Title

Enhancing the Performance of Advanced Wireless Systems via Passive Beamforming

Author

Li, TIanxiang

Publication Date

2023

Peer reviewed|Thesis/dissertation

UNIVERSITY OF CALIFORNIA
Los Angeles

Enhancing the Performance of Advanced Wireless Systems via Passive Beamforming

A dissertation submitted in partial satisfaction
of the requirements for the degree
Doctor of Philosophy in Computer Science

by

Tianxiang Li

2023

ABSTRACT OF THE DISSERTATION

Enhancing the Performance of Advanced Wireless Systems via Passive Beamforming

by

Tianxiang Li
Doctor of Philosophy in Computer Science
University of California, Los Angeles, 2023
Professor Omid Abari, Chair

Contemporary wireless networks are experiencing an era of unprecedented advancements, driven by the escalating demand from new wireless applications such as augmented and virtual reality, and further bolstered by the widespread deployment of the Internet of Things (IoT). These advancements encompass a range of technologies, comprising progress in wireless communication, wireless sensing, and wireless power transfer. mmWave technology is considered the key enabler of ultra-high data rates and capacity for future wireless communication, addressing the escalating demands of applications like high-definition video streaming and augmented reality. WiFi technology, the cornerstone of indoor wireless communications, has also undergone significant advancements in the various generations, offering higher throughput and network capacity. Meanwhile, the proliferation of wireless access points has sparked interest in harvesting power from Radio Frequency (RF) signals to power up the mass number of IoT devices. Despite these advancements in wireless technology, there remains a distinct disconnect between the evolution of wireless protocols and antenna hardware, with each failing to fully benefit from the progress of the other. In this thesis, we adopt a combined hardware-software co-design methodology to address the challenges of modern

wireless networks, synergizing the latest developments in both wireless network protocols and antenna technology. In particular, we draw inspiration from the passive beamforming principle of Frequency Scanning Antenna (FSA), traditionally utilized in the field of radar and imaging, and integrate it in the field of wireless communication, sensing, and power transfer. In contrast to active beamforming technology, which uses intricate and energy-consuming electronic components to steer the beam, FSA utilizes the physical structure of the antenna to steer the beam based on signal frequency. We integrate this unique passive beamforming feature of FSA with wireless protocols to enhance the range and performance of future wireless systems.

In this thesis, we first explore the challenges of modern-day wireless networks then discuss how we can address them using passive beamforming with FSA. A key challenge of mmWave networks is the significant signal attenuation due to high frequency. To compensate, base stations transmit mmWave signals using narrow beams that can be easily blocked by physical obstacles, greatly impacting their real-world deployment. In the first part of this work we propose mmXtend, a low-cost, low-power mmWave repeater that uses passive beamforming to provide high-data-rate links to a large number of users simultaneously in scenarios where the line-of-sight path is blocked. Following this, we explore the evolution of WiFi technology. Despite the advancements of WiFi protocol over the years, the performance of WiFi networks is still constrained by the inherent limitations of its antenna hardware design. Today's WiFi devices mainly use omni-directional antennas, which fail to capitalize on the advancements in WiFi protocols, and conversely, these protocols do not leverage the potential of antenna technologies. This disconnect markedly hampers the overall performance of WiFi systems. In the second part of this thesis, we introduce Wi-Pro, a plug-and-play module, which enhances WiFi performance by integrating passive beamforming with the WiFi protocol. It can be deployed on any WiFi device without requiring firmware or chipset modifications. Additionally, for wireless power transfer, although it has been a long-standing topic of discussion, its practical applications in the real world remain limited. The main barriers include the

restricted range for energy transfer and the lack of an efficient, low-power method for beam alignment, which is essential for effective energy transfer. In the third part of this thesis, we introduce mmCharge, a mmWave power harvesting system which uses passive beamforming to increase the range of mmWave wireless power transfer.

Our research shows that by integrating the concept of passive beamforming in the field of wireless communication, sensing, and power transfer, we can enhance performance and enable new capabilities. This thesis provides a comprehensive exploration into the development of end-to-end wireless systems that employ passive beamforming via FSA, which paves the way for future research in this area.

The dissertation of Tianxiang Li is approved.

Tony Nowatzki

Deepak Vasisht

Songwu Lu

Omid Abari, Committee Chair

University of California, Los Angeles

2023

TABLE OF CONTENTS

LIST OF FIGURES

LIST OF TABLES

ACKNOWLEDGMENTS

It has been a long, challenging, and fruitful journey. As I look back at the many twists and turns along my academic path, I am glad to have reached this significant milestone. I would like to express my gratitude for all that has supported me along the way. First and foremost, I extend my deepest thanks to my Ph.D. Advisor Omid Abari. His unwavering support and insightful guidance have been pivotal throughout my Ph.D. years. I would like to thank him for sparking my interest in the field of wireless networking, and supporting me through some of the hardest times in my academic journey. I have learned many things from him over the years on how to become an independent researcher, from creative thinking, writing, presentation, to conducting experiments, formulating research plans, and managing projects. His insights and feedback have not only shaped this research but have also profoundly influenced my professional growth. It has been a great honor to work with him.

I would like to further thank my thesis and oral qualification exam committee members, Prof. Songwu Lu, Prof. Deepak Vasisht, Prof. Tony Nowatzki, and Prof Achuta Kadambi for their valuable feedback to further improve my research. Their expertise across diverse fields has not only broadened my perspective on interdisciplinary studies but also enabled me to uncover new challenges and explore alternative approaches within my research domain. I sincerely appreciate the time and effort they put in helping me to refine my research and my thesis.

In my long academic journey, I have been fortunate to work with many talented colleagues, Haofan, Mohammad, Reza, Haochen, Chris, Jianting. I would like to thank them for tackling the various research challenges we faced together and the moments of laughter we shared. I will forever cherish the friendship and memories at ICON Lab. I would also like to extend my thanks to my previous collaborators, Zhaoning, Zhiyi, Haitao, Xin, and Spyros for their help on the various projects we pushed out. I wish them the best of luck in their research and careers.

A special thanks to my tennis pals, Jeff, Tong, James, Yizhou, Kobe, Zetao, Xuanyi, Yaxuan, and Shuaijing for hitting those late night tennis games with me and relieving our academic stress together. I also extend my sincere gratitude to all my friends who have supported me in my Ph.D. journey Minqi, Yadi, Wenxin, Jiacheng, Zhenning, Sibo, and the countless others who I could not all name here. I cherish the time we have spent together at UCLA as well as the companion and friendship they have provided.

Finally, I would like to express my deepest gratitude to my parents Xiaohan and Haizhou for their long enduring support throughout my many years of academic journey. My dad Haizhou, who taught me the value of strict discipline in the pursuit of professional excellence from a young age, and constantly reminded me of the important things I should be focused on in life. My mom Xiaohan, a great researcher and a loving mother, who has taught me the essential qualities of a researcher: patience, perseverance, the pursuit for knowledge, and the constant curiosity of understanding new things. She played a pivotal role in inspiring me to embark on this Ph.D. journey and will forever be a role model in my life. I dedicate this achievement to them, for always believing in me and for providing their unyielding support.

VITA

2010–2014 B.S., e-Commerce Engineering with Law, QMUL, London, UK

2014–2017 M.S., Computer Science, Tsinghua University, Beijing, China

2017–2023 Graduate Student Researcher, Computer Science Department, UCLA, Los Angeles, CA, USA

2018–2022 Teaching Assistant, Computer Science Department, UCLA, Los Angeles, CA, USA

2019 Summer Software Engineer Intern, Cisco Systems, Inc., San Jose, CA, USA

2021 Summer Software Engineer Intern, Facebook, Inc., Menlo Park, CA, USA

2022 Summer Software Engineer Intern, Meta Platforms, Inc., Menlo Park, CA, USA

PUBLICATIONS

Tianxiang Li, Mohammad Hossein Mazaheri, Omid Abari. "Enabling On-Demand Low-Power mmWave Repeaters via Passive Beamforming", MobiCom 2024.

Tianxiang Li, Mohammad Hossein Mazaheri, Kalaivani Kamalakannan, Haofan Lu, Omid Abari. "Can IoT Devices be Powered up by Future Indoor Wireless Networks?", HotMobile 2024.

Tianxiang Li*, Haofan Lu*, Reza Rezvani, Ali Abedi, Omid Abari. "Bringing WiFi Localization to Any WiFi Devices". HotNets 2022.

Tianxiang Li, Mohammad Hossein Mazaheri, Omid Abari. "5G in the Sky: The Future of High-speed Internet via Unmanned Aerial Vehicles", HotMobile 2022.

Tianxiang Li*, Haofan Lu*, Reza Rezvani, Mohammad Hossein Mazaheri, Omid Abari. "Enhancing WiFi Protocols via Smarter Antenna Design". In submission.

CHAPTER 1

Introduction

In recent decades, the increasing demand for high-throughput low-latency services in new wireless applications, combined with the rapid expansion of Internet of Things (IoT) deployments, has catalyzed significant advancements in various wireless technology domains. Millimeter-wave (mmWave) technology, in particular, has been pivotal in enabling a substantial increase in throughput for future wireless networks. Concurrently, WiFi technology has undergone significant evolution, offering enhanced throughput and greater network capacity. Furthermore, the growing proliferation of wireless access points has sparked interest in exploring the feasibility of harvesting power from Radio Frequency (RF) signals to power up the massive number of IoT devices. However, despite these exciting advancements in wireless technology, they consistently face challenges and limitations rooted in the inherent disconnect between the wireless protocols and the hardware designs, which constrain the full realization of their potential. This thesis presents a cohesive exploration into overcoming these challenges, by adopting an hardware-software co-design approach, synergizing the advancements in wireless network protocols, signal processing techniques, and antenna technology. At its core, this research aims to increase the range and performance of future wireless systems by employing innovative passive beamforming technology. We first explore the challenges of modern wireless networks, then discuss how we can integrate passive beamforming technology to address them.

Millimeter-wave (mmWave) technology, operating in the expansive high-frequency spectrum of 24 GHz and above, holds the promise of meeting the demands of popularization

of wireless applications that require ultra-high data rates and low latency, including high-definition video streaming, autonomous vehicles, augmented/virtual reality (AR/VR), and industrial automation [FMT17, RQH20, SNR20, WCC17, ZWH19, MAA19a, MRG23]. The primary challenge facing millimeter wave (mmWave) technology is its signal coverage. The high-frequency signals inherently experience significant path loss, necessitating the use of power-intensive and costly phased array antennas to concentrate signal power into a directional beam. However, these beams can be easily blocked by obstacles such as a wall, a person or even furniture, resulting in a drop of 20 dB or more in Signal-to-Noise ratio (SNR) [ABD17, Zha13]. Therefore, mmWave networks cannot provide reliable high-data-rate links in environments with static or mobile obstacles. To overcome this problem, researchers have designed mmWave relays, repeaters and intelligent surfaces [mov, ABD17, CMG23, PLS20, TSK18, GPO21], to reroute the signal around obstacles. However, these existing systems are costly, power hungry, and require frequent feedback from the transmitter or receiver. This drives the need for a solution that is low-cost, low-power, capable of providing reliable high data-rate links to multiple users simultaneously, and can be deployed seamlessly on-demand without requiring significant changes to the communication endpoints.

Beyond the pursuit of higher-quality services, the growing proliferation of wirelessly connected devices also introduces new challenges and opportunities. The number of worldwide Internet of Things (IoT) devices is expected to grow to more than 29 billion by 2030 [Sta]. On one hand, the rapid increase in connected devices requires the network to handle massive connectivity while supporting high-data-rate, low-latency applications such as video conferencing, and multiplayer gaming. On the other hand, the ubiquitous WiFi deployment brings up new opportunities for WiFi sensing, which also raises challenges in seamlessly integrating the communication and sensing capability of future WiFi network. To deal with these challenges, WiFi manufacturers have adopted numerous techniques and advancements along with the evolution of WiFi standards over the past two decades. These advancements include but

not limited to: expanding the channel bandwidth, adding more antennas, and implementing advanced multiplexing and multiple-access techniques (such as MIMO and OFDMA). While most of these advancements are around WiFi algorithms, protocols and circuit, the design of WiFi antenna itself has remained relatively static over the years. In particular, most WiFi devices have been using typical omni-directional antennas (such as monopole or diplole antennas). Unfortunately, these antennas do not benefit from the advancement of WiFi protocols or vice versa. We argue that the current antennas used in WiFi devices do not fit well with the evolving standards and it is time to rethink about how to design WiFi antennas in a cross-layer approach (i.e. designing a WiFi antenna while considering WiFi protocols capabilities).

Besides network connectivity, another major challenge in deploying IoT devices is their battery life. Most today's IoT devices require their batteries to be replaced or recharged every couple of months. Considering the fact that the average number of IoT devices in an American household is expected to reach fifty in the next few years [Tim], we would need to change one to two batteries per week in our homes. Moreover, in many cases, IoT sensors are not easily accessible, making battery charging or replacement a significant effort. With the increased deployment of wireless access points, there is a growing interest in the potential of harvesting energy from RF signals to power low-energy IoT devices. Although this sparks exciting new opportunities, many questions remain in this field. For example, which frequency is best for wireless power transfer considering the trade-offs of energy propagation, hardware efficiency, and regulations? In this thesis, we show that mmWave bands are much better candidates for transferring power to IoT devices than lower frequency signals. However, to efficiently transfer power using mmWave, the main challenge is beam alignment of the power transmitter and harvester. Although past mmWave work has proposed different approaches and schemes for creating a directional beam and searching for the best beam direction [HAR18a, EAH15], they are not practical for low-power IoT devices. This is mainly due to the fact that existing schemes require phased array antennas. Unfortunately, phased

arrays are costly and consume a significant amount of power which makes them impractical for energy harvesting IoT. This drives the motivation to pursue alternative methods to perform beamforming and beam alignment to power up energy-constrained devices.

1.1 Our Contribution

This thesis adopts a hardware-software co-design approach, which combines advancements in wireless network protocols with innovative passive beamforming technology to address the challenges of modern wireless networks. Unlike active beamforming technology, which requires complex and power-intensive electronic components to shape and steer the beam of radio waves, passive beamforming technology offers a low-power, low-complexity solution to direct the signal based on the physical structure of the antenna. In particular, we utilize passive beamforming principle of Frequency Scanning Antenna (FSA) previously used in the field of radar and imaging [ZKQ17, KZ13], and adapt it for novel applications in wireless network communication, wireless sensing, and wireless power transfer. FSA provides a method for passive beamforming and beam steering based on signal frequency. We demonstrate how this unique feature can be seamlessly integrated with wireless protocols, enhancing the range and performance of future wireless systems.

1.1.1 mmXtend: Extending the Coverage of mmWave Networks via Passive Beamforming

To address the limited coverage problem of mmWave networks, we present mmXtend, the first mmWave repeater which uses passive beamforming technique. mmXtend is low-cost, low-power, supports multi-user, and can be easily deployed on-demand (without requiring any feedback from the network to operate). We design a 2D passive beamforming and steering structure which can be easily implemented on printed circuit board (PCB). More importantly, we show the applicability of passive beamforming in wireless repeaters for the

first time. We built mmXtend and empirically evaluated its performance in a variety of scenarios. Our results show that mmXtend solves the blockage problem, and enables data rate of more than 250 Mbps link to each user when there are up to 200 users. Even when there are 1000 users, it can provide each user with a 70 Mbps link, which is sufficient for 4K video streaming [Qua18].

1.1.2 Wi-Pro: Enhancing WiFi Performance via Passive Beamforming

To enhance the performance of future WiFi networks in the era of massive IoT connectivity, we introduce Wi-Pro, a system which incorporates a new plug-and-play antenna for WiFi devices based on FSA technology and integrates it with the existing WiFi protocols. We demonstrate the dual advantages of Wi-Pro in enhancing the performance of modern WiFi protocols. First, it increases the data rate and communication distance of WiFi devices. Second, it facilitates the Angle-of-Arrival (AoA) measurement on any WiFi device, including low-cost, low-power units with a single transceiver chain, all without requiring firmware or chipset modifications. We build a prototype of Wi-Pro and demonstrate 10 to 120% data rate improvement and more than three times range improvement for communication. Our prototype can also measure the AoA with an average precision of 1.34 degrees.

1.1.3 mmCharge: Increasing the Range of mmWave Wireless Power Transfer via Passive Beamforming

We study the feasibility of using different indoor signals to transfer power to IoT devices considering constraints such as FCC regulations, antenna size, etc. Our results show that mmWave signals are much better candidates to transfer power compared to traditional wireless signals such as WiFi and sub-GHz signals. We propose a system architecture and link establishment protocol for IoT devices to harvest energy from indoor mmWave access points. Our design is based on passive beamforming and backscatter technology, which greatly re-

duces the energy consumption for beam alignment and increases the range of mmWave power transfer. We evaluate our system in terms of power transfer at different distances. Our results show that it is possible to harvest 1 mW and 0.1 mW power at the distances of 7.5 m and 15 m indoors, respectively. This enables IoT devices to significantly increase their batterylife.

1.2 Organization of the Dissertation

This dissertation is organized into the following chapters. Chapter 2 introduces the basic principles of beamforming and beam steering as well as discusses the limitations of the beamforming solutions adopted in modern wireless networks. It then introduces the concept and working principle of Frequency Scanning Antennas (FSA). Chapter 3 introduces our mmXtend system, and illustrates how we use passive beamforming technology to design and implement a low-cost, low-power repeater to address the mmWave signal blockage challenge. Chapter 4 presents Wi-Pro, our plug-and-play module which uses passive beamforming to enhance WiFi performance. Chapter 5 investigates the feasibility of mmWave wireless power transfer and presents mmCharge, a system which uses passive beamforming to increase the range of mmWave wireless power transfer. In Chapter 6, we summarize our contributions and propose potential directions for future research.

CHAPTER 2

Background

In this chapter we will first explain the basic principles of *beamforming* and *beam steering*, emphasizing their pivotal roles in wireless communications. Then, we will introduce the conventional methodology of beamforming and beam steering using phased arrays, while examining its limitations. Finally, we will introduce the concept of *passive beamforming*, implemented through Frequency Scanning Antenna (FSA), a cutting-edge approach that offers new potentials in the field of wireless communication.

2.1 Basic Principle of Beamforming and Beam Steering

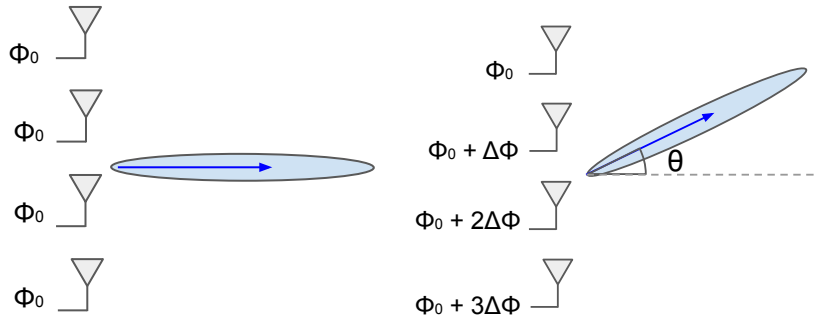

(a) Beamforming (b) Beam Steering

Figure 2.1: Basic Principle of Beamforming and Beam Steering.

Beamforming and beam steering are signal processing techniques used to optimize the performance of wireless communication systems. These techniques are especially important for higher frequency signals, such as mmWave signals, which experience higher propagation loss compared to lower frequency signals. Therefore, it is important to focus the signal power

at a particular direction through *beamforming*, and control its transmission direction using *beam steering* techniques. First let me explain the basic principle of beamforming. A single isotropic antenna simply radiates the signal uniformly in all directions. By aligning an array of antenna elements with fixed-spacing, and transmitting signals with the same phase (ϕ_0) to all the antenna elements, the signals radiated out of each antenna element will combine constructively in the broadside direction, forming a beam, as shown in Figure 2.1a. By controlling the amount of phase shift ($\delta\phi$) between each antenna element, the angle of the beam θ will change accordingly as shown in Figure 2.1b.

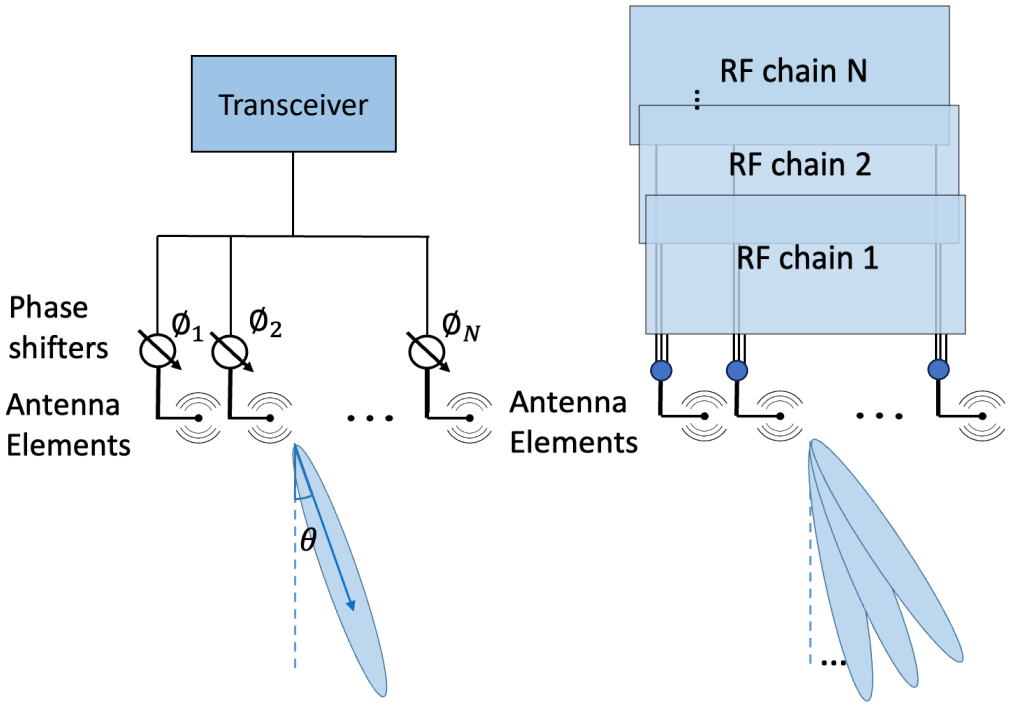

(a) Phased Array Beamforming (b) Multi-Beam Phased Array

Figure 2.2: Phased Array Principle.

A well known approach for beamforming and beam steering is to use phased arrays [Mai17]. Phased array consists of an array of fixed-spacing antenna elements, where each antenna element is connected to an electronically controlled phase shifter, as shown in Figure 2.2a. The radio waves from multiple antennas elements will interfere with each other constructively, forming a narrow beam with stronger signal strength. By electronically controlling

the amount of phase shift between each antenna element using a central computer, the beam angle θ will change accordingly. This allows the phased array antenna to form a narrow beam and steer it in different directions. The main limitation of phased arrays is that it requires calibration and extensive control over the phase shifters which makes the system very complex and costly. Moreover, to generate multiple beam simultaneously with independent data streams, phased arrays require multiple transmitter and receiver chains as shown in Figure 2.2b. As a result, the required hardware becomes extensively costly and complex, making it unsuitable to be deployed flexibly on-demand at different locations. To address these challenges, and design a low-power, low-complexity beamforming system, we develop passive beamforming solutions using Frequency Scanning Antenna (FSA).

2.2 Passive Beamforming using FSA.

Frequency Scanning Antenna (FSA) is a passive structure which focuses and transmits a signal toward a direction, where the direction of the signal depends on the signal frequency, as shown in Figure 2.3a. FSA realizes beamforming and beam steering based on the physical structure of the antenna, instead of relying on active components like phase shifters, so it is regarded as a *passive beamforming* technique. This approach significantly reduces both the power requirements and the cost of beamforming systems compared to traditional phased arrays, which rely on expensive and power-intensive phase shifters. Owing to its passive nature, Frequency-Scanning Antenna (FSA) technology has been employed as a cost-effective beam scanning solution in various applications such as radar [ZMZ13, SRT19], and imaging [LLI18, LLL16, ZKQ17].

There are mainly two categories of FSAs: leaky-wave antennas [CHW10, XWZ09, WZC20] and antenna arrays [VGA13, KZK13]. First, we will explain how FSA achieves passive beamforming using leaky-wave antennas as an example. For a leaky-wave based FSA, when a signal is fed to the FSA structure, the signal gradually leaks into space through the ra-

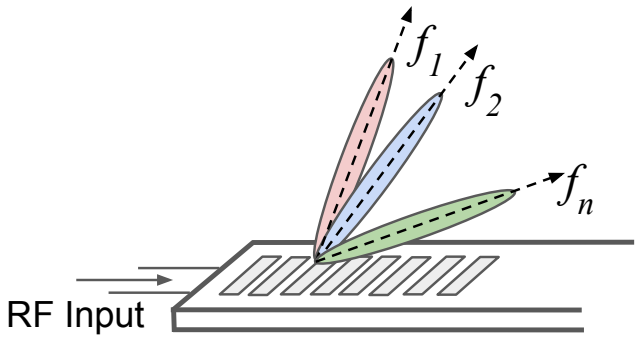

(a) The input signal leaks into space as it travels through the antenna structure, forming highly directional beams. The beam angle is dependent on the input signal frequency.

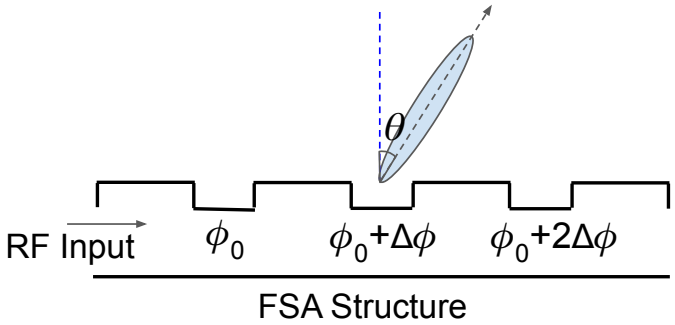

(b) The input signal experiences a different phase shift at each radiating slot, which causes the radiated signals to combine constructively in a certain direction θ.

Figure 2.3: FSA Principle: Leaky-Wave Antenna

diating slots on the top of the structure, as shown in Figure 2.3b. The signal experiences a different phase shift at each radiating slot, which causes the radiated signals to combine constructively in a certain direction, forming a beam. The angle of beam radiation depends on the frequency of the signal. Next we will explain how FSA achieves passive beam steering based on signal frequency. Signals of different frequencies have different wavelengths, thus it experiences a different amount of phase shift at each radiating slot, forming beams in different directions. Therefore, this structure is similar to an array of emitting elements, where the phase shift of the signal at each element is a function of the distance of the element from the signal feed and frequency of the signal. This natural phase shift enables the structure to receive or transmit a signal toward a direction, where the beam direction is a function of

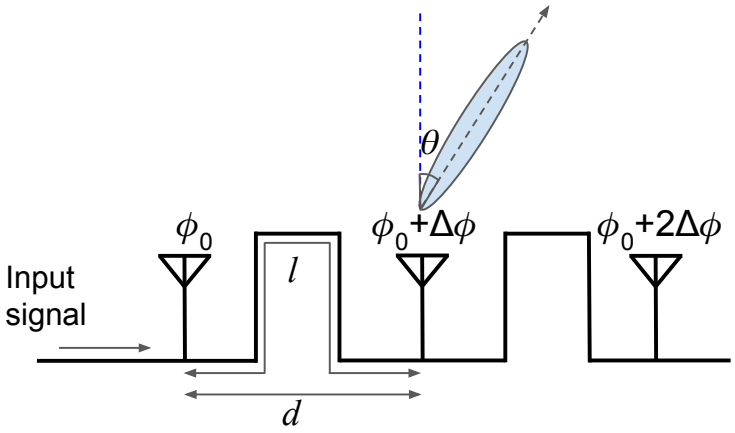

Figure 2.4: FSA Principle: Antenna Array

signal frequency. In particular, the angle of the beam, θ, can be expressed as:

$$sin(\theta) = \frac{\beta}{k_0}, \tag{2.1}$$

where β is a parameter of the design, known as the waveguide number and k_0 is the free space wavenumber [Gua18]. In (2.1) both β and k_0 change with frequency but in a FSA structure, the variation of β is much higher. Therefore, the beam rotates with the change of the frequency.

The array-based FSA structure consists of an array of antenna elements connected by a transmission line as shown in Figure 2.4. When a signal is fed into this structure, it travels along the transmission line. The signal experiences a different amount of phase shift at each radiating element. This natural phase shift enables the signals at different antenna elements to combine constructively in a certain direction. The relationship between the signal wavelength and the radiated beam angle can be expressed using the following equation:

$$\sin(\theta) = \frac{\Delta\lambda \cdot l}{2 \cdot \lambda_0 \cdot d}, \tag{2.2}$$

where $\Delta\lambda$ is the change in the signal wavelength, λ_0 is the signal wavelength which generates the beam in the broadside direction, d is the spacing between adjacent antenna elements, and

l is the length of the transmission line between adjacent antenna elements. As the structure of the FSA is fixed, therefore the transmitting or receiving direction is a function of the signal's wavelength or frequency.

In summary, FSA provides a passive way to steer the beams to different directions based on signal frequency. Instead of relying on active phase shifters like phased arrays, FSA utilizes the physical structure of the antenna to create natural phase shift, which provides a low-power, low-complexity solution to beamforming and beam steering. Furthermore, to generate multiple beams simultaneously, FSA simply requires input signals of different frequencies, which greatly lowers the complexity of the hardware system compared to phased arrays.

CHAPTER 3

mmXtend: Extending the Coverage of mmWave Networks via Passive Beamforming

This chapter introduces mmXtend, our on-demand low-power mmWave repeater, which uses passive beamforming technology to overcome the signal blockage challenge of mmWave networks.

3.1 Problem Statement and Challenges

In this section, we begin with an overview of the coverage problem of today's mmWave networks. Following this, we will outline the key objectives in designing an effective mmWave repeater system to tackle these issues. Finally, we will analyze the shortcomings of existing solutions and highlight the unique aspects of our approach that set it apart.

3.1.1 mmWave Coverage Problem

One of the main challenges of mmWave technology is signal blockage. As shown in Figure 3.1, it is generally hard to guarantee LOS non-blockage communication link directly between the mmWave access point and the user device. A path with obstacles between the transmitter and receiver can cause significant attenuation to the mmWave signal. For example, a single wall located between the user and the outdoor base station results in penetration loss of 20

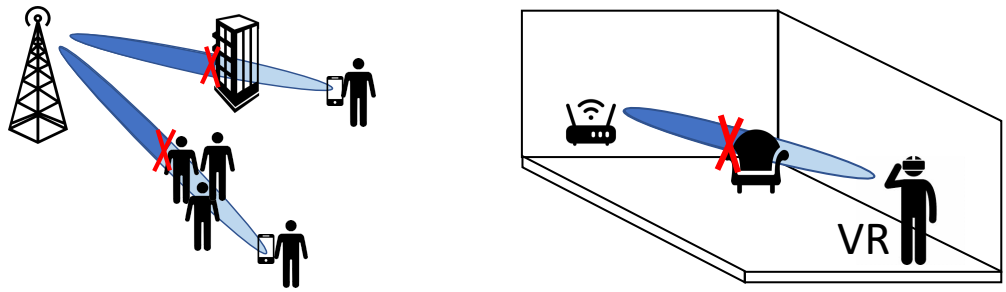

(a) Outdoor (b) Indoor

Figure 3.1: mmWave networks problem. mmWave signals are directional, and hence they can be blocked by obstacles.

to 40 dB [Zha13] at 28 GHz [1]. Similarly, a person standing between the user and the access point, attenuates the signal by 10 to 12 dB [ZWL16, ABD17].

To illustrate the effect of blockage on the throughput, we present a link-budget calculation using a real world example as shown in Figure 3.1a. We consider a typical cellular base station with an Effective Isotropic Radiated Power (EIRP) of 60 dBm [Qua19], and a typical mmWave receiver with 10 dB antenna gain, and noise floor of -89 dBm. The communication frequency is 28 GHz, and the channel bandwidth is 100 MHz. The distance between the user and the base station is 200 meters, which results in around 107 dB free space path loss. For our calculation, we only consider the downlink, where the base station is the transmitter and the user device is the receiver. However, similar link budget calculation can be done for uplink too. We calculate the received signal power P_{rx} based on eq.(1), where P_{tx} is the transmitter EIRP, A_{rx} is the receiver antenna gain, L_{path} is the free-space path loss, and L_{obs} is the penetration loss of the obstacles.

$$P_{\text{rx}} = P_{\text{tx}} + A_{\text{rx}} - L_{\text{path}} - L_{\text{obs}} \tag{3.1}$$

[1]We will use the commercial mmWave frequency band of 26.5 GHz to 29.5 GHz and channel bandwidth of 100 MHz in our examples, as this is the spectrum band used by a number of carriers

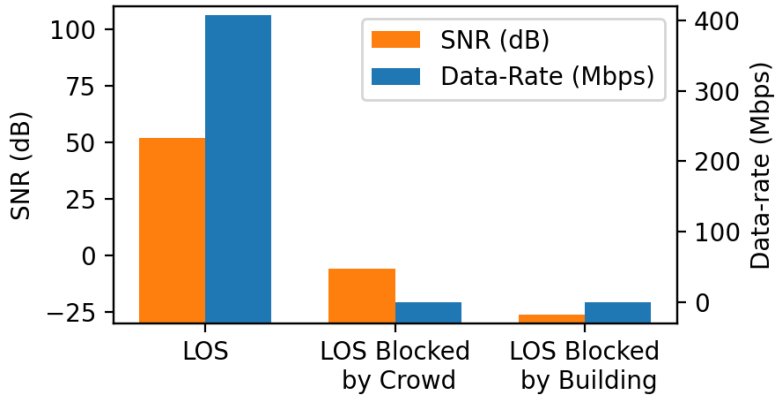

Figure 3.2: Blockage Impact on SNR and Data Rate of mmWave.

We then calculate the receiver SNR value based on eq.(2), where P_{nf} is the noise floor value.

$$SNR = P_{\text{rx}} - P_{\text{nf}} \tag{3.2}$$

Figure 3.2 shows the calculated SNR of the received signal and the data rate of a single user in three different scenarios. In the case with LOS path between the base station and the user, the receiver SNR is 52 dB. When there is a crowd of people blocking the path, the SNR decreases to -6 dB. In the case of a building blocking the signal path, the SNR drops to -26 dB. To evaluate the effect of blockage on data rate, we ran simulations with a single base station and a single user using the ns-3 mmWave simulator [Mez18]. We set up the parameters as mentioned above. The simulation results show that the data rate of a single user is 408 Mbps when there is no blockage [2]. The user data rate drops to 0 Mbps when a crowd or a building is blocking the signal path. This result shows that blockage of a mmWave signal has significant impact on the throughput.

To solve the mmWave blockage problem, we propose mmXtend, a low-cost, low-power repeater system for mmWave communications.

[2]The channel throughput is computed based on single component carrier, single MIMO layer, time division multiplexing, and adaptive modulation and coding [Mez18]

3.1.2 Design Goals of mmXtend

Ideally, an mmWave repeater needs to satisfy multiple requirements to effectively achieve the goal of making mmWave networks scalable and ubiquitous:

•*On-demand and Rapid Deployment:* It must work seamlessly with the base stations and clients without requiring any cooperation or feedback from them. This enables on-demand and rapid deployment of the repeater, extending reliable mmWave networks to wherever and whenever needed. For example, during an emergency response, or an event in a part of a city, we can quickly use this repeater and enable high-data-rate low-latency mmWave networks to users.

•*Low-Cost and Low-Power:* Its design and implementation need to be low-power, low-cost, and lightweight, such that it can be battery (or solar) powered, and be easily deployed on a pole or a drone whenever and wherever high-data-rate connectivity is needed.

•*Multi-user Support:* Finally, it needs to provide reliable high-data-rate links to many users. Otherwise, it cannot be used in emerging applications such as multiuser virtual reality, smart home, and stadium augmented reality, where ten to thousands of mobile devices need reliable, high-data-rate, low-latency mmWave connectivity.

If the above requirements are satisfied, we can envision making reliable mmWave networks scalable and ubiquitous. However, to the best of our knowledge, no current system satisfies all of these requirements. To address these challenges, we introduce mmXtend, a low-power low-cost repeater system which can be battery (or solar) powered, and be easily deployed on a pole or a drone whenever and wherever high-data-rate connectivity is needed. mmXtend can form beams to multiple users, simultaneously, without requiring phased arrays, or other complex and power-hungry hardware such as radios, FPGAs, or processors. Moreover, our solution can work seamlessly with the base station and the client. Therefore, it can effectively address the coverage limitations of mmWave networks in both outdoor and indoor scenarios whenever and wherever is needed such as crowded events, disaster recovery, smart factories,

and smart homes as shown in Figure 3.3.

3.1.3 Limitations of Current Solutions

In recent years, there has been a growing interest in solving the blockage problem in mmWave networks [QYZ22, JWG19, SPZ18, CMG23, SZR16]. There are some works on building mmWave repeaters [mov, FRT22, Met21, ABD17]. However, they either do not support multiple users or use complex, expensive, and power-hungry phased arrays. They also require significant feedback and cooperation with the base stations and users, to operate and keep its beams aligned toward users. Some recent work has proposed smart and intelligent surfaces [CMG23, PLS20, GPO21, TSK18, Met18]. These surfaces typically consist of a large array of passive elements which can reflect and refocus mmWave beams in certain directions passively. Although these systems do not need to use phased arrays, they are either non-reconfigurable [QYZ22] or require a large number of mmWave diodes (or varactors) and a processor such as FPGA to control individual elements, which makes the design complex and expensive. Moreover, they require feedback from the client and base station to operate and typically do not support multiple users simultaneously. In contrast, mmXtend introduces a mmWave repeater which supports multiple users, does not require any processor (such as FPGA), and does not require any feedback from the client or base station to operate. mmXtend achieves this by designing, building, and integrating a passive 2D beamforming structure into mmWave repeaters.

Past work has explored passive 1D and 2D beamforming methods in the mmWave frequency. However, they all have certain limitations, and none of them targets repeater systems. For example, some past work has shown the potential of using Rotman lens for passive beamforming at mmWave frequencies [EHT21b, EHT20]. However, the only support 1D beamforming. Some other work has also proposed passive designs for 2D beamforming. However, these approaches [CVF17, KHL22, LWL17] are very complex in design since they are interconnecting multiple layers of substrates in orthogonal planes. In contrast, our

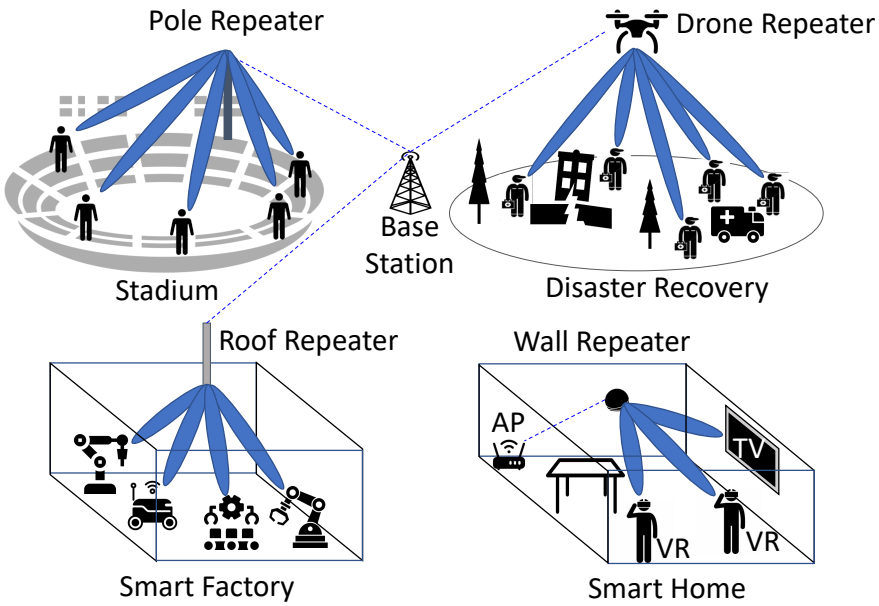

Figure 3.3: mmXtend applications. Our repeater can be deployed on-demand in outdoor and indoor scenarios, solving the blockage problem of mmWave networks.

design is integrated into a single-layer substrate, which is compact, low cost, and easy to fabricate. It can be flexibly deployed at various locations on-demand. Finally, the authors in [WCH18] proposed a 2D beamforming design using FSA and Rotman lens, however it is designed for near-field scenarios with limited coverage of tens of millimeters and FSA beam steering range of less than 25 degrees, which makes it impractical to be used for applications such as cellular communication, where a large number of users need to be covered in a large area. In contrast, our design can achieve a working distance of hundreds of meters and FSA beam steering range of more than 50 degrees. Moreover, we also incorporate Multi-User Multiple Input Multiple Output (MU-MIMO) enabling a repeater system which supports multiple users and works seamlessly with existing mmWave networks.

3.2 mmXtend Overview

mmXtend is a low-power low-cost repeater system which can be battery (or solar) powered, and be easily deployed on a pole or a drone whenever and wherever high-data-rate connec-

tivity is needed, as shown in Figure 3.3. In a scenario where the line of sight between a base station and a user is blocked, mmXtend receives the signal from the base station and forms beams to the user. mmXtend can support multiple users simultaneously, without requiring phased arrays or other complex and power-hungry circuits. Moreover, our solution works seamlessly with the base stations and users. Hence, it can effectively address the coverage limitations of mmWave networks in both indoor and outdoor environments. To develop and build mmXtend, we need to address multiple challenges. First, we need to design a technique which forms beams to multiple users simultaneously, without consuming any power. Second, we need to extend our beamforming approach to 2D and build a repeater which covers the whole space. Finally, our design needs to seamlessly support protocols for multi-user communication, link establishment, and mobility.

To address the first challenge, we develop a Frequency Scanning Antenna (FSA) operating at mmWave. Our design enables 1D passive beamforming while it can be fabricated using only printed circuit board (PCB). Such a design enables our repeater to perform Frequency Division Multiple Access (FDMA) for users in different directions since FSA creates multiple beams while each radiating only a specific frequency channel. Moreover, since the direction of the beam is a function of the signal frequency, the base station or client can simply steer the repeater beams without its cooperation. To address the second challenge, we then design a mmWave Rotman lens and integrate it to our FSA design on the same PCB. Rotman lens is a passive structure with multiple ports which enables 1D beamforming where each beam is fed by a different port. Hence, integration of a FSA and Rotman lens enables our repeater to perform 2D beamforming, supporting multiple users in each frequency channels. In particular, by incorporating Multi-User Multiple Input Multiple Output (MU-MIMO) into our design, our repeater can support multi-user in each frequency channel through Space Division Multiple Access (SDMA). Finally, we integrate low-power amplifiers to our design, enabling low-power repeaters which amplifies and refocuses mmWave signals while it can be deployed seamlessly, without requiring any cooperation or feedback from base station or

client.

In the next few sections, we will explain in detail the components that contribute to the design of mmXtend.

3.3 1D Passive Beamforming.

To enable low-power, low-cost beamforming and multi-user access, our novel idea is to develop a repeater system based on Frequency Scanning Antenna (FSA) technique. FSA is a technique used primarily in radar imaging and weather forecast to perform measurements [ZKQ17, KZ13]. It is a passive structure which focuses and transmits (or receives) a signal toward a direction, where the direction of the signal depends on the frequency of its input signal, as discussed in § 2.2. One can design an FSA on PCB consisting of a substrate with many radiating elements (slots). When a signal is fed to the input of the FSA structure, the signal gradually leaks into space through these radiating slots. However, the signal experiences a different phase shift at each radiating slot, which causes the radiated signals to combine constructively in a certain direction. Since signals of different frequencies have different wavelengths, they experience different amounts of phase shift at each radiating slot. Hence, FSA forms a transmitting beam toward a direction which depends on the frequency of the signal. Note, FSA performs the same for receiving a signal too.

Our idea is that an FSA can provide a passive way to create multiple beams simultaneously when the signal contains multiple channels with different center frequencies. Moreover, we can steer each beam based on the shift in its signal center frequency, without relying on any phase shifters or active components. Hence, by integrating an FSA on a repeater, the repeater can create multiple beams toward the users, simultaneously. In particular, when the base station transmits/receives a signal consisting of multiple frequency channels (centered at f_1 to f_n) to/from the repeater, the FSA on the repeater is able to passively split the different frequency channels into separate high-gain beams to cover different areas on the

ground. We note that compared to phase arrays, our design has much lower power, lower complexity, and lower cost for beamforming and creating multiple beams simultaneously since it is purely based on a passive structure. Moreover, it does not require any processor or feedback from the base station (or the client) since they can steer the repeater's beam themselves by changing the frequency channel. In § 3.6, we will provide more details on how this design would enable a repeater which can be easily deployed without any need for a change or feedback to the base station or client.

Traditional mmWave FSA designs have multiple limitations which we need to address before using them in our repeater design. First, their designs require a large bandwidth to achieve a wide range of steering angles. Unfortunately, such a large bandwidth is not available in the commercial mmWave bands such as 5G and 6G. Second, they only support beam scanning from 0° to positive angles. This is due to the fact that the wave traveling in the structure only provides positive phase shift between consecutive radiating elements. Therefore, for our repeater, we need to design an FSA which (a) requires smaller bandwidth for beam steering and (b) covers negative angles.

(a) Requiring smaller bandwidth for beam steering: To achieve a reasonably large range for beam steering angle while using a small frequency change, we need to create large phase changes between the FSA radiating slots. To achieve this, our idea is to reduce the speed of the traveling wave inside the FSA. To control the speed of the wave, we build on a technique used in meta-materials, known as Spoof Surface Plasmon [KCQ16]. In particular, we place slots on the back of the FSA antenna. These back plate slots do not radiate the signal, but they act as a speed bump to reduce the wave velocity in the structure. Reducing the wave velocity provides a higher phase variation with frequency change, enabling larger beam steering angle in a smaller bandwidth.

(b) Covering negative angles: To enable beam steering for negative angles, we use modulated periodic slots on the top plate of our FSA. Specifically, as shown in Figure 3.4, the sizes of the radiating slots vary along the FSA structure. This periodicity in structure pro-

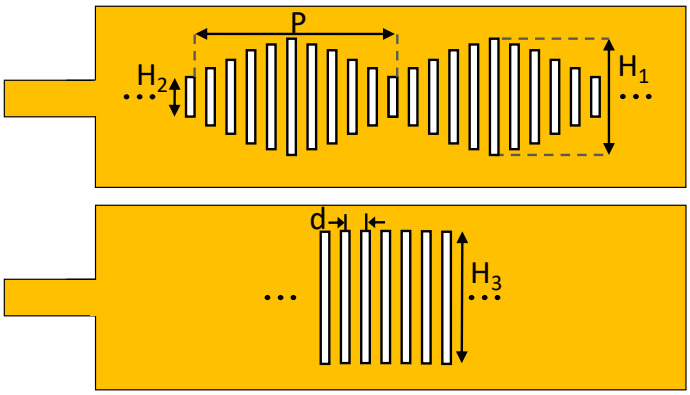

Figure 3.4: Our Designed FSA Antenna. The top and bottom layers of the antenna with modulated and equal length periodic slots, respectively.

vides spatial amplitude modulation (AM) [3] of the wave in the FSA structure, which creates infinite number of space harmonics [Bri53, Ito04, WZC20]. However, only the first harmonic radiates. This space harmonic creates negative phases for lower frequencies while positive phase for higher frequencies. Therefore, at the lower part of the frequency band, the FSA beam is pointing toward negative angles, while at higher frequencies, the beam is steered toward positive angles.

The design parameters to control the characteristics of the FSA are H_1, H_2, H_3, P, and d, as shown in Figure 3.4. As mentioned above, the slots in the back plane of the FSA do not radiate the signal. Rather, they are used to decrease the wave velocity. The proper wave velocity is achieved by adjusting the value of H_3 and d. For the slots in the top plane, the lengths of the slots are modulated. The period (P) and the amplitude of slots (H_1, H_2) define the backward and forward scanning range. Finally, the total number of slots and the length of the structure define the 3 dB beamwidth of the FSA.

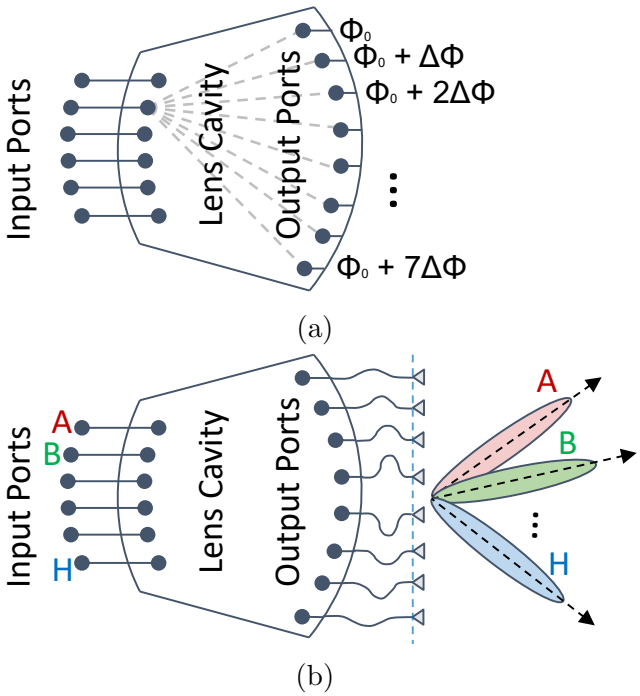

Figure 3.5: Rotman Lens. Rotmann Lens is passive structure which can be fabricated using just PCB. (a) It creates a specific phase change from each input port to the output port. (b) When the output ports are connected to individual antennas, it creates beams toward directions, depending on which input port is used. It can also create multiple beams simultaneously.

3.4 2D Passive Beamforming

In the previous section, we explained how we develop a passive structure for beamforming. However, since the proposed structure is a linear array of emitting elements, its beamforming works only in 1D. To support multiple users in an area, our system needs to generate beams in 2D. Hence, the next question is how can we achieve passive 2D beamforming?

To address this question, our novel solution is to integrate our FSA design into a Rotman lens. Rotman lens is a passive structure mostly used in radar systems to detect targets in different directions [VSS14]. The basic structure of the Rotman lens is shown in Figure 3.5. It consists of a number of input ports, a lens cavity, and a number of output ports which are

[3]Note spatial AM is different from temporal AM which is commonly used in wireless communication.

typically connected to individual antennas.

This structure can create a beam where its direction depends on which input port is used to feed the signal. The lens cavity, which can be fabricated using only a PCB, is designed such that it adds specific phase changes to the signal as it propagates from each input port of the Rotman lens to its output ports. Note, due to the shape of this structure, the amount of these phase changes depends on which input port is used for feeding the signal. Therefore, the antennas connected to the output ports of the Rotman lens emit the signal with different phases, creating a beam toward a direction that depends on which input port is used. Here, we explained how Rotman lens work for transmitting signals, it also works the same for receiving.

Note, both FSA and Rotman lens enables beamforming in only 1D. However, FSA steers the beam with change of frequency, and the Rotman lens steers the beam with change of input port. Hence, to enable 2D passive beamforming, our idea is to develop a Rotman lens at mmWave and integrate it with our FSA design on the same PCB substrate, as shown in Figure 3.6. In particular, our design connects each output port of the Rotman lens to the input of a separate FSA structure instead of just a typical antenna. Below, we explain how this structure enables 2D beamforming.

When a signal with a particular frequency is fed into one of the Rotman lens input ports, all FSAs receive the signal with different phase shifts created by Rotman lens cavity. Since the signal frequency is the same for all FSAs, they all create beams toward the same direction in 1D. However, since their signals have different phases caused by Rotman lens, their 1D beams are combined and create a 2D beam toward a specific direction. This novel structure enables passive beamforming in 2D. In other words, by changing the frequency of the signal, we can steer the beam in one dimension, and by changing the input port which we feed the signal into Rotman lens, we can steer the beam in the other dimension. Thus, we can create multiple beams simultaneously in 2D by feeding signals of different frequencies to different ports.

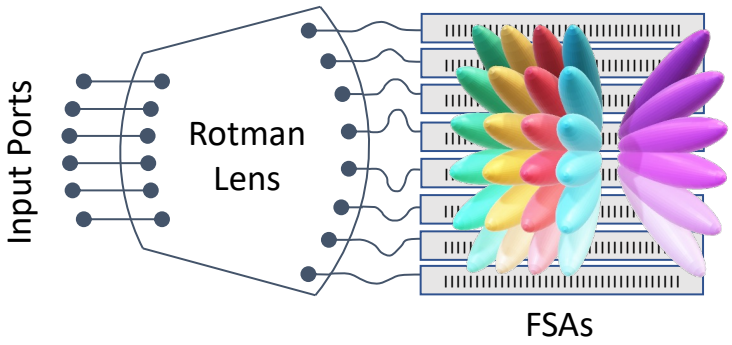

Figure 3.6: Our 2D Passive beam forming and steering. It can be fabricated on a thin PCB substrate (without any ICs) to passively form and steer narrow high-gain beams toward a direction that depends on which port and frequency is used. It can also create many beams simultaneously.

3.5 Supporting Multi-User

So far, we have explained how to design a passive structure which can create beams in 2D without consuming power or using any circuit components. Here, we explain how we use this structure to build a repeater which supports multiple users.

To build a repeater, we connect each input port of our passive structure shown in Figure 3.6 to a horn antenna. Such a design enables a repeater which can receive/transmit the signal from/to a base station using horn antennas and transmit/receive it to/from the clients using beams created by our passive structure. We are able to use horn antennas for backhaul (i.e. the link between the repeater and base station) since base stations and repeaters are typically fixed. Hence, they only need to perform the beam alignment process once, during the manual installation of the repeater.

To support multi-user communication, mmXtend divides users into different frequency channels in one dimension using FSA beams. Hence, they can communicate simultaneously using Frequency Division Multiple Access (FDMA). To support multiple users in the other dimension, mmXtend divides users into different beams created by Rotman lens and use Multi-User Multiple Input Multiple Output (MU-MIMO), which is already provided in most

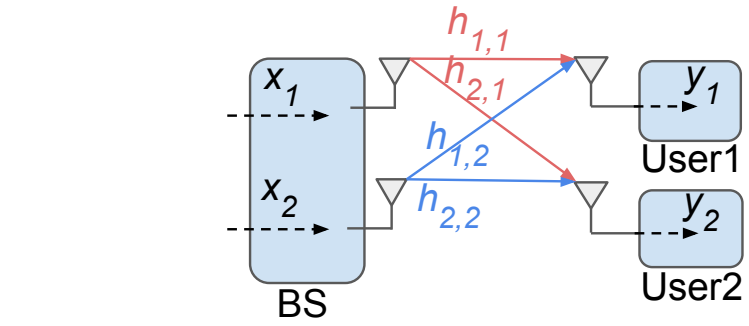

(a) Typical MU-MIMO

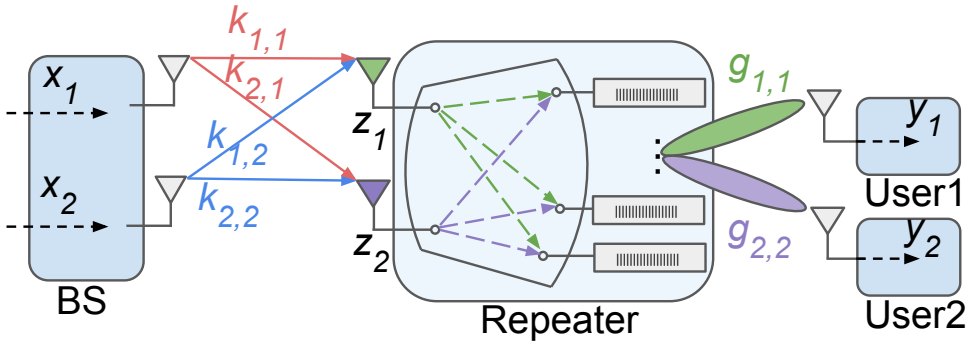

(b) MU- MIMO with mmXtend

Figure 3.7: MU-MIMO Examples. A typical 2×2 MU-MIMO system (a) without, and (b) with mmXtend's repeater.

mmWave base stations (such as 5G). Below, we will first explain the basics of MU-MIMO, then we will explain how our design seamlessly operates in MU-MIMO scenarios.

3.5.1 MU-MIMO Integration

MU-MIMO enables a base station to simultaneously communicate to multiple users over the same frequency channel. In a typical MU-MIMO system (when there is no repeater), the vector of received signals by users, y, can be written as follow: $y = HWx$, where H is the matrix of channels between the base station and users, W is the precoding matrix, and x is the vector of the data sent by the base station. Figure 3.7a shows an example of a typical 2×2 MU-MIMO. In these systems, the channel matrix H is measured in the channel estimation stage, and then the precoding matrix W is set to the inverse of the channel matrix. Hence,

by transmitting Wx instead of x, the base station can simultaneously transmit multiple data streams while each user receives only its own data stream.

When we use our repeater in a typical MU-MIMO system as shown in Figure 3.7b, the only difference would be the channel matrix. The signals transmitted by the base station antennas will be first received by the backhaul antennas, and then they will be forwarded to users through separate beams created by the passive structure. Hence, the channel matrix will be $H = GK$, where K is the matrix of channels between the base station and the repeater's backhaul antennas, and G is the matrix of channels between the repeater and the user devices. Note, G is a diagonal matrix since the signal received at each backhaul antenna of the repeater creates a separate beam towards each user as shown in Figure 3.7b.

To enable MU-MIMO, the base station needs to set the precoding matrix W to the inverse of GK. Note that as our repeater is transparent to the base station and performs no processing on the signals, during the MU-MIMO channel estimation stage, the base station and users will measure GK as the channel matrix between the base station and users, and use it to compute the precoding matrix. The signals received by the backhaul antennas of the repeater can be presented as $z = KWx$, where $W = (GK)^{-1}$. Therefore, we can show that $z = G^{-1}x$. Note since G is a diagonal matrix, its inverse is also diagonal. This enables MU-MIMO from the base station to the repeater's backhaul antennas. Recall that the signal received at each repeater's backhaul antenna is directed toward a user via a beam using our repeater. Hence, the base station has supported MU-MIMO to the users without any additional complexity on the repeater. Finally it is worth mentioning that here we focused on the downlink, however, the uplink works in a similar way.

3.6 Network Details

In the previous sections we presented the key components of mmXtend and explained how they are put together to enable a low-cost, low-power, on-demand repeater for mmWave

networks. In this section we explain the networking details in using mmXtend in practice.

3.6.1 End-to-end Link Establishment

First, we explain how mmXtend establishes an end-to-end communication link between the base station (BS) and the user. In a typical mmWave network, the BS and the user need to perform beam searching to find the best direction for their beams to enable a communication path between the BS and the user [3GP17a, Sha22]. This path is typically the direct line-of-sight (LOS) path between them. Below we first explain how this process is done in today's 5G networks as an example, and then describe how mmXtend's repeater can seamlessly be integrated without interfering with the standard process. Although we use 5G network as an example, but this can be extended to any mmWave network such as 6G and beyond..

In the standard 5G mmWave beam alignment process, the BS sends groups of synchronization signals [3GP17b, 3GP21b] periodically in multiple spatial directions and different frequency channels, to detect users in different areas. On the user side, the user initiates a beam sweeping process using a wide beam and scans for available frequencies. It then reports to the BS which one of the BS's beams (i.e. frequency and direction) resulted in the highest received power [5GW20, Twe22]. Based on the feedback from the user, the BS then aligns its beam direction to the user. Then the user begins beam sweeping using a narrow beam and aligns its beam toward the BS using received signal power measurements.

When a mmXtend's repeater is installed and the LOS path is blocked, the BS and the user still tries to find the best communication path using the same standard process. Figure 3.8 shows the steps in end-to-end beam alignment when a repeater is deployed. In the first step, the repeater needs to have its backhaul beam aligned toward the BS. As mentioned before, the repeater is using fixed beam antennas (e.g. horn antenna) for its backhaul beams. Hence, during installation, the beams of the antennas can be manually adjusted toward the BS. Note, this is a one time process since the BS and repeater location is fixed in most scenarios. In the second step, the BS sweeps its beams and sends synchronization signals

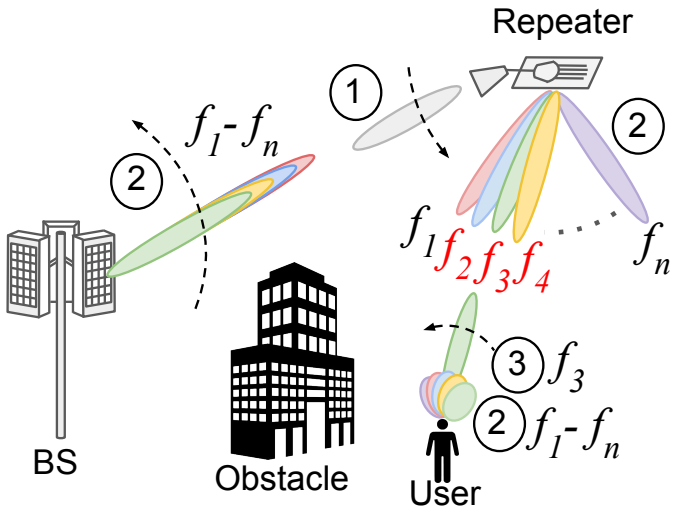

Figure 3.8: mmXtend Beam Alignment

in multiple directions and frequency channels [4] $(f_1 - f_n)$. This process is the same as the standard beam alignment process. However, when the beam of a particular frequency channel is steered in the direction of the repeater, its signal will be forwarded by the repeater to a specific direction based on its frequency. On the other side, the user also performs standard beam sweeping to find the direction and operating frequencies of the nearby base stations. The user provides feedback to the BS in the frequencies with the highest signal strength. This feedback will be transmitted back to the BS which allows it to determine which beam direction and which frequency provides the best performance for that user. This will be the direction which aligns the beam of the BS to the repeater, and the frequency which aligns the FSA beam to the user. This process will be repeated for each user. Note that in 5G mmWave bands, the same frequency channel is utilized for both uplink and downlink communication between a user and the BS through Time Division Duplexing (TDD) [3GP23], so a user does not need to switch beams (frequencies) when transitioning between uplink and downlink communication. Finally, in the third step, the user performs the standard beam alignment

[4]Cellular base stations and user devices typically support multiple frequency bands and channels [Nok23, App23]. In the commercial mmWave bands, the available bandwidth is between 1 to 4 GHz [3GP23], which is a large enough bandwidth for the FSA to operate. For example, the n257 band consists of 3 GHz bandwidth, which can be split into thirty 100MHz channels.

process to find the best direction for its beam. This results in the alignment of the user's beam toward the repeater. After the beams are aligned, the user and the BS exchanges additional information to initiate downlink and uplink communication.

It worth mentioning that this entire process and all steps is done without the BS or user knowing there is a repeater. The repeater relays the signal between the BS and the user while the BS and user perform their standard beam search process. Hence, mmXtend repeater can be seamlessly deployed wherever and whenever needed without requiring any cooperation or feedback from the BS or user.

3.6.2 Channel Resource Allocation

Next, we explain how mmXtend can provide opportunities for more flexible channel resource allocations to the users. In today's mmWave network, when we have a dense number of users in the same area, their network performance drops due to the sharing of the same frequency channel resource. In the design of mmXtend, we address this problem by providing partially overlapping channels of different frequencies to cover each area. As we mentioned earlier, our FSA shifts its beam continuously with respect to frequency. The scan ratio of our FSA design is 0.0167 degrees/MHz, meaning that for a channel bandwidth of 100 MHz and 400 MHz, the angle of the beam will shift by 1.67 degrees and 6.67 degrees, respectively. On top of this, we designed our FSA to achieve a 3 dB beamwidth of around 10 degrees for a single frequency. This means that the beamwidth of a single frequency is much larger than the amount of angle shift caused by the bandwidth of a frequency channel. Therefore, our design guarantees not only good coverage for each FSA beam, but also that each user will be covered by the FSA beams from a few different frequency channels.

This overlapping FSA beams provides an opportunity to enable more flexible channel resource allocation schemes for the users. In particular, the BS can allocate resource blocks based on the quality of each channel relative to the user location, as well as the occupancy of each channel. This enables more efficient bandwidth utilization of each channel when

there are many users located in the same area, and ensures higher data rate for each user. When there are less number of users in each area, the overlapping channels also provides the opportunity to improve performance through carrier aggregation which is an existing feature in cellular networks [3GP21a].

Finally, in the case of user mobility, a user may move from one FSA beam to another beam. As the direction of the FSA beam is determined by the channel frequency, the operating channel of the user needs to be updated. Note that the BS is able to determine the best frequency channel to allocate to the user based on the continuous exchange of reference signals between the BS and the user, which are transmitted within the frequency of each channel on a periodic basis. Channel overlap in mmXtend, also enables a smoother hand-off process when the user moves between different channels, as the user can remain connected to a channel while initiate the hand-off procedure with adjacent channels at the same time. In particular, the BS dynamically adjusts the channel resources allocated to a user when it moves across different FSA beams. With the graceful hand-off process, the BS could schedule resources in advance in adjacent channels.

3.7 Link Budget Analysis

In this section, we provide a link budget analysis for mmXtend. We only consider the downlink, where the base station is the transmitter and the user device is receiver. However, similar link budget calculation can be done for uplink too.

We calculate the received signal power P_{rx} of the user device based on the following equation:

$$P_{\text{rx}} = P_{\text{tx}} + A_{\text{rx}} + A_{\text{repeater}} - L_{\text{path1}} - L_{\text{path2}} \tag{3.3}$$

where P_{tx} is the transmitter's Effective Isotropic Radiated Power (EIRP), A_{rx} is the receiver antenna gain, A_{repeater} is the total gain of the repeater, L_{path1} is the free-space path loss from the base station to the repeater, and L_{path2} is the free-space path loss from the repeater to

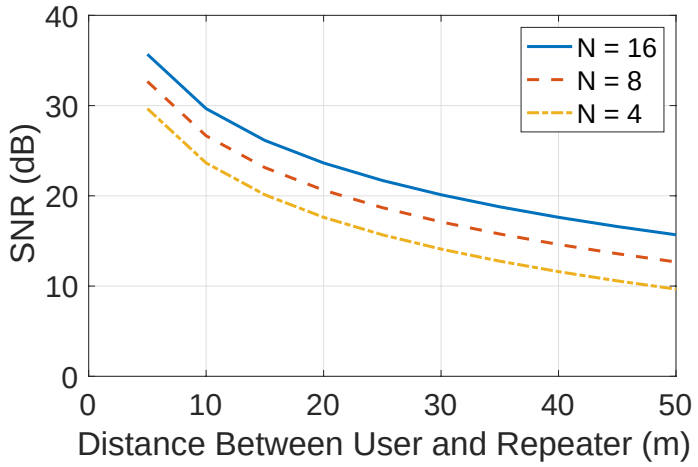

(a)

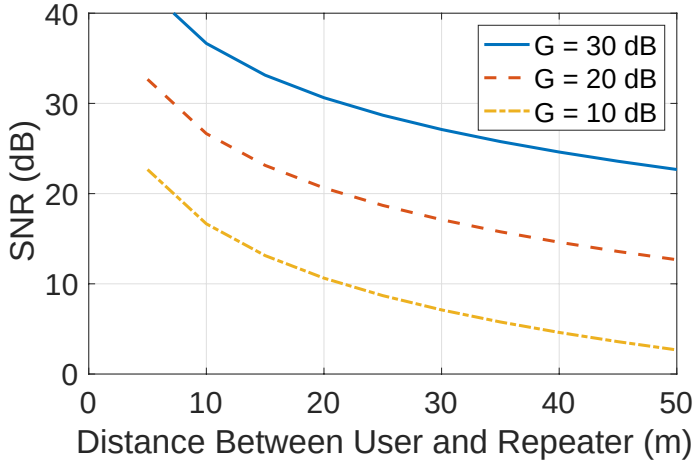

(b)

Figure 3.9: Link Budget Analysis. SNR versus user to repeater distance when the repeater is 200 m away from the base station for (a) different number of FSA elements N, while the gain of the LNA is 20 dB, and (b) different LNA gains G, while the number of FSA elements is eight.

the user device.

For our analysis, we calculate the SNR of the signal at the user device based on the following setup. We consider a typical celluar base station with an Effective Isotropic Radiated Power (EIRP) of 55 dBm [Qua19], and a typical mmWave receiver with 20 dB antenna gain and noise floor of -88 dBm. We calculate the receiver SNR value based on the following

equation:

$$SNR = P_{\text{rx}} - P_{\text{nf}} \tag{3.4}$$

where P_{rx} is the received signal power and P_{nf} is the noise floor value. We assume the repeater's backhaul antenna and each FSA has 20 dB and 10 dB gain, respectively, based on our measurement and simulation results presented in § 3.9.1. We consider the repeater's LNA gain and the number of FSAs as variables in our analysis. Finally, we assume that the distance of the mmXtend repeater is 200 meters from the base station, which is a reasonable distance to reach an outdoor base station to overcome signal blockage.

Figure 3.9a shows the SNR of the user versus distance of the user from the repeater. We plot the SNR for different number of FSA elements on the repeater where LNA gain is set to 20 dB. As the number of FSA elements increases, mmXtend enables higher SNR and/or longer communication range. However, as the number of FSA elements grows, the design becomes more complex. Hence, we fabricate a mmXtend repeater with eight FSA elements which is still easy to fabricate in a compact size while it provides SNR of 14 dB even when the user is 42 meters away from the repeater. Note, this SNR is sufficient to enable more than 240 Mbps data rate for a 100 MHz channel at 28 GHz.

Figure 3.9b shows the SNR of the user versus distance of the user from the repeater. We plot the SNR for different LNA gain where we use eight FSA elements on the repeater. As the gain of the LNA increases, the communication range of mmXtend increases too. However, using higher LNA gains increases the power consumption of the repeater. Moreover, we cannot use very high-gain since at some point the gain becomes larger than the leakage between the repeater's backhaul and fronthaul beams, causing the self-interference problem. Hence, we fabricate a mmXtend's repeater using 20 dB LNAs. This enables mmXtend to achieve good communication range (i.e. SNR of 14 dB even at 42 meters) without having self-interference problem or consuming significant amount of power.

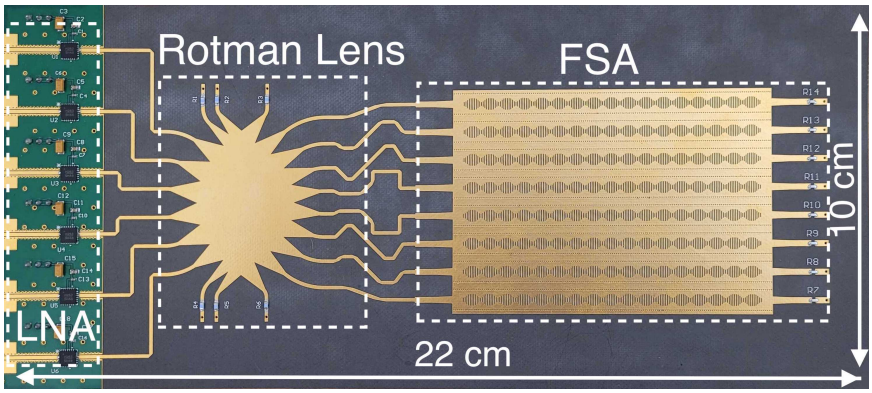

Figure 3.10: mmXtend Implementation Our fabricated prototype on a thin and compact PCB substrate.

3.8 Implementation

To evaluate the performance of the mmXtend system, we have built a prototype of mmXtend. We have designed and implemented our prototype using high-frequency structure simulator (HFSS) software. Based on our link budget calculation in § 3.7, we have designed a Rotman lens with eight outputs that connects to eight FSA elements. We integrated Rotman lens and FSAs on the same board andfabricated it in Rogers Duroid 5880 PCB substrate, as shown in Figure 3.10. Our prototype is only 22 cm by 10 cm and has a thickness of 0.5 mm. Our complete design operates in the 28 GHz mmWave band, and supports more than 3 GHz of bandwidth.

For backhaul antennas, we used Mi-Wave horn antennas (261-34-20-595), and connected them to the input port of our fabricated design. The combination of the horn antennas and FSA beams provides significant gain for our repeater. However, to provide further gain, we also placed a Low Noise Amplifier (LNA) between each horn antenna and our passive structure input ports. For LNAs, we have used HMC263LP4E from Analog Devices where each provides 20 dB LNA gain and consumes 174 mW of power. The LNAs are integrated on the same PCB board, as shown in Figure 3.10. Note, these six LNAs are the only components in our design which consumes power and the rest are passive.

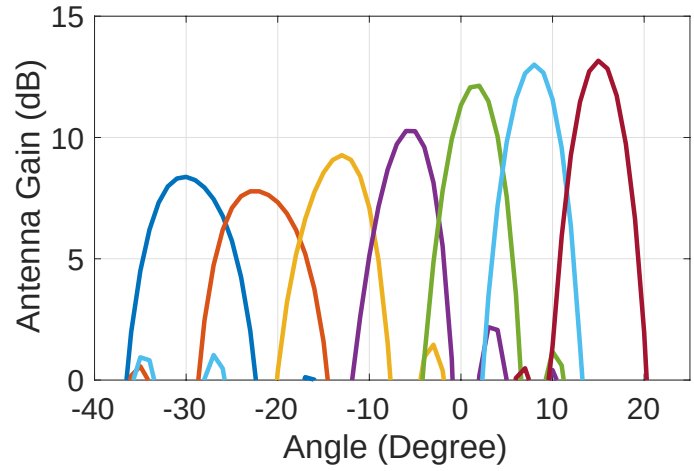

(a)

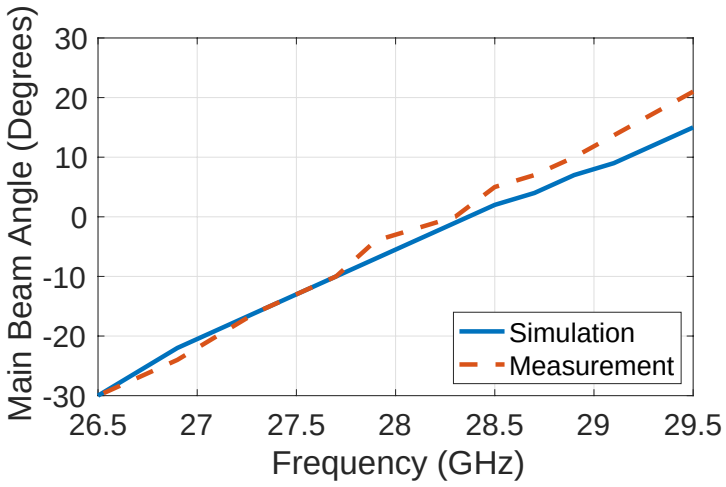

(b)

Figure 3.11: FSA Beam Steering Performance. (a) Radiation pattern of the FSA for different signal frequencies. (b) The direction of FSA beam and its corresponding frequency.

3.9 Evaluation

In this section, we present the performance of mmXtend under various conditions and scenarios. First, we investigate the radiation properties and scanning capability of mmXtend under microbenchmark testbeds. Then we explore the performance of mmXtend in extending mmWave coverage when the LOS between the base station and the user is blocked. We define different test scenarios and study the performance of the system (such as achievable

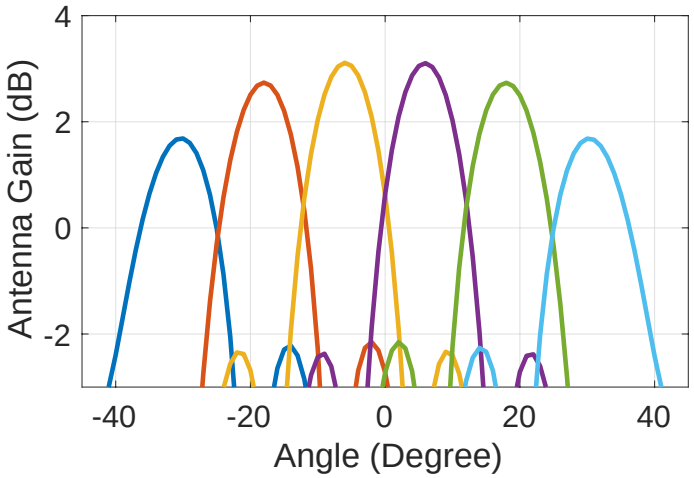

Figure 3.12: Rotman Lens Beam Steering Performance. Radiation pattern of our Rotman lens for different input ports.

SNR and data rate) in each case. We perform our experiments in both indoor and outdoor scenarios. We have used Keysight 5G R&D test bed [Key23] as our base station (BS) and user device to evaluate the performance of mmXtend. Our base station is equipped with a 20 dB gain antenna and uses transmission power of 35 dBm for both indoor and outdoor scenarios, which complies with FCC 28 GHz band regulation [FCC23c]. Our user device is equipped with a 20 dB gain antenna.

3.9.1 Micro Benchmark

As discussed in §3.4, mmXtend forms and steers beams in 2D. In particular, mmXtend can steer its beam in one dimension by changing the signal frequency and in another dimension by using Rotman lens. Here, we evaluate mmXtend's capability to do so.

(a) FSA Beam Steering: mmXtend designs FSAs to create and steer beams in the elevation plane. In particular, FSA steers its beam when the frequency of the signal changes. Here, we evaluate the performance our designed FSA to do this. Figure 3.11a shows the radiation pattern of our FSA as the signal frequency changes. For simplicity, the figure shows the radiation pattern for seven different frequencies. However, it is worth mentioning

that the FSA beam steering is continuous. The figure shows that our FSA design generates narrow beams with more than 8 dB gain. Moreover, the beam is steered as the frequency of the signal is changing. These results show that mmXtend can successfully form and steer multiple beams to multiple users by just using different signal frequencies. Figure 3.11b shows the relation between the direction of the beam and the frequency of the signal. This result implies that our design can steer its beams by more than 50 degrees by changing the frequency of the signal over the commercial mmWave band. Note repeaters are typically installed on a wall or ceiling and hence 50 degrees is enough to cover a large area. The figure also compares these results with the HFSS simulation results, implying that our fabricated prototype performance closely follows the expected results.

(b) Rotman Lens Beam Steering: mmXtend designs a Rotman lens to steer its beam in the Aimuth plane. Here we evaluate the performance of our designed Rotman lens in creating and steering the beams. In particular, the Rotman lens steers its beam when different input ports are used for transmitting or receiving a signal. The radiation pattern of our designed Rotman lens is shown in Figure 3.12, where the vertical axis is the antenna gain in dB and the horizontal axis is the angle. The figure shows the radiation pattern for the six input ports of the Rotman lens. This result shows that our Rotman lens design is able to form narrow beams (with 1.5 to 2 dB gain) in different directions while a different port is used. This rotman lens can also create these beams simultaneously, spanning more than 65 degrees which in enough to cover a large area.

3.9.2 Angle Performance

So far we have evaluated the performance of individual components of mmXtend (i.e. our FSA and Rotman lens). Here, we evaluate the performance of the complete mmXtend in beamforming and repeating the signal toward a user, placed in different angles with respect to the repeater. We conducted this experiment in an indoor environment. We place the base station and repeater at fixed locations. We then place the user 3.5 meters away from the

repeater and change its angle with respect to the user while measuring the SNR at the user. In particular, we are interested to see whether the repeater can steer its beam successfully toward the user (i.e. enabling reliable link without experiencing significant SNR drop) when the user is located at different azimuth and elevation angles. To examine only the effect of angle changes, we make sure that the distance of the user to the repeater is kept constant, and monitor the change in the SNR as we change azimuth and elevation angles of the user respect to the repeater.

Figure 3.13a and 3.13b show the change in the SNR (with respect to the SNR at zero degree) for different azimuth and elevation angles of the user, respectively. The figures show that the repeater can steer its beam toward the user without significant SNR loss within the azimuth angle of -30 to 30 degrees and elevation angle of -40 to 40 degrees. Specifically, the worst SNR drop is 2 dB in elevation and 1 dB in azimuth plane. As we will show in the next evaluation, in most scenarios, mmXtend enables SNR of more than 20 dB, and hence a few dB drop in SNR will not have an impact on the achievable maximum data rate. Finally, considering that the repeaters are typically installed at a height (such as a pole, top of a building, or on a wall), the achieved angular range will be sufficient to cover a large area.

3.9.3 Range Performance

We evaluate the performance of mmXtend in solving the blockage problem and supporting reliable high SNR links in both indoor and outdoor scenario. We install our repeater at a fixed distance with respect to our base station, and measure the SNR of the signal received at the user placed at different distances with respect to the repeater. We make sure that the line-of-sight (LOS) path is always blocked, and the base station and the user communicate through our repeater.

a) Indoor Scenario mmXtend promises to enable reliable mmWave connectivity in indoor environments with blockages. Here, we verify if it delivers on this promise. We place a base station and a user device in our building where their LOS path is blocked by a concrete wall.

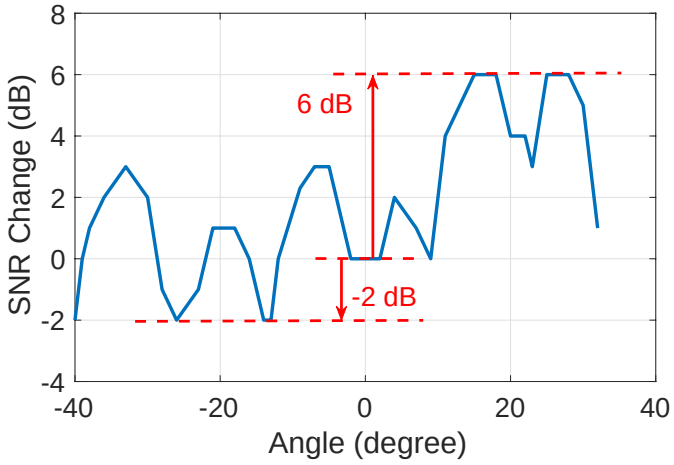

(a) Elevation Angle

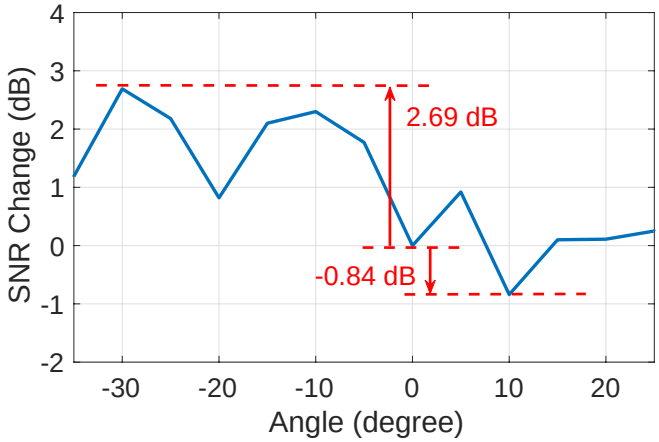

(b) Azimuth Angle

Figure 3.13: mmXtend Angle Performance. SNR change with respect to the SNR at zero degree.

We then place mmXtend in a position which has LOS to both the base station and user. The distance between the base station and repeater is eight meters while we change the distance between the user and repeater from 2 to 45 meters. For each distance, the base station is transmitting, and we measure the SNR at the user side. Note, since the LOS is blocked, the communication link is established through our repeater. Figure 3.14a shows the result of this experiment. The repeater has successfully enabled high SNR at the user. In particular, even when the user is 45 meters away from the repeater, the user still achieves more than 40 dB SNR. Note, SNR of more than 20 dB is sufficient to enable the maximum data rate

in mmWave networks. These results imply that mmXtend enables reliable high-data-rate wireless connectivity in indoor environment despite having blockage.

b) Outdoor Scenario. Next, we perform the same experiment as the previous one except in outdoor scenario. In this experiment, the base station and repeater are 170 meters apart [5]. We then place the user at different distances with respect to the repeater while its LOS path to the base station is always blocked. Figure 3.14b shows the achievable SNR of the user when we change the distance between the user and the repeater from 3 to 30 meters. The user has achieved the SNR of more than 20 dB in all locations. Such SNR is sufficient to enable the maximum data rate in this frequency band. These results imply that mmXtend provides reliable high-data-rate wireless connectivity in outdoor environment, enabling emerging applications such as augmented sport and concert events, and autonomous robots to improve disaster recovery.

3.9.4 Data Rate Performance

So far we have evaluated the SNR performance of mmXtend at different angles and distances. Here, we evaluate its performance in terms of user's data rate where multiple users seek communication with the base station via the repeater.

For this purpose, we use the following setup to conduct our evaluation. As shown in Figure 3.15, the repeater is placed on a pole at 14 meters above ground. The repeater establishes a backhaul link with a BS at 170 meters away while it relays the signal to cover a 2D plane on the ground noted by the x and y axis. Along the x axis, the plane is divided into 30 frequency channels, where each channel is covered by a single FSA beam (f_i). The bandwidth of each channel is 100 MHz. Along the y axis, the plane is divided into 6 sections, where each section is covered by a single Rotman lens beam (l_j). In total, it creates $30 \times 6 = 180$ cells. Users in different frequency cells (e.g. f_1 and f_2), communicate with

[5]The distance is limited by the space we had available for our tests.

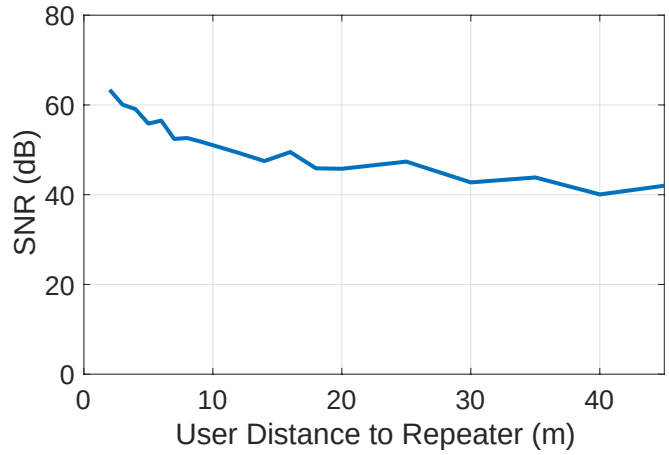

(a) Indoor

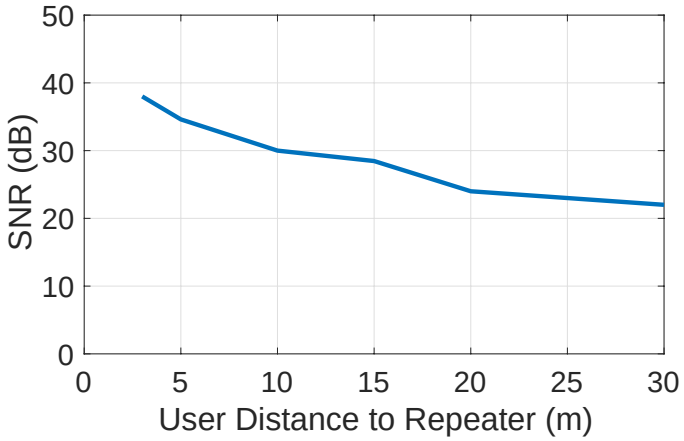

(b) Outdoor

Figure 3.14: mmXtend Range Performance. (a) is an indoor scenario where the base station and the repeater are eight meters apart. (b) is an outdoor scenario where the base station and the repeater are 170 meters apart.

the BS using different channels. For users located in the same frequency cell but different Rotman lens cells (e.g. (f_1, l_1) and (f_1, l_2)), they communicate with the BS through MU-MIMO in the same channel. If the users are in the same frequency cell and Rotman lens cell, the channel resource is shared through time-division multiple access. Finally, the coverage of mmXtend repeater along the x axis is 60 degrees and along the y axis is 72 degrees using FSA and Rotman lens, respectively.

To evaluate the performance of mmXtend in a network of users, we randomly distribute

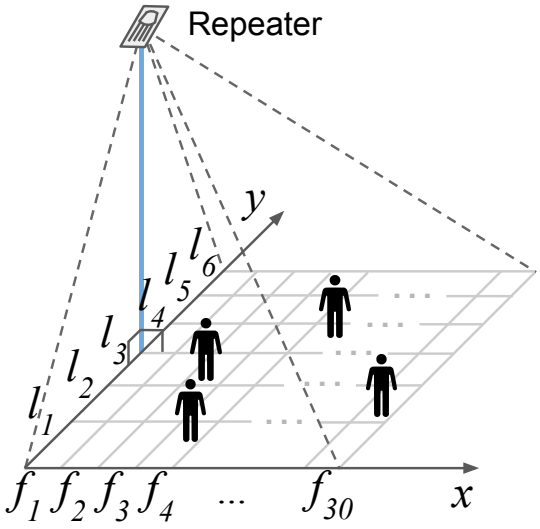

Figure 3.15: mmXtend Evaluation Setup. In the x axis, the area is divided into 30 channels covered by FSA beams, noted by f_1 to f_{30}. In the y axis, the area is divided into 6 sections covered by Rotman lens beams, noted by l_1 to l_6.

different number of users in the 2D plane covered by mmXtend and evaluate the average data rate of each user. To do so, since we do not have hundreds of user devices, we empirically measure the SNRs at different angles and distances (i.e. different cells) and use it to compute the data rate of each user in post-processing using the mmWave NS3 simulator [6] [Mez18]. Figure 3.16a shows the average user data rate with respect to the different number of users covered by the repeater. For each number of users, we ran our experiment 50 times with random distributions of users to calculate the average user data rate. The figure shows that when we have less than 100 users, the average data rate per user is as high as 300 to 400 Mbps. When the user number increases to 1000, we can still achieve an average user data rate of more than 70 Mbps. which is more than enough for streaming Ultra High Quality 4K videos. Figure 3.16b shows the aggregated data rate of all the users with respect to the different number of users. This figure shows that as the number of users increases, the aggregate data rate can reach more than 73 Gbps. These results shows mmXtend's capability

[6]The BS communicates in the mmWave commercial frequency band of 26.5 to 29.5 GHz, the max downlink data rate per layer in a 100 MHz channel is 408 Mbps based on 3GPP standard [3GP22]. For our evaluation, we assume the BS can provide the max data rate for all 30 channels in this spectrum at the same time.

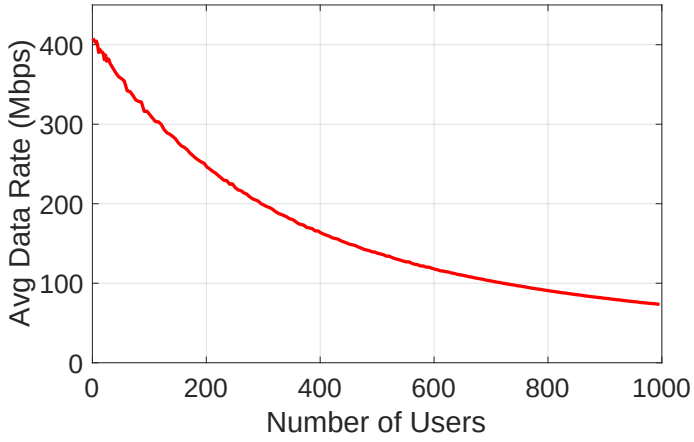

(a)

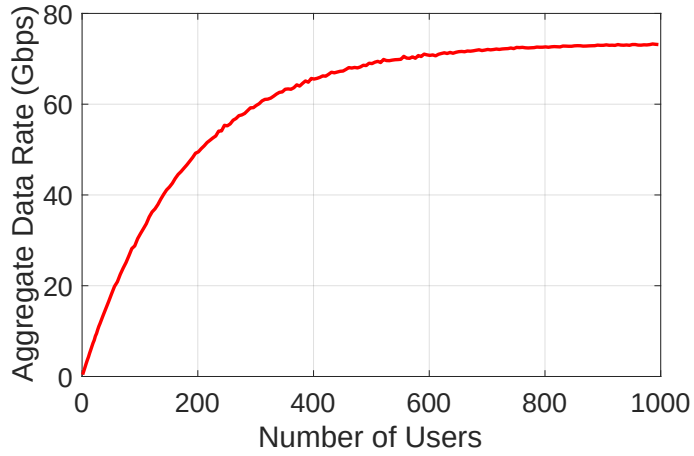

(b)

Figure 3.16

to provide high data rate links to a large number of users in a wide area when the LOS path between the user and the BS is blocked.

3.9.5 Power, Weight and Cost Analysis

The total power consumption of mmXtend is only 1.05 W which can be power up by a small solar panel (9 × 11 cm) [Sys23] or a drone's battery without impacting on its flying time. Even small drones typically have batteries with 20-100 Wh capacity [DJI23] which are not impacted by the low power consumption of mmXtend. Note, the total power consumption of

mmXtend can be even further reduced to 300 mW by using recent released LNAs instead of the ones used in our prototype [Dev22]. mmXtend design includes a custom designed PCB, LNAs and horn antennas. Our mmXtend implementation (including 6 LNAs) as shown in figure 3.10, costs only $980 [7]. Note, this is the cost to fabricate one prototype device and hence it will be much lower in mass production. Finally, it is worth mentioning that horn antenna and our 2D passive repeater structure (including 6 LNAs) weigh only 48.19 g and 70.02 g, respectively. Hence, our design is very light and can seamlessly be deployed on a pole or drone [li2].

3.10 Conclusion and Discussion

In this chapter we presented mmXtend, an on-demand repeater which solves the blockage problem of mmWave networks in outdoor and indoor scenarios. mmXtend is low cost, low power, and can be seamlessly deployed whenever and wherever is needed. We achieved this by introducing a novel design which enables the repeater to passively create and steer beams to multiple users simultaneously. Finally, we implemented mmXtend and empirically evaluated its performance. Our results show that mmXtend enables reliable high-data-rate connectivity to hundreds of users even when they are hundreds of meters away from the base station and their line-of-sight path to it is blocked. There are also some parts of this work which could be further extended. The current implementation of mmXtend focuses on the downlink communication from the base station to the user. This limitation stems from the uni-directional LNAs used in our design. To extend mmXtend for bi-directional communication, one could explore different alternatives such as using bi-directional LNAs or deploy two separate uni-directional repeaters dedicated to downlink and uplink communications respectively.

[7] For comparison, the cost of the radio equipment for a commercial mmWave 5G base station typically exceeds $35,000. [Exp21]

CHAPTER 4

Wi-Pro: Enhancing WiFi Performance via Passive Beamforming

This chapter introduces Wi-Pro, a plug-and-play module, which uses passive beamforming technology to enhance the performance of future WiFi networks.

4.1 Problem Statement and Challenges

In this section, we first provide an overview of the challenges of modern WiFi networks. Next, we present the key design goals and contributions of our solution: Wi-Pro. We then illustrate the limitations of existing work and emphasize the distinct features of Wi-Pro that distinguish it from others.

As new applications emerge and user demands evolve, WiFi network is facing a series of new challenges. On one hand, Internet of Things (IoT) will connect more and more devices through WiFi, which leads to a busier wireless spectrum and higher latency. On the other hand, emerging real-time applications, such as video conferencing, multiplayer gaming and augment/virtual reality (AR/VR) require higher-datarate, lower-latency wireless links. Given the limited bandwidth of WiFi and the constraint on transmission power, there need to be new solutions to increase the performance of WiFi networks. Furthermore, in many scenarios such as smart factory and smart home, it is important to measure the Angle-of-Arrival (AoA) of WiFi signals to enable applications such as device localization. However, today's AoA measurement requires the use of multiple antennas and transceiver chains which

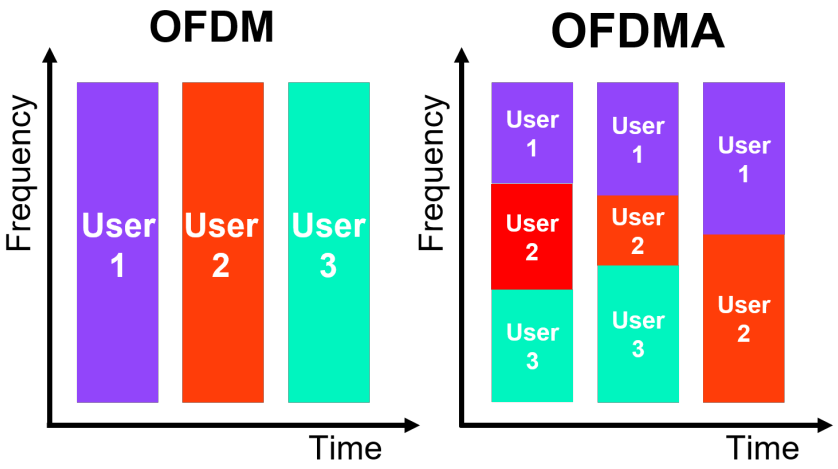

Figure 4.1: OFDM vs OFDMA Technology

is not available for the majority of WiFi devices.

To deal with these challenges, WiFi manufacturers have adopted numerous techniques and advancements along with the evolution of WiFi standards over the past two decades. These advancements include but not limited to: expanding the channel bandwidth, adding more antennas, and implementing advanced multiplexing and multiple-access techniques. While most of these advancements are around WiFi algorithms, protocols and circuit, the design of WiFi antenna itself has remained relatively static over the years. In particular, most WiFi devices have been using typical omni-directional antennas (such as monopole or diplole antennas). Unfortunately, these antennas do not benefit from the advancement of WiFi protocols or vice versa. In the following part of this section, we will explain how the antenna design hinders the performance and capabilities of modern WiFi devices.

4.1.1 Limitations of OFDMA in WiFi6

To meet the demand of high-throughput, low-latency communication, WiFi6 (802.11ax) introduced Orthogonal Frequency-Division Multiple Access (OFDMA). OFDMA enables a WiFi AP to simultaneously communicate with multiple user devices by partitioning the WiFi

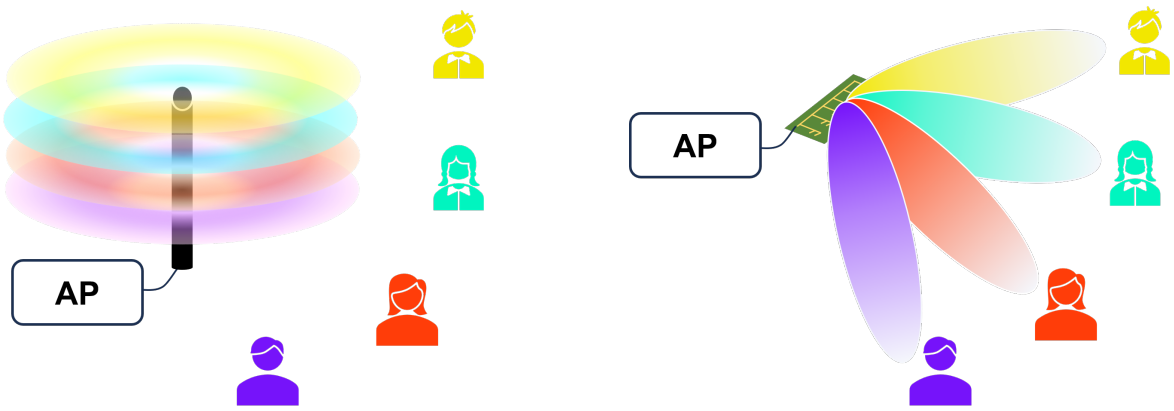

(a) Traditional WiFi Antenna (b) Wi-Pro's Antenna

Figure 4.2: Wi-Pro Overview. (a) Today's WiFi devices uses omni-directional antennas and hence the power allocated to each frequency (such as an RU in OFDMA) goes to all directions, wasting most power. (b) By replacing the traditional WiFi antenna with Wi-Pro's antenna, the power allocated to each frequency only goes to the targeted direction and user. This enhanced datarate and communication range of WiFi Networks and enable seamless Angle-of-Arrival estimation.

channel into multiple small trunks known as Resource Units (RUs), and allocating different RUs to different users. Figure 4.1 illustrates the concept of OFDMA in comparison with Orthogonal Frequency Division Multiplexing (OFDM), which is the key modulation technology in the past few generations of WiFi. OFDM divides the WiFi channel bandwidth into multiple subcarriers and modulates data symbols on the subcarriers. It has the advantages of high spectral efficiency and robustness to channel impairments. However, OFDM is not designed for optimal resource allocation for multiple users. As illustrated in figure 4.1, each OFDM packet only carries data for a single user, which causes insufficient spectrum usage and extra packet overhead. OFDMA solves this problem by allowing multiple users' data to be encapsulated in a single packet occupying different subsets of subcarriers. In this way, the spectral resources can be allocated dynamically according to the specific needs of user devices. OFDMA significantly reduces the latency in a dense deployment environment [qua] such as IoT networks where a large number of devices are distributed in different areas.

Despite the aforementioned benefits, the efficiency of OFDMA is notably constrained by

the design of modern-day WiFi antennas. As shown in Figure 4.2a, today's WiFi routers use omni-directional antennas, which means the power is uniformly distributed in all directions and across all frequencies. As a result, signals are transmitted to areas without users, and each user receives the same power level across all RUs, despite their data being modulated only in their assigned RU, which covers just a portion of the channel bandwidth. This leads to inefficient power distribution both in the spatial and spectrum domain, consequently diminishing the achievable communication range and data rates for individual users in an OFDMA network. These limitations highlight the need for innovative WiFi antenna designs that can enhance upper-layer protocols and vice versa.

4.1.2 Limitations of WiFi AoA Measurement

Beyond high-data-rate, low-latency communication, future WiFi networks are expected to support sensing services as well. In particular, device localization is one of the long-awaited services that has gained escalating attention in the past few years. The key challenge of device localization is AoA measurement. Over the past decade, there has been a significant amount of work on WiFi AoA measurement. Despite impressive improvements in accuracy and robustness of AoA measurement systems, unfortunately, all existing approaches have a major limitation: they cannot be integrated into low-cost low-power WiFi devices which only have a single transceiver chain. In particular, to perform AoA measurement, existing systems use multiple antennas and measure the phase differences of the received signal at the antennas to compute the AoA. In fact, this is exactly why today's single-device localization systems require multiple transceiver chains. Unfortunately, most low-cost WiFi chipsets (in particular the ones used in IoT devices) have only a single transceiver chain due to cost and power consumption constraints.

4.1.3 Design Goals of Wi-Pro

The design goal of Wi-Pro is to solve these challenges of modern WiFi networks by renovating the WiFi antenna design to benefit the upper-layer protocols and functionalities. Wi-Pro is a new system which enhances the communication and sensing capabilities of WiFi. The core of Wi-Pro is our new type of WiFi antenna which integrates seamlessly with WiFi protocols and make them much more efficient. Our design is a plug-and-play design, meaning that it can be easily connected to WiFi devices instead of their current antenna without requiring any changes to the WiFi hardware or firmware. Wi-Pro leverages Frequency Scanning Antenna (FSA) technology, a passive system that emits or receives signals in directional beams, with the beam direction varying according to the signal frequency. We have developed an FSA structure specifically for WiFi devices, demonstrating that its integration with advanced WiFi protocols make them much more efficient and capable. To demonstrate these benefits, we first show how the integration of Wi-Pro to WiFi devices makes a much more efficient Orthogonal Frequency-Division Multiple Access (OFDMA) in the MAC layer protocol of WiFi6. As another example, we also show how our design can enable AoA measurement to any WiFi devices, even those with a single transceiver chain.

Wi-Pro make the following contributions:

- Wi-Pro is a new plug-and-play antenna for WiFi devices based on FSA technology and it can be seamlessly integrated with the existing WiFi protocols.
- Wi-Pro offers dual advantages in enhancing the performance of modern WiFi protocols. First, it refines power allocation based on the spectral usage of users in each direction, which increases the data rate and communication distance of individual users. Second, it enables the the AoA measurement on any WiFi device, including low-cost, low-power units with a single transceiver chain, all without requiring firmware or chipset modifications.
- The prototype implementation of Wi-Pro demonstrates 10 to 120% data rate improve-

ment and more than three times range improvement for WiFi communication. Our prototype can also achieve AoA measurement with an average precision of 1.37 degrees.

4.1.4 Limitations of Current Solutions

Frequency Scanning Antenna (FSA) Wi-Pro's antenna design build on past work of Frequency Scanning Antenna (FSA). These antennas provide a directional radiation pattern that can be controlled by altering the frequency of the signal [JCI12]. Unlike past work which uses them for AoA measurement at Terahertz (THz) and mmWave bands [SVL21, GYS20, li2], our design is uniquely tailored for the WiFi band, which operates within a limited bandwidth and presents its own unique set of challenges. There are some past work on FSA operating at sub-6GHz bands [GPL21, PGP17, PGC20, GLP23]. However, none of them explored the integration of FSA with WiFi protocol to enhance communication efficiency and AoA measurement capabilities. In summary, Wi-Pro introduces an innovative WiFi antenna based on FSA technology, and combines it with the latest WiFi medium access protocol to provide improvement in both communication and AoA measurement, which has not been demonstrated in past work.

WiFi AoA Measurement Most work in AoA measurement utilizes the phase shift of the signal received across an antenna array to calculate the Angle-of-Arrival (AoA)[XJ13, KJB15, GHY21]. These work requires multiple antennas and multiple transceiver chains, which is not available for the majority of WiFi devices today, especially low-power IoT devices. In contrast, Wi-Pro uses FSA for AoA measurement which only requires analyzing the signal from a single antenna port, using a single transceiver chain. Some previous work have used a single-antenna wireless receiver to calculate the AoA based on the concept of Synthetic Aperture Radar (SAR) [KGK14, RKK12]. These works move the receiver antenna to different spatial locations to mimic a multi-antenna array. However, such methods not only necessitate relocating the measuring device but also depend on accurate information about the device's relative position to a fixed point. In contrast, Wi-Pro can perform AoA measure-

ment with a single FSA, without having to move the measurement device. Furthermore, the prior methods of AoA measurement require sophisticated algorithms, firmware or hardware modification and introduces extra traffic overhead. In contrast, Wi-Pro's AoA measurement is a simple plug-and-play solution that can be integrated with the communication system seamlessly.

4.2 Wi-Pro Overview

In this section we provide an overview of Wi-Pro, summarizing its key design ideas.

Wi-Pro is a new system that improves the communication performance and AoA measurement capabilities of WiFi. The core of Wi-Pro is our newly designed plug-and-play WiFi antenna module based on FSA. Unlike traditional WiFi antennas, which distribute power uniformly in all directions and across all frequencies, Wi-Pro's antenna passively focuses power in a particular frequency spectrum at a specific direction. This unique trait combined with the inherent features of WiFi protocol enables new capabilities for WiFi communication and sensing.

The first benefit of integrating Wi-Pro's antenna in a WiFi access point is improving the performance of OFDMA. As illustrated in figure 4.2b, in a dense WiFi network user devices are spread throughout an area, OFDMA allows multiple-user access by dividing the WiFi channel spectrum into small trunks of Resource Units (RUs) and allocating different RUs to different users. Unlike omni-directional antennas that transmits all RUs in every direction, Wi-Pro generates directional beams aimed at each user. Within each beam, the signal power is focused exclusively on the RU designated for that specific user. In this way, Wi-Pro can greatly increase the Signal-to-Noise Ratio (SNR) of the data transmitted to and from each user, thereby enhancing the network's communication range and throughput.

The second benefit of using Wi-Pro's antenna in a WiFi access point is enabling seamless AoA measurement which is crucial for device localization. Specifically, Wi-Pro effortlessly

enables an access point to determine the AoA of packets received from any WiFi device. This capability stems from the beamforming characteristic of FSA, which establishes a direct correlation between the beam direction and the signal frequency. By analyzing the signal pattern in the frequency domain, the AoA of incoming signals can be inferred using a single device with a single transceiver chain. This means that Wi-Pro can be integrated into any WiFi device without requiring firmware modifications.

4.3 Wi-Pro's Antenna Design

Wi-Pro's antenna need to create directional beams towards each user, where within each beam the signal power is only concentrated on the RU allocated for the corresponding user. To achive this, we design an antenna based on FSA, operating on the 5.8 GHz WiFi band (5.49 to.5.835 GHz). Note that our design can also be extended to the 2.4 GHz WiFi band. Our goal is to design an antenna with a compact size, good angle of coverage, narrow beamwidth, and good radiation gain. The biggest challenge in our FSA design is to achieve a wide angle of coverage in the limited WiFi frequency band, as traditional FSA design consumes a large bandwidth to achieve beam steering. This requires a high phase variation in the antenna hardware design, to create large angular shifts. In conventional FSA design, a common practice for generating phase shift is using a long transmission line, which facilitates more phase variation [ND95]. However, transmission lines take up a lot of space to create high phase variation and is not an efficient solution to provide a large scanning coverage. Another common way to implement passive phase shifters is using dispersive substrate integrated waveguides [XGZ19], which makes it possible to have larger scanning coverage withing narrow bandwidth. However, their main problem is the complexity of the design, as well as low efficiency as half of radiation power is dissipated. In our FSA design, we use bandpass filters as phase shifters, which creates a high phase variation with limited space. A bandpass filter is a passive component which creates phase shift to the input signal, where the amount of

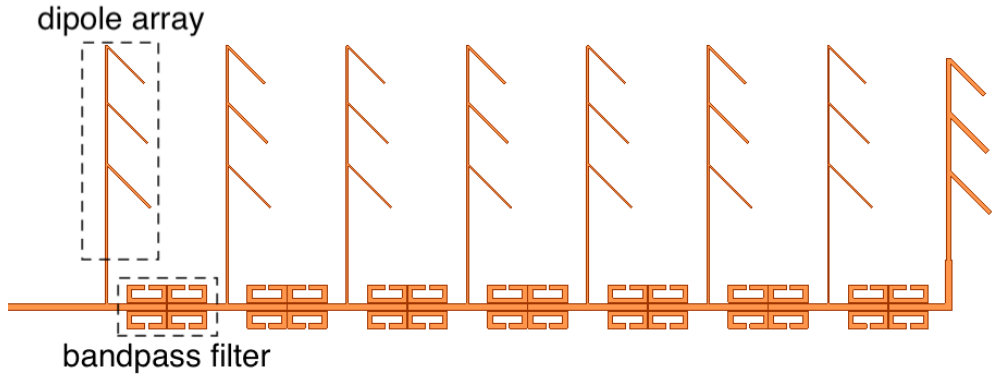

Figure 4.3: Wi-Pro's antenna design

phase shift is dependent on the signal frequency.

We adopt a series feed structure for Wi-Pro's antenna design, as shown in Figure 4.3. The structure consists of eight antenna elements connected by transmission lines with half-wavelength spacing. In our design, we integrate the antenna elements in between the bandpass filters, to radiate the signal. The linearly increasing phase shift among the antenna elements forms a directional beam. The orientation of this beam is dependent on the signal's frequency. This enables us to build an FSA with a wide steering angle given the limited bandwidth. The bandpass filter in our antenna design is based on split-ring-resonators [BJR17], which provides high phase shift values. The antenna elements we use in our design are arrays of dipole antennas, which creates higher gain and wider bandwidth.

4.4 Enhacing WiFi OFDMA using Wi-Pro

In this section, we explain how Wi-Pro integrates with OFDMA and boost communication performance of WiFi. We first discuss OFDMA's RU allocation mechanism. Then we explain how Wi-Pro works with OFDMA downlink and uplink communication.

OFDMA RU Allocation: OFDMA's RU allocation protocol is not fixed by standard. The specific implementation is left to be determined by vendors. A typical practice is to allo-

cates RUs based on channel condition [TBS21]. Using downlink as an example, the OFDMA AP first broadcasts pilot symbols to all the user devices engaged in the communication. Each user device evaluates its channel to the AP based on the received pilot symbols and sends feedback to the AP regarding the channel condition. Based on the feedback from multiple users, the AP decides how to allocate RUs to different users for downlink communication. This process works similarly for uplink where the user transmits the pilot symbol to the AP. The AP aims to assign RUs that offer the best channel conditions to each user. Wi-Pro also follows this practice to allocate the RUs with best SNR to each user; therefore, Wi-Pro does not require any firmware modification.

In Wi-Pro, when the pilot symbols are transmitted from the AP via the FSA, the power of the radiated signal is selectively amplified on specific subsets of subcarriers, depending on the direction of the user receiving the symbols. For example, as shown in Figure 4.4, User 1 may receive pilot symbols with higher signal power on subcarriers around frequency f_2, while experiencing weaker signals on other subcarriers. Consequently, User 1 provides feedback to the AP indicating the RUs around f_2 is have good channel condition for User 1. And the AP will allocate those RUs to User 1 with higher priority. In summary, Wi-Pro seamlessly integrates with the standard OFDMA RU allocation process based on channel condition, enabling the AP to allocate optimal RUs to each user in different directions. This builds the foundation for improving the performance of OFDMA. Next we explain how Wi-Pro improves the performance of OFDMA in both downlink and uplink communication.

OFDMA Downlink: In OFDMA downlink communication, once the communication channel is reserved, the Access Point (AP) transmits data for multiple users within a single aggregated Multi-User Downlink Physical Protocol Data Unit (MU DL PPDU). The format of an OFDMA downlink frame is shown in Figure 4.4. The preamble with common physical layer information is used to prepare the receiver for receiving subsequent data in the RU. The preamble uses the entire channel bandwidth to transmit, while the data symbols for each user is modulated on the RU subcarriers allocated to that user. The symbols in the

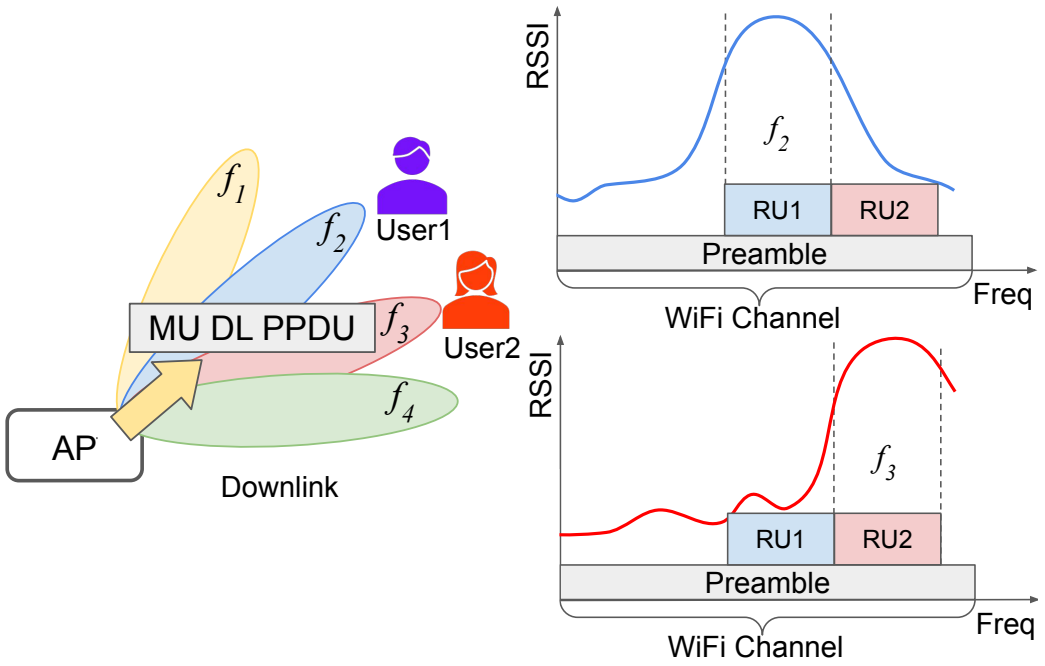

Figure 4.4: OFDMA Downlink

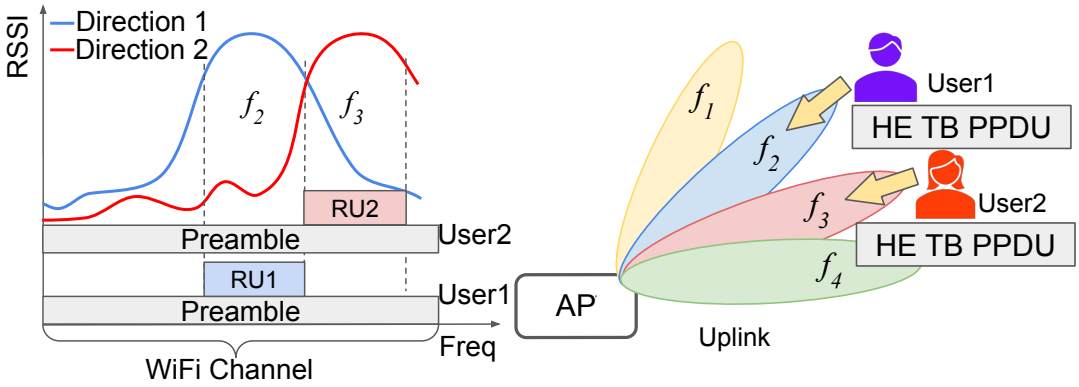

Figure 4.5: OFDMA Uplink

preamble are normally modulated using lower MCS schemes such as BPSK, which is more tolerable to lower SNR. Whilst data symbols modulated in the RUs typically use higher order modulation schemes, which could support higher datarate with the higher SNR.

In Wi-Pro, instead of distributing the signal power uniformly across the channel spectrum, we concentrate the power of the transmitted signal on the subcarriers within the RU allocated to each user for data transmission, which benefits the most from higher SNR. Conversely,

less power is distributed to the subcarriers containing preamble symbols, since it is more tolerant of lower SNR. For example, as shown in Figure 4.4, User 1 will be allocated RU 1 of frequency range f_2. The FSA concentrates the signal power in the direction of User 1 within the frequency range of f_2. In contrast, User 2 located in a different direction will be allocated RU 2 in the frequency range of f_3. In this direction, the FSA focuses the signal power in the frequency range of f_3. In summary, by combining Wi-Pro's antenna and OFDMA, we are able to allocate different RUs to users in different directions relative to the AP. For each user, the RUs with best channel condition is picked, whose power is further concentrated towards user's direction by Wi-Pro's antenna. In this way, Wi-Pro increases the SNR for downlink communication.

OFDMA Uplink: In OFDMA uplink, the AP first transmits a trigger frame to all the users to solicit the uplink transmission process. The users then transmit simultaneously on their allocated RUs in response to the trigger frame. The format of the user's uplink data frame, known as the High-Efficiency Trigger-Based Physical Protocol Data Unit (HE TB PPDU), is illustrated in Figure 4.5. Each user transmits a separate data frame containing data in its allocated RU subcarriers. As we mentioned earlier, Wi-Pro's antenna operates in a reciprocal manner for both transmitting and receiving signals. This means when the frame of each user is received by the AP, the signal power will be amplified on the RU containing the data symbols intended for that specific user. For example, as shown in Figure 4.5, User 1 is located in Direction 1 and User 2 is located in Direction 2. The frame transmitted by User 1 will be amplified in the frequency range of f_2 at the AP. This is because signals within the f_2 frequency range undergo constructive interference in the FSA when originating from User 1's direction. This increases the SNR of the data transmitted in RU 1. Similarly, the frame transmitted by User 2 will be amplified in the frequency range of f_3, which increases the SNR of User 2's data transmitted in RU 2.

4.5 Enhancing WiFi AoA Measurement Using Wi-Pro

In addition to enhancing the communication distance and data rate, Wi-Pro seamlessly enables WiFi Access Points (APs) to accurately measure the AoA of connected user devices as well as other WiFi devices in the area. We first explain how to measure the AoA of user devices connected to the AP using just a single transceiver chain, then we explain how to measure the AoA of any user devices in the vicinity.

4.5.1 Measuring the AoA of Connected Devices

Wi-Pro measures the AoA of a connected device by leveraging the special beamforming property of the FSA. Recall that FSA creates beams for different frequency signals towards different directions. Therefore, there is an one-to-one mapping relation between the angle and frequency. This enables the signal pattern received by the a user device to naturally contain the angle of arrival information of that device. First, since we allocate RUs to different users according to their channel condition, meaning each device is assigned the frequencies that matches the FSA beam directed towards the device. Therefore, the RU assignment implicitly encode the information of user's direction. Second, Wi-Pro can utilize the fine-grained Channel State Information (CSI) measured from uplink packets to further improve the accuracy of the angle of arrival estimation, based on the power distribution to different subcarriers. For the packet received from a user device, its signal power is selectively amplified across a subset of the subcarriers due to the frequency-dependent beamforming feature of FSA. CSI allows us to measure the received power of each subcarrier. This detailed information facilitates precise interpolation of the signal's peak frequency. By leveraging the direct correlation between frequency and beam angle of the FSA, the peak frequency of the incoming signal can be used to accurately measure the AoA of the user device. Note that the AP does all of these by analyzing the signal received from the single port of the FSA, this means Wi-Pro supports AoA measurement with just a single tranceiver chain.

4.5.2 Measuring the AoA of Unconnected Devices

In many situations we'd also want to measure the AoA any WiFi devices in the area even if they are not connected to the same AP. This sparks the opportunity for many interactions between WiFi devices, in scenarios such as smart homes or smart factories. In the rest of this section, we illustrate how we can utilize our smart antenna to measure the AoA of any WiFi devices in an area.

For devices which are not connected to the same network, it is difficult to measure their AoA based on overhearing their transmitted signals. First, as the transmitted WiFi frames are designated to different devices, they take up various WiFi channels and bandwidths, which makes it hard to design a general solution to measure the AoA based on the received signals. Second, we cannot extract the CSI information from individual WiFi frames as they are designated to other devices and are encrypted. We can only interpret the RSSI information of the received signal. To solve these challenges, we utilize an inherent trait of the WiFi protocol which is supported by all WiFi devices – WiFi probing [LLR22].

WiFi probe request packets are broadcast by each WiFi device in every frequency channel periodically for the purpose of discovering available networks in its communication range. Note that the probe request packets are sent even when the device is connected to a network, in order to update its list of available access points. As the probe request packet is transmitted on every frequency channel, it provides a perfect tool for us to measure AoA of the received signal using our FSA approach. In particular, FSA passively beam-forms in different directions based on the signal frequency. Hence, the probe request packet of a certain frequency channel will have a strong signal strength only if it arrives from a particular direction. This enables Wi-Pro to measure the RSSI at different frequency channels and use it to estimate the AoA. For compatibility with exisitng and legacy WiFi devices, probe packets by default are transmitted on every 20MHz channels. Our FSA is designed to operate in the WiFi frequency range of 5.49 to 5.83 GHz consisting of 17 20MHz channels.

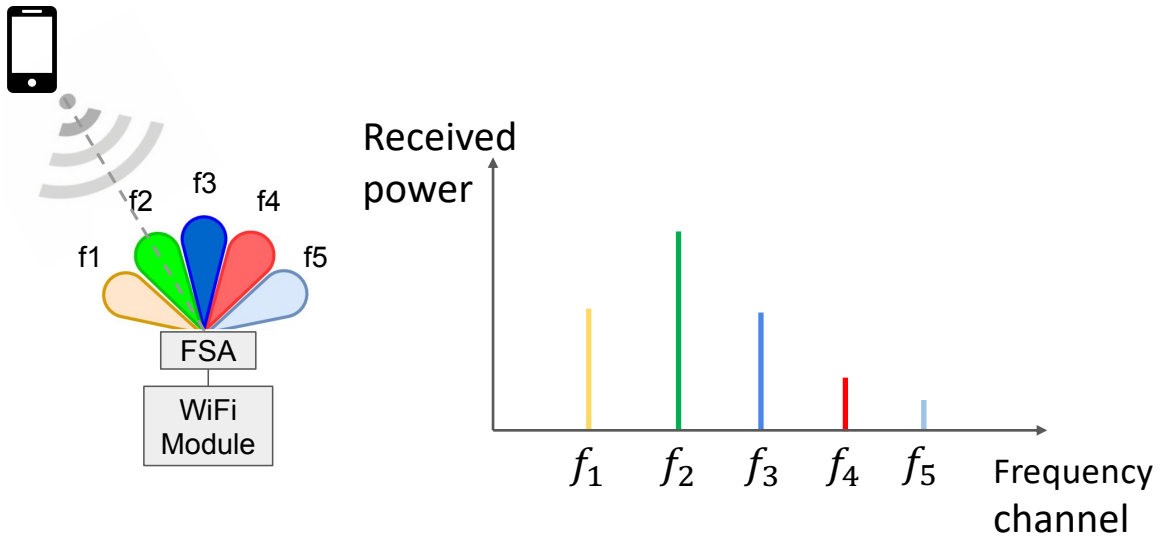

Figure 4.6: Measuring AoA using FSA

The angle of coverage for our FSA is 60 degrees, which should theoritically give us an angle measurement accuracy of 3.5 degrees using the RSSI of each channel.

Figure 4.6 shows a simple example of how our approach works where we have a WiFi module (measurement device) and a phone (target device). Assume we have an FSA whose beam forms in five different directions based on the signal frequency (i.e., f_1 to f_5). These frequencies are matched with WiFi channel center frequencies. The FSA is attached to a WiFi module as the substitute for the original antenna. As the phone transmits WiFi probe requests in frequencies f_1, f_3, f_4, and f_5, the WiFi module will receive the probe request with relatively low RSSI because the FSA's beams of those frequencies are pointing to the other directions. On the other hand, when the phone transmits a WiFi probe request in frequency f_2, the WiFi module will receive it with high RSSI because the FSA's beam direction at f_2 is pointing to the direction of the phone. Hence, by just comparing the five RSSI measurements, the WiFi device can estimate the AoA. Note, in this example the phone direction is perfectly aligned with the direction of one of the beams (i.e., beam f_2). However, in reality, there is a chance that the direction of the target devices is not perfectly aligned with any of the beam directions. In these cases, Wi-Pro can still use the RSSI profile from

multiple frequencies (different beam directions) to interpolate and estimate the correct AoA.

4.5.2.1 Measuring AoA of Multiple Unconnected Devices

The next question is how can we extend our approach to measure the AoA of multiple WiFi devices. In particular, since Wi-Pro needs to perform multiple RSSI measurements across different channels to estimate the AoA, it needs to differentiate probe request packets received from different devices. Our solution to solve this issue is to first identify the target devices based on their unique MAC addresses. Although this solution works for most WiFi devices (such as IoT and most laptops), it is not effective for Apple and Android phones. This is due to the fact that these WiFi devices perform MAC address randomization. Hence, Wi-Pro cannot simply use MAC addresses to differentiate RSSI measurements of a specific device from that of other devices in the area.

To solve this problem, we studied the behavior of Android and iOS WiFi devices in more detail. For Android devices, we found that the device probes with the same random MAC address on different channels as long as it is connected to an AP. However, for iOS devices, the story is slightly different. we found that when an iOS WiFi device is associated with an AP, it probes with the same MAC address only in the channel on which the AP is operating, and it uses other random MAC addresses for sending probe request packets on other channels. This is known as a *directed probe request*. Interestingly, we observed that this behavior is not dependent on the MAC address of the AP but on the SSID broadcast of the AP. In particular, in the channels where there is no AP with that specific SSID, the WiFi device still probes with randomized MAC addresses. On the other hand, in the channels where there is an AP with that specific SSID, the WiFi device probes with the same MAC address.

Wi-Pro leverages this property to push the target WiFi devices to use the same MAC addresses instead of randomizing them. In particular, the measurement device forges a

beacon frame, and put the SSID of the AP in its field[1] and broadcast it on every channel. This makes the target WiFi device assume there are multiple APs with the same SSID working on every single channel. As a result, the probing packets will always use the same source MAC address which helps Wi-Pro to identify each target device consistently. Finally, it is worth mentioning that we found that this technique not only works for target devices that are connected to a specific AP but also works for devices that were once associated with the AP and still have the SSID saved in their list of connected APs. Although these devices are no longer associated with that AP, they still probe with the same source MAC address on the channels where the AP's SSID is broadcasted.

In summary, Wi-Pro's measurement device broadcasts fake Beacons using the SSID of an AP. The WiFi devices which are in the range respond to this by sending Probe Requests on different channels with the same MAC address (i.e., without randomizing their MAC address). The measurement device which is equipped with an FSA antenna measures the RSSI of these probe request packets at different channels. Since the FSA's beam direction changes as a function of the frequency, the channel (beam direction) with the highest RSSI corresponds to the AoA of the signal from the target device.

4.6 Implementation

To evaluate the performance of the Wi-Pro system, we have implemented a prototype FSA based on our design as shown in Figure 4.7. Our FSA is implemented on RT/Duroid 5880 substrate, with a size of $22 \times 10\ cm^2$, and a thickness of $0.5mm$. Everything is integrated on the substrate with no additional components. The antenna element of this FSA is a three-element dipole with 7.5 dB gain. The structure is completely passive, with no energy consumption. For our experiments, we used four Zimaboards [zim], which are low-cost single board mini-PCs, with AX210 NIC as user devices. We use a TP-Link AX3000 Dual-band

[1]Note, since the SSID field of an AP is not encrypted, it can be easily obtained by sniffing the traffic.

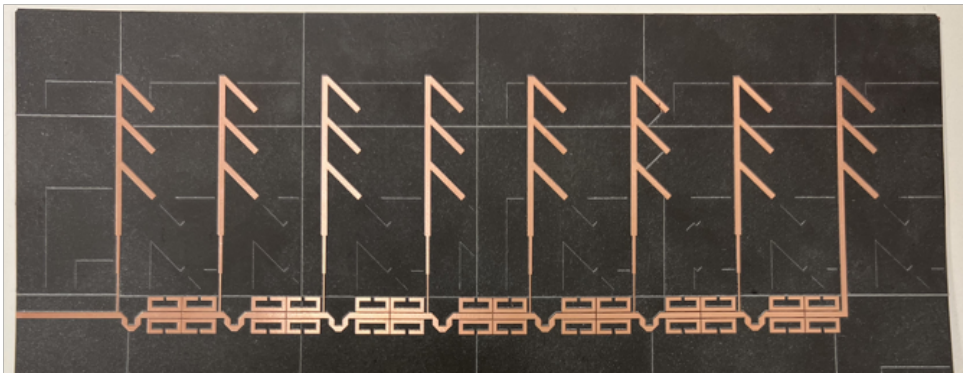

Figure 4.7: Wi-Pro FSA Implementation. It has single port which can be easily connected to WiFi devices instead of their current antenna. The design is also paper-thin and small. Hence, it can be placed on a wall, ceiling, or on a router box itself

WiFi 6 router as the AP. Both devices support 802.11ax OFDMA and channel bandwidths up to 160 MHz. For evaluating our system, we used PicoScenes [JLR21] for CSI measurement. We use Remcom Wireless Insite v3.4.4 [Rem23] for indoor RF propagation simulation, and CST [Das23] for our antenna design and simulation.

4.7 Evaluation

In this section, we present the performance of Wi-Pro. We first investigate the properties of our custom-designed FSA interms of its beamforming and steering capabilities in relation to frequency. Subsequently, we assess the Wi-Pro's effectiveness in extending the transmission distance and data rate of indoor WiFi6 devices based on large scale simulation as well as a variety of real indoor scenarios. Finally, we present our evaluation results for device measurement using Wi-Pro and show the AoA measurement accuracy.

4.7.1 Wi-Pro's Antenna Performance

(a) FSA Beamforming Capability

As we mentioned earlier, our FSA operates in the WiFi 5 GHz frequency range of 5.5 to

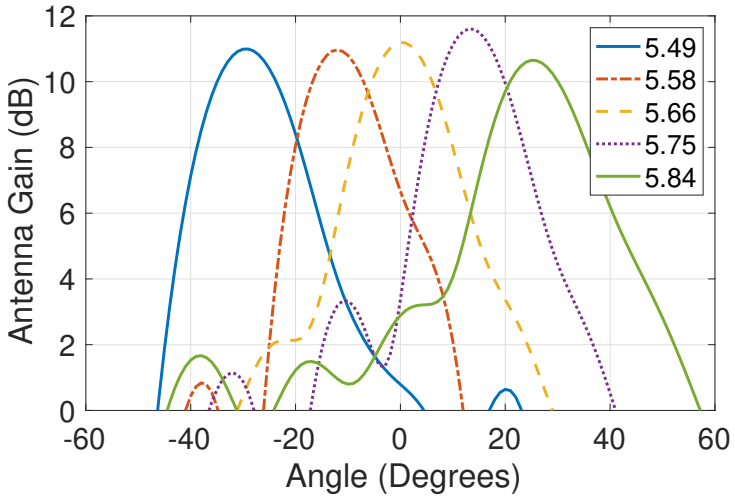

Figure 4.8: FSA Radiation Pattern at Five Frequencies

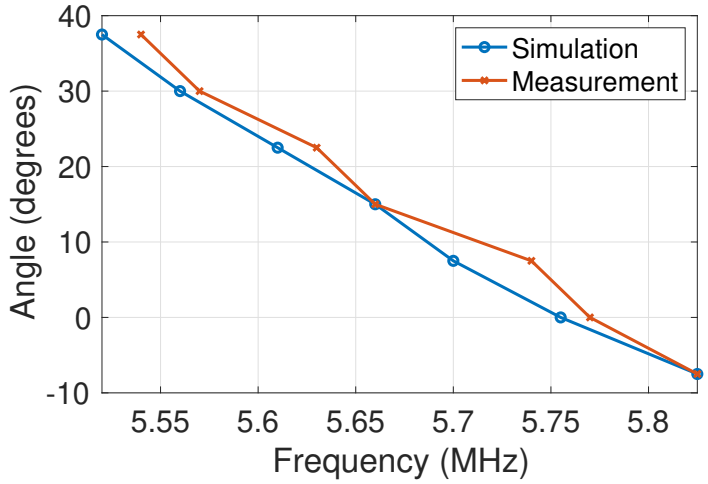

Figure 4.9: FSA Beam Angle Versus Frequency

5.825 GHz, and forms beams at different angles for different signal frequencies. Figure 4.8 shows the radiation pattern of the FSA with respect to the change in frequency. We chose five example frequencies to show the beam pattern, however it is worth mentioning that the FSA steers its beam continuously with the change in frequency. The horizontal axis is the angle of which the antenna radiates and receives energy in the unit of degrees, while the vertical axis is the antenna's gain at a specific angle in the unit of dB. The FSA can generate

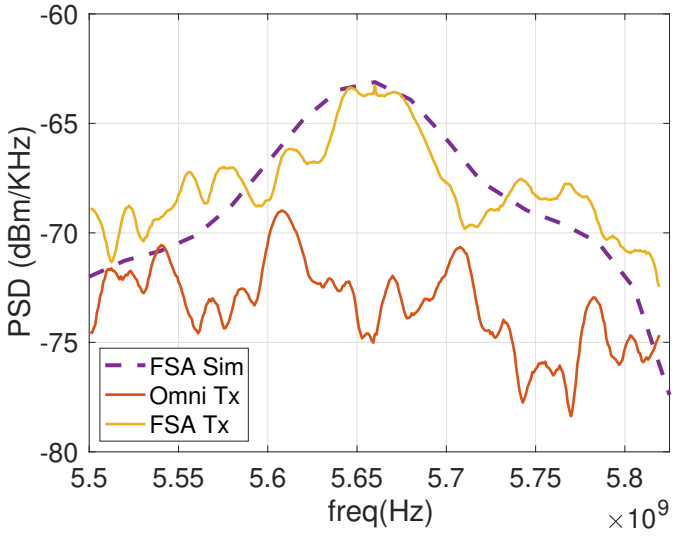

(a) 15 degree

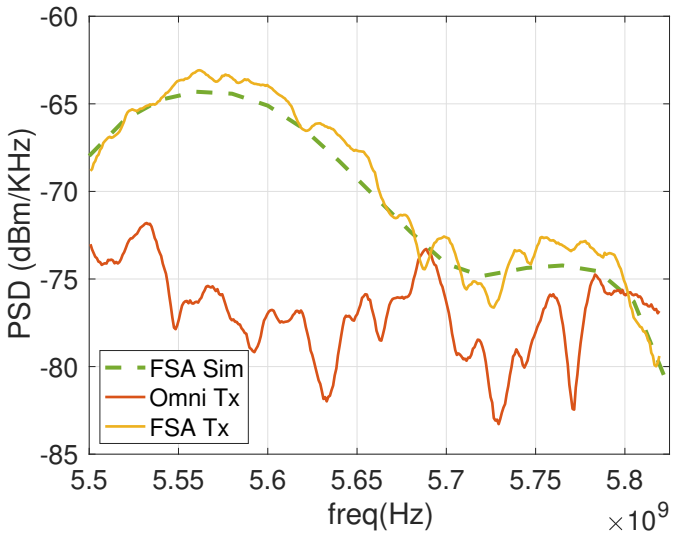

(b) 30 degree

Figure 4.10: FSA Power Distribution Across Frequency at Different Angles

narrow beams, achieving beam gains between 8.6 to 11.3 dB. The antenna beamwidth ranges from 12 to 26 degrees.

Figure 4.9 shows the relationship between the direction of the beam and the frequency of the signal based on both simulation and real-world measurement. The results indicate

that our FSA is capable of steering the beam by approximately 50 degrees across the WiFi 5 GHz band. This range is sufficient for extensive coverage, especially considering that typical APs are usually mounted on the walls or corners of a room. The figure also shows that the simulation result from CST closesly matches with the real world measurement, meaning our prototype implementation closely aligns with our design.

(b) Power Allocation Measurement

We further measured the performance of our FSA in terms of signal transmission in comparison with traditional omni-directional WiFi antenna in an indoor environment. For this assessment, we employed the Keysight 5G R&D test bed [Key23] as the platform for both transmitting and receiving signals. In our setup, the transmitter consists of a signal generator connected to the FSA, operating at a transmit power of 10 dBm. We transmitted a wideband signal spanning the entire operational frequency range of the FSA (5.5 GHz to 5.825 GHz), and measured the power spectral density (PSD) of the signal at different frequencies. On the receiving end, we used a spectrum analyzer connected to an omni-directional antenna, with a transmission distance set at 1.5 meters. For comparative analysis, we conducted a parallel experiment where the transmitter was connected to an omni-directional WiFi antenna BFN00456.

Figure 4.10 shows the measurement result of the received signal when the receiver is at two distinct angles with respect to the transmitter. As can be seen from the result, in the frequency domain the power of the signal is concentrated within certain frequency ranges, where the concentration of power depends on the position of the receiver. The power distribution pattern closely follows the simulation result (adjusted magnitude). In comparison, when omni-directional antenna is used by the transmitter, then power is more uniformly distributed across the entire frequency spectrum. These results show that our FSA closely follows our design, and is able to focus the transmission power at different frequencies in different directions. While not depicted here due to space constraints, additional tests have verified that our FSA exhibits similar performance in receiving signals. This implies that

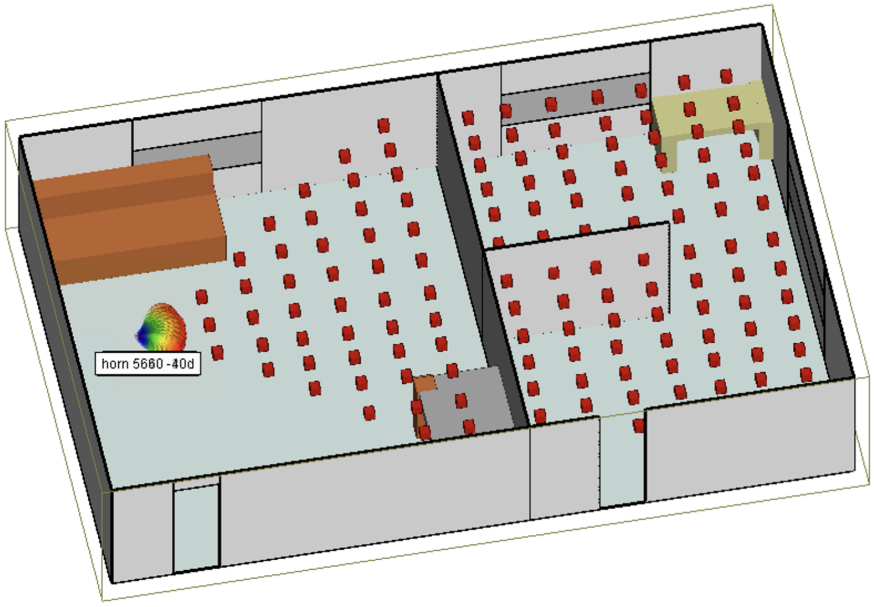

(a) Indoor Simulation Setup

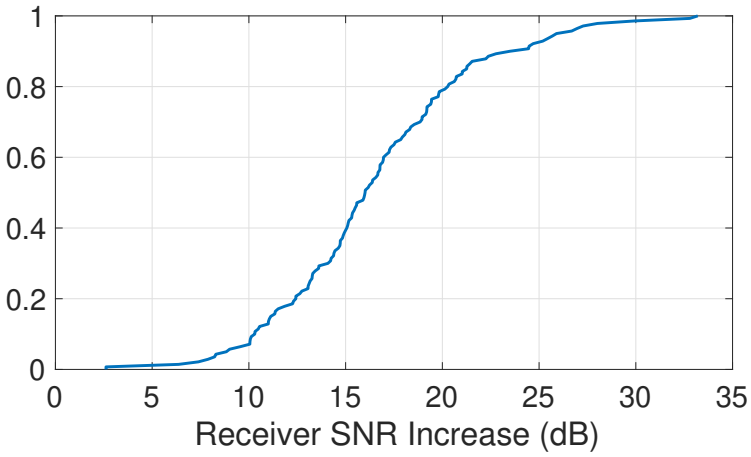

(b) SNR Improvement

Figure 4.11: Indoor Simulation Performance

the power distribution characteristics are consistent for both uplink and downlink communications.

4.7.2 SNR Improvement Performance

4.7.2.1 Simulation Results

We first evaluate the performance of our system in an indoor environment with a large number of distributed users, we ran simulations using Remcom Wireless InSite, to model the signal propagation dynamics in indoor settings. Our simulation environment replicates an indoor building with dimensions of $16 \times 10 \times 3m$ with various rooms and furnitures, as shown in Figure 4.11a. We simulated an ideal FSA with eight beams pointing to different directions. The total coverage of the beams is 60 degrees similar to our designed FSA, each beam has a center gain of 15 dB and transmits signal using non-overlapping 20 MHz frequency blocks in the range of 5.50 GHz to 5.66 GHz (160 MHz channel). For comparison, we also used an omni-directional antenna as the transmitter which transmits signal in the same frequency range (5.50 GHz to 5.66 GHz). For each of the 140 receivers inside of the rooms, we recorded the max SNR across all the 20 MHz subchannels for both antenna types. We then compared how much the receiver SNR increased for the FSA transmitter compared to the omni directional transmitter.

The CDF plot of the receiver SNR improvement is shown in Figure 4.11b. Based on the result, FSA is able to achieve an SNR improvement at 100% of the time. Moreover, the FSA can achieve atleast 17 dB of SNR improvement at 50% of the time.

4.7.2.2 Measurement Results

We evaluated the performance of our system in different indoor environments, an office with lots of desks and cubicles, as well as a lab space. We collected measurements for 26 different locations. Our setup is shown in Figure 4.12 where we connected our FSA to the antenna output port of the WiFi6 router (instead of its typical antenna). We terminated the other antenna ports of the router with 50 ohm terminators. Our user devices are Zimaboards plus AX210 NIC with omni-directional antenna. The user devices are all associated to the same

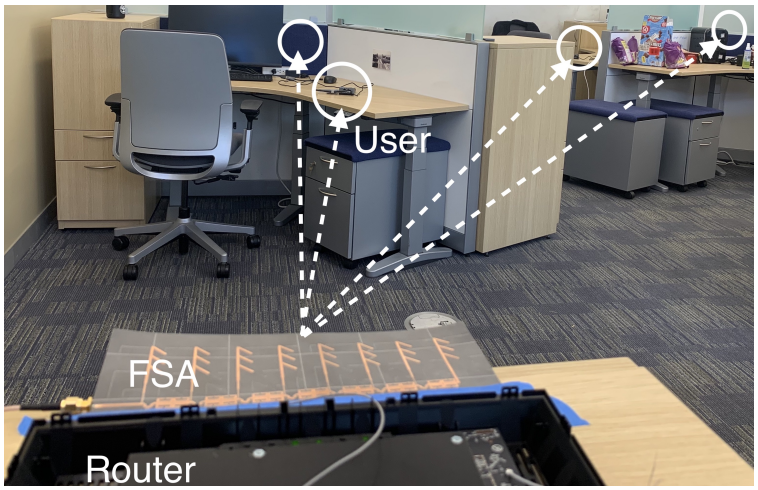

Figure 4.12: Indoor Experiment Setup

AP. The Zimaboards are running Ubuntu 20.04 systems with PicoScenes software installed for analyzing the CSI of the received signal. We conducted our experiment by collecting the CSI of the received signal on the user device at each location, when the AP is using our FSA and when the AP is using an omni-directional antenna respectively.

To compare the performance of Wi-Pro to a regular AP with omni-directional antenna, we first analyze the SNR difference of the received signal at the RU with the strongest signal power. As the RU with the best channel quality is allocated to each user, this allows us to compare how much FSA helps improve the SNR of an RU compared to omni-directional antenna. More specifically, for each location, assume there are m RUs in the received signal, the power of i-th RU in the received signal from the FSA antenna is denoted by $P_{\text{fsa},i}$ and the power of the j-th RU in the received signal from the omni-directional antenna is denoted by $P_{\text{omni},j}$. Then the SNR improvement of FSA can be defined as follow:

$$\Delta\text{SNR(dB)} = \max_{i=1}^{m} P_{\text{fsa},i}(\text{dBm}) - \max_{j=1}^{m} P_{\text{omni},j}(\text{dBm}) \tag{4.1}$$

We calculate the SNR difference for RUs of 20 MHz and 40 MHz bandwidth respectively, we perform this calculation for all 26 positions of measurement. Figure 4.13a shows the

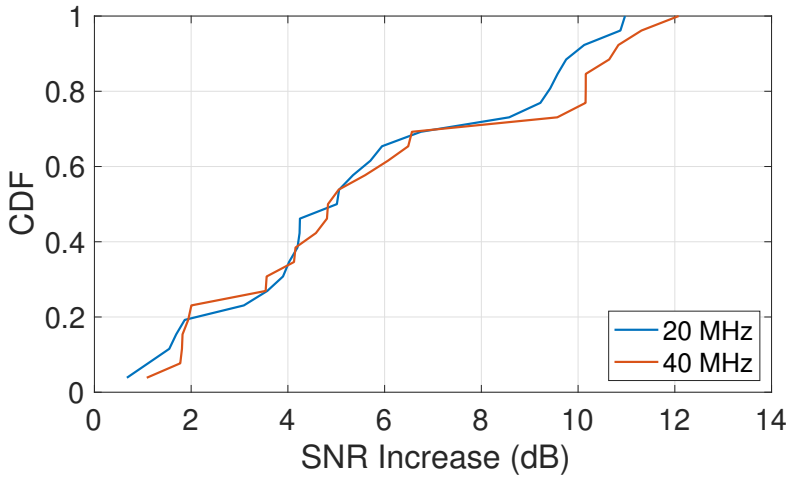

(a) SNR Improvement

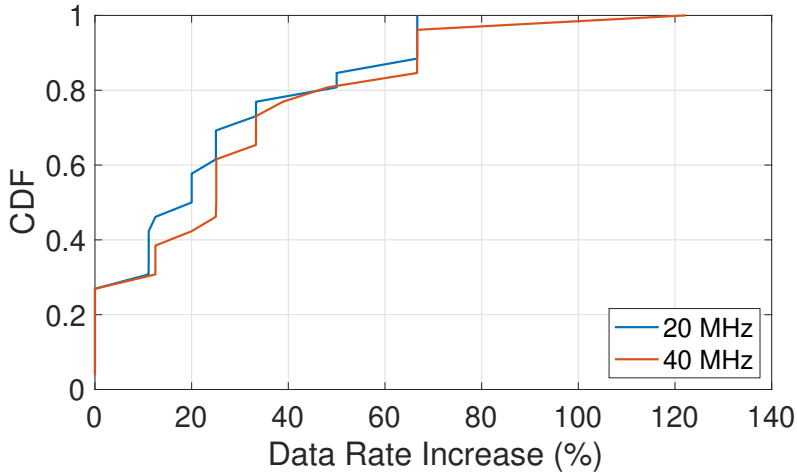

(b) Data Rate Improvement

Figure 4.13: Wi-Pro Performance Improvement

SNR improvement of FSA compared to omni-directional antenna for RU bandwidth of 20 MHz and 40 MHz respectively. This results show that FSA achieves higher SNR for RUs compared to omni-directional antenna. More specifically, 55% of the time the FSA is able to achieve more than 5 dB higher SNR compared to omni-directional antenna, which results in an increase in the operating range of device by around two times or improve their data rate. At certain positions the SNR increase can reach more than 10 dB, which results in an increase in the operating distance by more than three times.

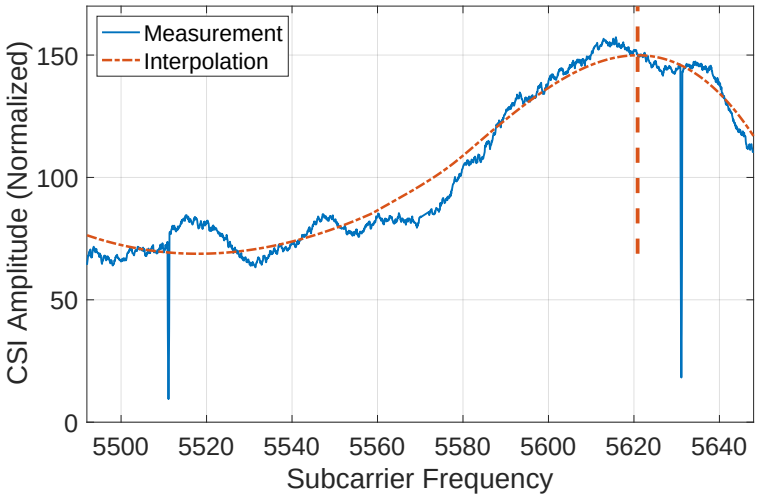

Figure 4.14: CSI Measurement at 23 Degrees

As our design enables higher SNR per user device at each location, it also enables higher modulation and coding schemes to be used, which increases the data rate of the user. Figure 4.13b shows the data rate increase for users at different positions based on the measurement of the RSSI of the received signal as well as the SNR difference between the FSA and omni-directional antenna. The result is calculated based on the average data rate increase for RU of specific bandwidth (20 MHz and 40 MHz) across different guard band intervals at a given modulation and coding scheme [IEE21a]. Wi-Pro improves the data-rate by more than 20% in average. In fact, in some cases, the data rate is almost doubled.

4.7.3 AoA Measurement Performance

For our AoA measurement, we setup a Zimaboard as the AP and connects it to the FSA for receiving signals. As before, we are transmitting 160 MHz 802.11ax WiFi packets with the center frequency of 5.57 GHz. We conducted our experiment at angles of 19, 23, 30, and 40 degrees respectively. For each angle, we positioned the transmitter at distances of 2, 2.5, 3, and 4 meters away from the receiver. To calculate the AoA, we analyzed the CSI of the received signal and attempted to interpolate its peak frequency. We then identified the angle corresponding to this frequency based on the angle versus frequency measurement we

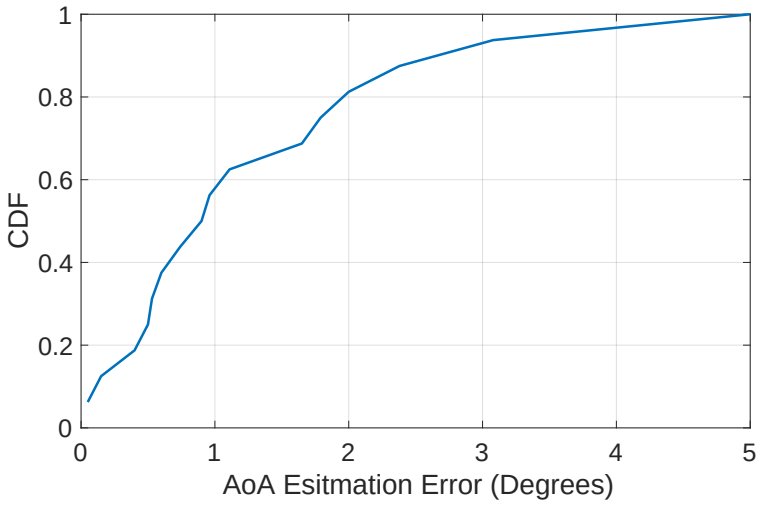

(a) Wi-Pro AoA Estimation Error

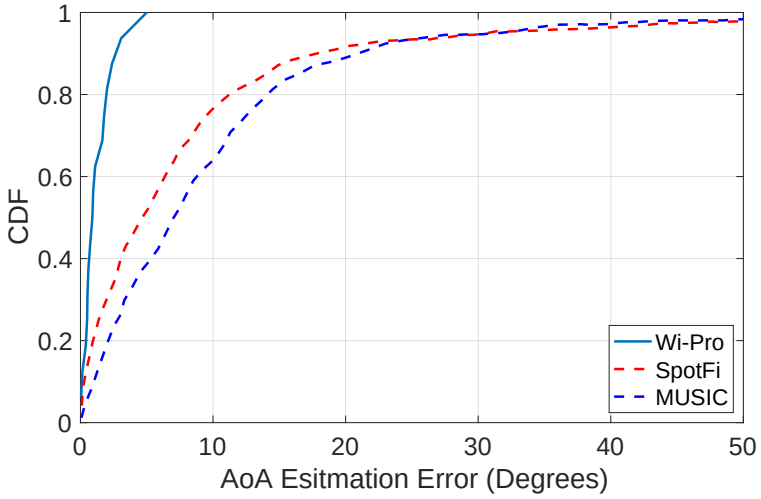

(b) Wi-Pro vs Existing Work

Figure 4.15: Wi-Pro AoA Estimation Performance.

plotted in Figure 4.9. For example, Figure 4.14 shows the CSI magnitude of the received signal for subcarriers across the 160 MHz WiFi channel. We used an interpolation algorithm to smoothen the shape of the CSI plot and estimated the peak frequency is at 5.620 GHz , which corresponds to an estimated AoA of 23.6 degrees, resulting in a 0.6 degree estimation error. We use the same method to calculate the estimated AoA versus the expected AoA, and plotted the AoA estimation error in Figure 4.15a. Based on these mreasurement results, we show that Wi-Pro can achieve an AoA estimation error of less than 1 degree 50 % of

the time, with a max estimation error of around 5 degrees. Figure 4.15b shows Wi-Pro's AoA estimation error compared to existing solutions [KJB15, Sch86] in a similar indoor setting. Based on the result we can see that Wi-Pro can greatly increase the AoA estimation accuracy without using multiple access points, multiple antennas, and complex interpolation algorithms.

4.8 Conclusion and Discussion

In this chapter we presented Wi-Pro, a system which integrates a new plug-and-play FSA antenna with commodity WiFi devices. By combining FSA with the inherent features of existing WiFi protocol, Wi-Pro is able to improve the performance of WiFi. We first introduce a novel design for WiFi power allocation based on spectral usage of users at different locations. We then propose methods to measure the AoA of any WiFi devices in the vicinity, including low-cost, low-power devices with a single transceiver chain, without requiring firmware or chipset updates. Finally, we implemented Wi-Pro and evaluated its performance in various indoor settings. There are certain limitations of Wi-Pro that warrant further discussion. Wi-Pro is most beneficial for scenarios with a large number of users scattered in different directions, such as smart home or smart factories. In networks with fewer users, the advantages of Wi-Pro are not as pronounced. This is because, in such scenarios, each user could potentially utilize a more significant portion of the channel. However, the system is designed to amplify the signal on a subset of subcarriers for each specific direction. When the users are clustered in a single direction, it is better to use a fixed direction beam which amplifies the signal for all frequencies to enhance communication.

CHAPTER 5

mmCharge: Increasing the Range of mmWave Wireless Power Transfer via Passive Beamforming

This chapter introduces mmCharge, a system which uses passive beamforming to increase the range of wireless power transfer.

5.1 Problem Statement and Challenges

In this section, we will first explain the motivation of wireless power transfer and its key challenges. Subsequently, we will explain the limitations of existing wireless power transfer systems. Next we will introduce the design goals of mmCharge and how we address these challenges. Then we explain the limitations of existing mmWave wireless power transfer systems and illustrate how mmCharge differs from these work.

The number of worldwide Internet of Things (IoT) devices is expected to grow to more than 29 billion by 2030 [Sta]. Although this is exciting, there is a major challenge in deploying IoT devices: *their batterylife*. Most today's IoT devices require their battery to be replaced or recharged every couple of months. For example, smart home sensors such as motion, temperature and moisture sensors require their battery to be changed every 6 months. Similarly, WiFi home security cameras require their battery to be recharged every 4 months. Although a batterylife of a few month might seem long enough for a device, unfortunately, this would not be the case in a few years. In particular, considering the fact that the average number of IoT devices in an American house is expected to reach fifty in the next

few years [Tim, For], we would need to change one to two batteries per week in our homes. Moreover, in many cases, the IoT sensors are not even in reach, so the battery charging or replacement requires lots of effort.

In this chapter, we ask whether future indoor access points (such as WiFi or 5G) can transfer power to IoT devices to recharge their battery and/or significantly increase their batterylife. In particular, we are interested to learn which frequency bands are the best for transferring power wirelessly. On one hand, high frequency signals (such as mmWave bands) experiences greater path loss than low frequency RF signals (such as WiFi bands). Therefore, at first glance, mmWave signals may seem unsuitable for transferring power. However, on the other hand, FCC allows much higher transmission power for indoor mmWave networks than traditional indoor wireless networks [FCC23b]. Moreover, due to small wavelength of mmWave signals, their antennas are tiny and many of them can be packed into a small area to create high gain antenna to harvest more energy. Therefore, due to these trade-offs, it is not clear whether low frequency signals are more suitable than mmWave signals for transferring power or vice versa.

In order to transfer power to IoT devices using mmWave signals, we first need to address multiple challenges. The main challenge is that indoor mmWave access points and mmWave harvester devices use directional antennas with narrow beams, and hence, the maximum power is transferred when these beams are aligned [HAR18b]. Moreover, when a node moves, it needs to search again for the best beam direction. Although past mmWave work has proposed different approaches and schemes for creating a directional beam and searching for the best beam direction [HAR18a, KM14, EAH15, RVM12], they are not practical for our application. This is mainly due to the fact that existing schemes require phased array antennas. Unfortunately, phased arrays are costly and consume a significant amount of power which makes them impractical for energy harvesting IoT devices [MAA19b, AHR16]. In the following part of this section, we will explain in detail the limitations of existing wireless power transfer systems and literature.

5.1.1 Design Goals of mmCharge

Our goal is to first perform a comprehensive end-to-end performance evaluation of using 900 MHz (RFID), 2.4 GHz (WiFi), 5.8 GHz (WiFi), and 28 GHz (mmWave 5G) signals for transferring power to IoT devices, to determine the most suitable band for wireless power transfer while considering their trade-offs. We focus our evaluation on the indoor environment such as smart home or smart factory. Our results show that mmWave bands are much better candidates for transferring power to IoT devices than lower frequency wireless signals. To address the challenges of mmWave wireless power transfer, we propose mmCharge, a mmWave wireless power transfer system which uses Frequency Scanning Antenna (FSA) and backscatter technology. The goal is to design a low-power low-complexity mmWave power harvesting system which can be integrated to power-constrained IoT devices. In particular, we develop a directional energy harvesting antenna which is completely passive while enables the access point to steer the harvester device's beam. Furthermore, we propose an efficient and low power beam alignment mechanism based on backscatter technology which enables the access point to align its beam and the harvester device beam, even when they move. Different from previous work, the power harvester uses nearly zero power to achieve accurate beam alignment.

Our contributions are as follow:

- We study the feasibility of using different indoor signals to transfer power to IoT devices considering constraints such as FCC regulations, antenna size, etc. Our results show that mmWave signals are much better candidates to transfer power compared to traditional wireless signals such as WiFi and sub-GHz signals.

- We propose a system architecture and link establishment protocol for IoT devices to harvest energy from indoor mmWave access points. Our design is based on passive beamforming and backscatter technology.

- We evaluate our system in terms of power transfer at different distances. Our results show that it is possible to harvest 1 mW and 0.1 mW power at the distances of 7.5 m and 15 m indoors, respectively. This enables the IoT device to significantly increase their batterylife.

5.1.2 Limitations of Current Solutions

Existing wireless power transfer systems can be divided to two types: near-field magnetic coupling and far-field electromagnetic radiation [ENA16]. Magnetic coupling in wireless power transfer, such as in smartphone wireless chargers, involves the transmission of electrical energy between a transmitting coil and a receiving coil through an oscillating magnetic field. However, despite their high efficiency, these systems have a very short operating range (i.e. less than a foot) since the strength of the field falls off inversely with the cube of the distance from its source. In contrast to the near-field magnetic coupling approach, the far-field electromagnetic radiation approach uses RF signals to transfer power between two devices. In these systems, a charger device transmits a signal using its antenna. Then user devices receive the signal on their antennas and use harvesting circuits to harvest energy. Existing systems mostly operate at ISM bands such as 900 MHz, 2.4 GHz, 5.8 GHz and mmWave bands [LWN15, ENA16]. Given the inherent trade-offs across various frequency bands in terms of communication distance, antenna size, and power regulations, there lacks a a comprehensive analysis on which frequency band is best for wireless power transfer. Although there are a few survey work which discuss the potential and challenges of higher frequency bands such as mmWave for power transfer [WWB20], none of them provide a conclusive end-to-end comparison with different frequencies. Moreover, they do not take into account various parameters such as the FCC regulations, the antenna aperture, and the power conversion efficiency based on recent hardware advances. In work, we perform a comprehensive study and an end-to-end performance evaluation of using different frequency bands for transferring power, while considering practical factors such as FCC, antenna size,

path loss, hardware efficiency, etc.

While various systems for mmWave power harvesting have been proposed in the past, they exhibit certain limitations. Existing mmWave power harvesting systems such as GuRu [HAB23, HAB20, SWC23] require the power harvester to constantly monitor the received power level and provide feedback to the power transmitter through a communication module, thereby increasing both the design complexity and power consumption on the harvester. Furthermore, it requires time synchronization between the power transmitter and harvester. In contrast, mmCharge employs a backscatter technique, reflecting the signal back to the power transmitter for beam alignment, which not only simplifies the design of the harvester but also avoids introducing additional power consumption or delay. Additionally, a major challenge with most existing systems lies in their use of fixed beam antennas on the harvester, thereby limiting power harvesting efficiency across various orientations and during mobility [NST16, CLC20, HAB20, WHW22]. These systems also combine the DC output power of each antenna element on the harvester [HAB20, WHW22], leading to suboptimal power conversion efficiency, limiting the system's working distance. This is due to the input power requirement of mmWave frequency rectifiers, it requires high received power per element to achieve a good power conversion efficiency. The authors in [EHT21a] proposed a multi-beam mmWave energy harvester using Rotman Lens and patch antennas. However, the Rotman Lens has multiple output ports, and therefore it requires a DC combiner network to combine the power of all ports. This adds complexity and reduces the efficiency of the system. In contrast, our design, based on Frequency Scanning Antenna (FSA), not only creates multiple spatial beams, but also naturally combines all the power harvested from beamforming via a single output port. Moreover, we propose a link establishment protocol based on backscatter communication which enables the access point to steer the harvester's beam, and align it toward itself without any need for a separate module.

5.2 Which Spectrum Band is the Best for Wireless Power Transfer?

A typical wireless power transfer system consists of a power transmitter which sends power using radio waves signals and a power harvester which collects these waves and convert it to DC power through a rectifier circuit. In this section, we perform an end-to-end performance evaluation of wireless power transfer system operating at four different frequency bands: 900 MHz (RFID), 2.4 GHz (WiFi), 5.8 GHz (WiFi), and 28 GHz (mmWave 5G). Our evaluation is based on commodity devices which are compliant with Federal Communications Commission (FCC) regulations. Our goal is to see whether using mmWave signals have any advantages or disadvantages compared to other signal frequencies.

5.2.1 Link Budget Parameters

A typical wireless power transfer system consists of a power transmitter which sends power using radio waves signals and a power harvester which collects these waves and convert it to DC power through a rectifier circuit. In this section, we perform an end-to-end performance evaluation of wireless power transfer system operating at four different frequency bands: 900 MHz (RFID), 2.4 GHz (WiFi), 5.8 GHz (WiFi), and 28 GHz (mmWave 5G). Our evaluation is based on commodity devices which are compliant with Federal Communications Commission (FCC) regulations. Our goal is to see whether using mmWave signals have any advantages or disadvantages compared to other signal frequencies.

FCC regulation and Transmit Power: We first investigate how much power a power transmitter can radiate to the air based on FCC regulation. The total output power radiated in a transmitting direction is known as the Effective Isotropic Radiated Power (EIRP), which consists of the transmitter output power and the transmitter's antenna gain. The max EIRP at each frequency band is regulated by the FCC. The max EIRP permitted for 900 MHZ band and indoor WiFi access points at 2.4 GHz and 5.8 GHz is 36 dBm [FCC23b]. At mmWave

frequency of 28 GHz, the max EIRP for indoor access points is 55 dBm [FCC23a], the max EIRP for outdoor access point can reach up to 75 dBm [FCC23a]. Hence, a transmitter operating at 5G mmWave bands can radiate almost 20 dB higher power than a transmitter operating at other frequency bands for indoor scenarios and this number further increases for outdoor scenarios.

Propagation Path Loss: Next, we compare the propagation path loss for signals at different frequencies. The equation for calculating the received power (P_r) is shown in Eq.(5.1), where P_t is the transmitter output power, G_t is the gain of the transmitting antenna, G_r is the gain of the receiving antenna, d is the distance between the transmitter and the receiver, f is the signal frequency, and c is the speed of light in vacuum.

$$P_{\mathrm{r}}(dB) = P_{\mathrm{t}}(dB) + G_{\mathrm{t}}(dB) + G_{\mathrm{r}}(dB) + 20log\frac{c}{4\pi fd} \tag{5.1}$$

Based on Eq.(5.1), the path loss of the signal is determined by the transmission distance (d) and the frequency of the signal (f). This means that given the same transmission distance, the higher the signal frequency, the higher the propagation path loss.

Antenna Size: The relationship between the antenna gain (G) and the effective antenna aperture (A_e) is shown in Eq.(5.2).

$$G = \frac{4A_{\mathrm{e}}\pi f^2}{c^2},\ G(dB) = 10log(\frac{4A_{\mathrm{e}}\pi f^2}{c^2}) \tag{5.2}$$

When the antenna aperture size is the same, the higher the transmission frequency, the higher the gain of the antenna. This means that for the same antenna area, the gain of the receiving antenna will be much higher for mmWave compared to lower frequencies. Note, higher antenna gain means that the receiver can collect more power to harvest energy. For example, for the same aperture size, an antenna operating at 28 GHz has almost 100, and 1000 times higher gain compared to an antenna operating at 2.4 GHz and 900 MHz,

Frequency	Input power to rectifier (dBm)				
	-20	-10	0	10	20
900 MHz	16%	26-60%	60-69%	N/A	N/A
2.4 GHz	20%	45%	57-72%	53-73%	84%
5.8 GHz	N/A	23%	18-34%	50%	60-82%
24-35 GHz	N/A	N/A	10-12%	15-35%	37-62%

Table 5.1: Power Conversion Efficiency. This table shows the PCE of rectifiers used in existing literature at different frequencies and different input powers [VD14, WWB20, VKM21].

respectively.

Energy Harvester Efficiency: Once the RF signal is received at the output of the receiving antenna, it has to be converted to DC power for usage. This conversion is done using a circuit called rectifier. In a rectifier, the ratio of output DC power to input RF power is quantified as the Power Conversion Efficiency (PCE). This conversion efficiency is impacted by the quality of RF to DC converter components and various losses due to mismatch in the circuits. Unfortunately, the losses worsen at higher frequencies. Table 5.1 shows PCE of existing circuits operating at different frequencies for different range of input powers. As the table shows, the higher the signal frequency, the lower the PCE.

5.2.2 Link Budget Analysis

So far, we have explained the trade-offs between mmWave and lower frequency signals in terms of FCC EIRP limit, path loss, antenna size, and energy conversion efficiency. Next, we will combine all the above factors and provide an end-to-end link budget calculation. By substituting Eq.(5.2) in Eq.(5.1), and considering the circuits efficiency, the harvested DC power at the IoT device can be calculated using the following equation.

$$P_{\mathrm{DC}} = EIRP + 10log(A_{\mathrm{e}}) - 20log(d) - 10log(4\pi) + 10log(\eta) \tag{5.3}$$

Note, in our calculation, we replaced $P_t + G_t$ with $EIRP$, as defined by FCC regulations. Furthermore, we assume that the IoT node dimensions are constant regardless of the operating frequency, meaning that the allowable antenna aperture size will be the same regardless of the operating frequencies. Finally, we convert the received power to DC power by considering the RF to DC PCE (η).

As Eq.(5.3) shows, the harvested power at the IoT is a function of $EIRP$, IoT antenna aperture size (A_e), distance (d), and RF to DC conversion efficiency (η). Interestingly, the harvested power is not dependent on the operating frequency. This is due to the fact that although higher frequency signals suffer from higher path loss but their antennas have much higher gain (for the same aperture size). Therefore, these two factors counterbalance each other's effects. Finally, it is worth mentioning that although η is lower for mmWave, mmWave has much higher EIRP which compensates for its lower circuit efficiency. In particular, mmWave EIRP is 100 times (20 dB) higher than EIRP of lower frequency signals, while its efficiency is just 20-30% lower as shown in Table 5.1. In Figure 5.7, we calculate the harvested DC power for different distances and different operating frequencies, from 900 MHz up to 28 GHz. Our results shows that mmWave is a much better candidate than other frequencies to transfer power.

5.3 Addressing the Challenges of mmWave Power Transfer

In this section we illustrate the challenges of mmWave power transfer and introduce mmCharge, a mmWave power transfer system for indoor low-power IoT devices. To build mmCharge we need to address three challenges: achieving low-power beamforming at the IoT node to harvest power from multiple directions; integrating a low-power protocol for beam alignment; and addressing the self-interference issue. For illustration, we use a typical indoor scenario with multiple IoT nodes that harvests power from a mmWave access point (AP), as shown in Figure 5.1. In this scenario, one or more nodes which receives power from

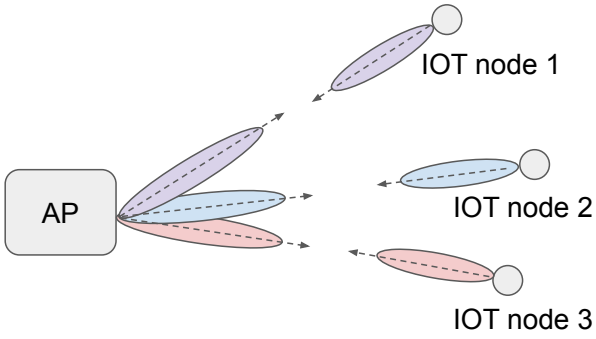

Figure 5.1: mmWave Power Transfer Example

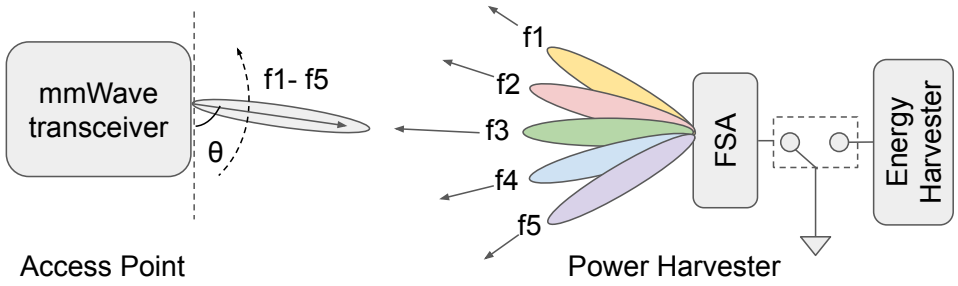

Figure 5.2: mmCharge Beam Alignment

a mmWave access point (AP) and uses it to charge their battery. First, the AP and the node find needs to find the best direction to align their beams. Once both transmitter and receiver beams are aligned, the AP transmits a high-power signal to the node. The node receives this signal and passes it to its harvesting circuit to convert it to the DC power.

Beamforming Challenge: Due to the property of mmWave signals, both the AP and the IoT node need to first create beams and then align them before transferring power. We assume the AP is equipped with a phased array and hence can electronically create and steer its beam toward the node. However, for the IoT node, we cannot use phased array due to complexity and power consumption. Existing mmWave power harvesters generally use an array or grid of antenna elements, forming a fixed beam to receive power [NST16, HAB20]. This limits the power harvesting efficiency at different orientations and during mobility. To achieve low-complexity and low-power beamforming on the IoT node, enabling it to harvest

power across multiple directions, we design a passive antenna system based on Frequency Scanning Antenna (FSA). FSA is a passive structure which transmits or receives signals from a specific direction such that the angle of the direction is a function of the signal frequency, as shown in Figure 5.4(b). Compared to traditional beamforming techniques such as phased arrays that utilize power-hungry phase shifters to form beams in different directions, FSA forms beams based on the natural effect of phase shift caused by the difference in signal wavelength when the signal travels through the structure of the FSA [li2]. Hence, FSA can form beams in multiple directions, while being simple, passive, with no power consumption.

Beam Alignment Challenge: Secondly, we need a low-power solution to align the beams of the AP and the IoT node. Most existing mmWave power transfer systems require the power harvester to constantly monitor the received power level and provide feedback to the power transmitter through either Bluetooth or WiFi [HAB23, SWC23], while the transmitter adjusts its beam direction. However, this significantly increases the power consumption on the harvester, rendering it impractical for low-power IoT devices. We propose a system that combines frequency scanning technique with backscatter technique to address this challenge. Due to the special nature of FSA, to align the AP's and node's beams, the AP needs to determine two parameters: (1) the optimal direction to transmit the signal; (2) the optimal frequency of the signal. Note, the signal frequency is important since only a specific frequency results in the FSA beam to become aligned toward the AP. In particular, the AP must sweep these two parameters to find the combination which results in the highest received power at the IoT node [1]. To enable the IoT node to provide feedback to the AP about its received power without consuming energy, we propose a solution similar to RFID and backscatter technology. In particular, instead of directly connecting the FSA to the energy harvesting circuit, we connect it to a switch which connects the FSA to either a ground or the harvesting circuit, as shown in Figure 5.2. During the beam alignment process,

[1]Beam sweeping is an inherent part of cellular and WiFi standards for mmWave communication [3GP17b, IEE21b]. These mmWave access points generally support multiple frequency channels. We believe this will also be the expected behaviour for future mmWave access points.

the node connects the FSA to the ground. In this mode, the FSA works as a reflector and reflects the received signal back. The strength of the reflected signal is determined by the direction of the FSA beam for that frequency in relation to the direction of the AP's beam. The AP then measures the power of the reflection for all combination of the frequency and transmitting beam angle and pick the combination which results in the highest reflection power. However, one issue with this solution is that it takes a long time to find the best beam alignment. For example, if the AP has to try N different directions for its beam, and there are M different signal frequencies to try, it would take $N \times M$ measurements. To speed up this process, instead of sweeping both frequency and direction, the AP transmits at all frequency choices simultaneously, and only sweeps its beam direction. For each beam direction, the AP receives the reflected signal and creates a profile of received signal strength across frequency. Finally, the AP compares all the measured profiles and picks the direction and frequency that provide the highest reflection power. Once the optimal frequency and transmitter beam direction is discovered, the node moves to the harvesting mode.

Self-Interference Challenge: The third challenge is that the reflected signal from the FSA is much weaker than the AP's transmitted signal. In particular, the AP needs to extract the weak reflected signal from its own transmitted signal which creates a strong self-interference. To solve this self-interference problem, one solution is to use full-duplex radio at the AP. However, full duplex radios are very complex and are not available in today's mmWave access points. To overcome this problem, the FSA switches between reflection and absorption modes to modulate the the reflected signal to a different frequency. For example, if the AP transmits at frequencies f_1, f_2 and f_3 the IoT node modulates this signal by turning the FSA on and off at the rate of f_s. Hence, the frequency of the reflected signal will be $f_1 + f_s$, $f_2 + f_s$ and $f_3 + f_s$. Thus this makes it much easier for the AP to measure the reflected signal from its own transmitted signal. Finally, it worth mentioning that the backscatter modulation can be easily implemented by switching the FSA switch (as shown in Figure 5.2) between the ground and harvester circuit.

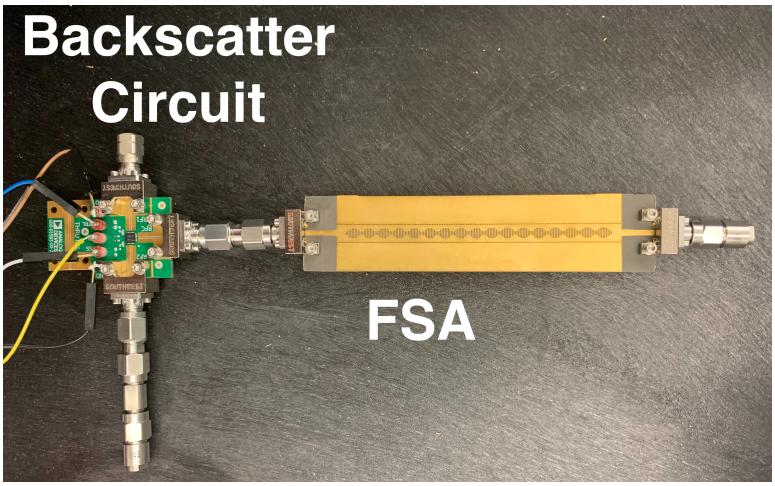

Figure 5.3: mmCharge Implementation.

5.4 Implementation

To evaluate the performance of the mmCharge system, we have implemented a prototype as shown in Figure 5.3. We have implemented an FSA operating at the mmWave frequency band between 26.5 to 29.5 GHz with an beam steering angle around 50 degrees. We connected our FSA to a backscatter circuit to reflect the received signal back to the AP for beam alignment. To address the self-interference challenge, the backscatter circuit is also connected to a switch which modulates the reflected signal by a fixed frequency shift. Our prototype can be further connected to a power harvesting circuit to convert the received signal to DC power. In this implementation, we can manually switch between power harvesting mode and backscatter (beam alignment) mode.

5.5 Evaluation

Below, we evaluate the performance of mmCharge using both simulation and real-world experiments. We designed and simulated a mmWave FSA similar to the technique presented

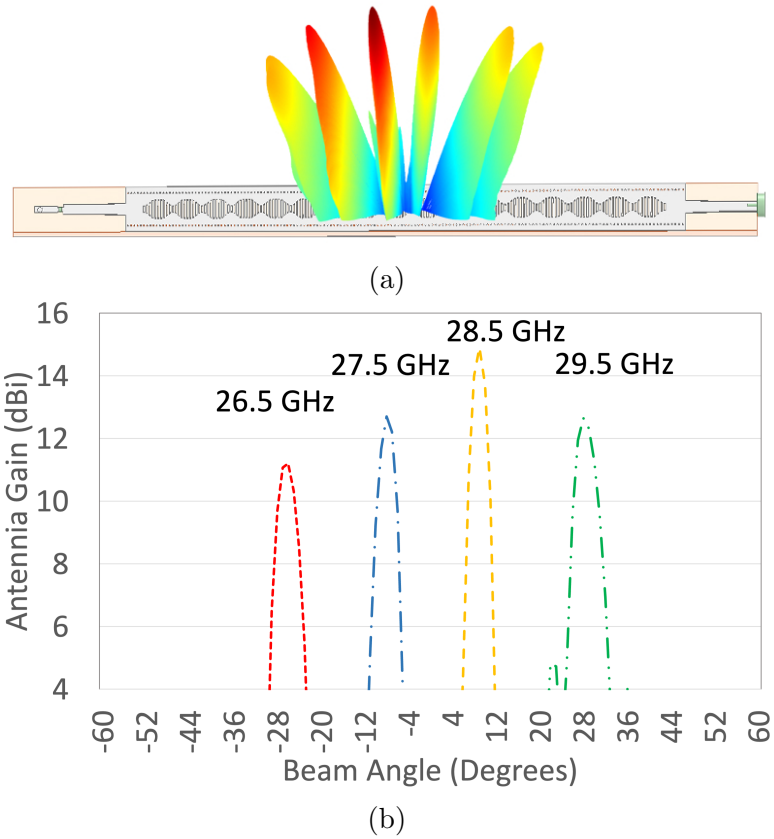

Figure 5.4: Our Designed FSA and its receiving pattern.

in [li2]. First, we present the performance results of the FSA design. Then we present the performance of mmCharge in receiving and converting the mmWave signal into DC power.

5.5.1 FSA Results

Figure 5.4(a) shows the structure of our designed FSA. It is very compact in size, with dimensions of $110 \times 7 \times 0.5$ mm. Figure 5.4(b) shows the radiation (or receiving) pattern of the FSA at different frequencies simulated by CST Microwave Studio. These results show that the FSA is able to effectively create a beam and steer it by changing the signal frequency. In particular, the design achieves a beam steering angle of approximately 56 degrees (-28^o

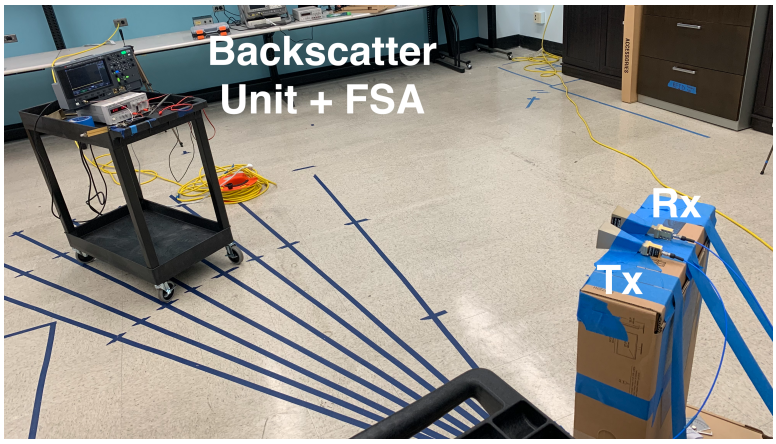

Figure 5.5: mmCharge Beam Alignment Setup.

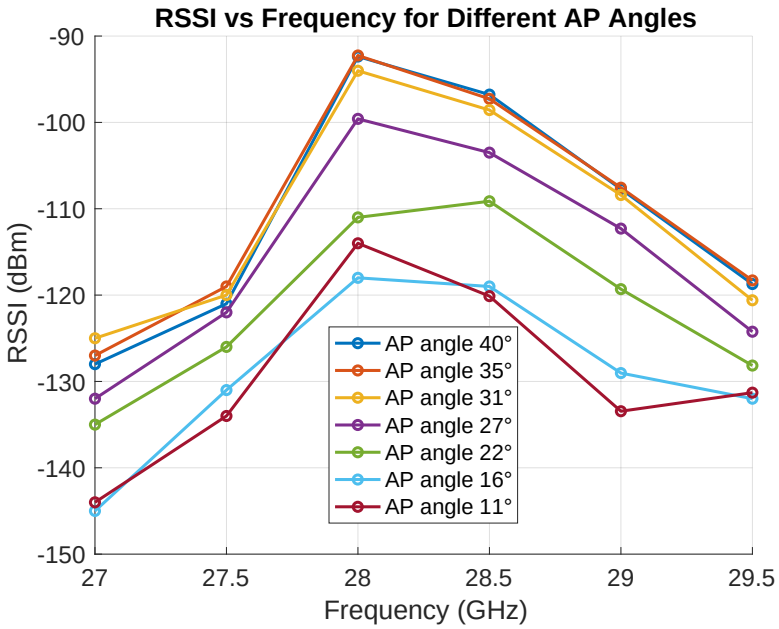

Figure 5.6: Measured RSSI Profile at Different Angles

to 28^o) across the mmWave 5G band of 26.5 to 29.5 GHz [2].

5.5.2 Beam Alignment Performance

Next, we evaluate the performance of mmCharge's beam alignment protocol. In this experiment, our goal is to evaluate how accurate mmCharge's beam alignment protocol can align the beam angle and signal frequency of the AP based on the feedback from the power harvester. Our experiment setup is shown in Figure 5.5. On the power harvester side, we connected our designed FSA to a backscatter circuit to reflect the signal transmitted by the AP. The backscatter circuit is also connected to a switch which modulates the reflected signal by 100 KHz, to avoid the self-interference problem at the AP. The distance between the AP and the power harvester is 1.5 meters. On the AP side, we connected a transmitter antenna (Tx) and a receiving antenna (Rx) to the AP for transmitting the signal and receiving the backscattered signal respectively. We then placed the power harvester at 37 degrees relative to the AP. Following the beam alignment protocol, the AP steers its transmitter beam to different angles and different frequencies, while we measure the received signal power of the backscattered signal at the AP. Figure 5.6 shows the received signal pattern on the AP. We can clearly distinguish the peak angle to be between 35 and 40 degrees, and the peak frequency is 28 GHz. This means, mmCharge is able to efficient align the beam direction and signal frequency of the AP based on our beam alignment protocol. The AP is able to select the best beam angle and signal frequency for transmitting power to achieve the best power transfer efficiency.

5.5.3 End-to-End Performance

Next, we evaluate the performance of mmCharge in transferring power from an AP to IoT devices in an indoor environment. We use our analysis presented in Section 5.2.2, and perform an end-to-end simulation to estimate the amount of power an IoT device can harvest.

[2]The bandwidth of cellular or WiFi mmWave bands ranges between 1 to 8.64 GHz GHz [Wik23, IEE21b], which is more than enough to achieve a good angle of coverage for the FSA.

To evaluate the correctness of our simulations, we also run some real-world measurements in an indoor environment. Figure 5.7 shows the result of our simulation. The figure shows the amount of power an IoT can harvest across different distances between an indoor AP and an IoT node for different operating frequencies. As the figure shows, mmWave signals can transfer much higher power compared to other frequencies. As mentioned earlier, this is due to the fact that mmWave AP can transmit much higher power (EIRP) based on FCC regulations. Moreover, for the same antenna aperture, mmWave antennas have much higher gain and hence they collect higher power. Note, in our evaluation, we assume an EIRP of 55 dBm for the mmWave AP (which is based on FCC). We also assume that the aperture size of the IoT device is $100cm^2$ which is equivalent to the size of two credit cards. Our results show that mmCharge's nodes can harvest 1mW and 0.1mW power when they are 7.5 m and 15 m away from an indoor mmWave AP, respectively. The figure also plots the average power consumption of a typical IoT device using a solid purple line [3]. Interestingly, mmCharge provides more power than the device average power consumption even when they are 15 meters spaced, which is more than enough for most indoor scenarios. In an outdoor scenario, due to much higher FCC EIRP limit [FCC23a], this power transmission distance can reach to 150 meters based on our link budget analysis. It is worth mentioning that the distance can be further improved by using larger antenna aperture for the IoT node. One of the main limiting factors of mmWave wireless power transfer is the PCE of the rectifiers [WWB20]. Figure 5.7 is based on the performance data of mmWave rectifiers shown in recent literature (Table 5.1). With the development of semiconductors, the PCE of rectifiers at mmWave frequency is expected to improve further, thus the harvested power at mmWave frequency would continue to increase in the future. This results show that mmCharge has the potential to transfer power from an AP to IoT devices and significantly improve their batterylife.

[3]We use the Google Nest Temperature Sensor as an example. It can run on a single CR2 3V lithium battery of 800 mAh capacity for two years. Considering 2400 mWh capacity and two years lifetime, the average power consumption of the device is around 0.14 mW.

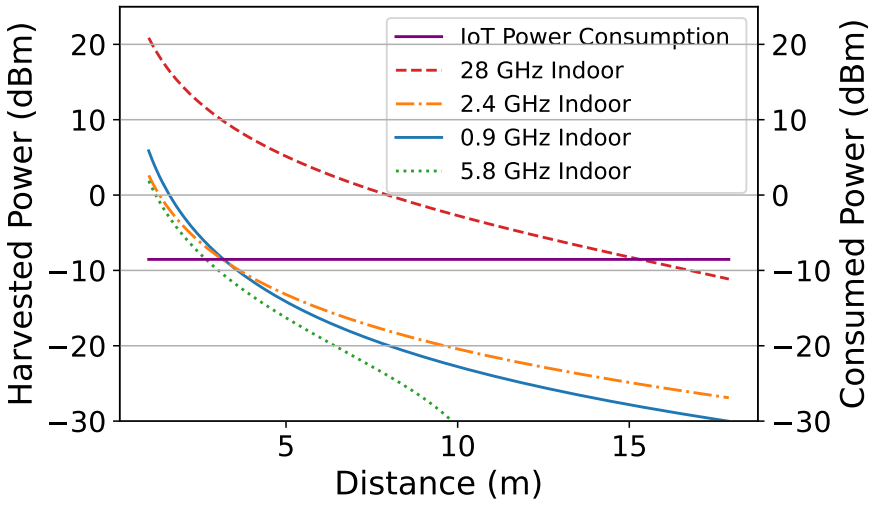

Figure 5.7: Harvested Power vs Distance ($100cm^2$ Aperture), based on our link budget analysis.

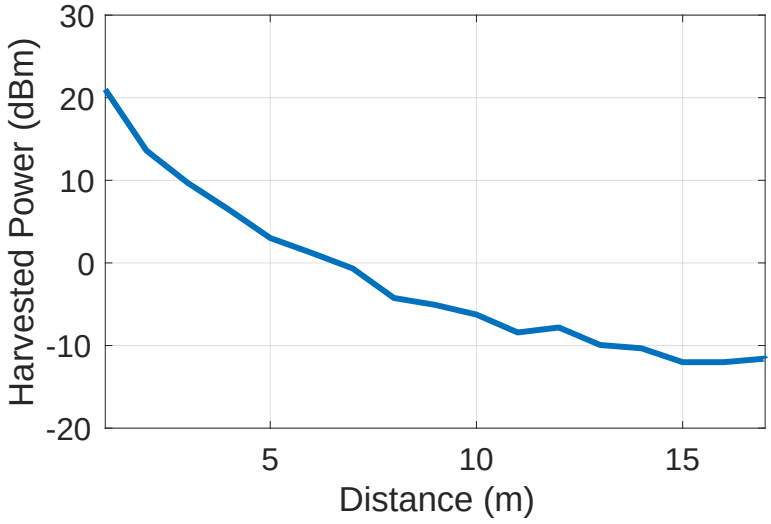

Figure 5.8: Measured Harvested Power vs Distance

Finally, we perform some real-world experiments to validate our simulation results. We used a signal generator (HP 83650B) as a mmWave AP and we used a spectrum analyzer (Agilent 8565EC). We connect them to to horn antennas and measure the received power at different distances. Note, although the EIRP can be as high as 55 dBm, the EIRP of the equipment was limited to 20 dBm. Hence, we performed the experiments at 20 dBm and then added 30 dB to it in post-processing. Finally, we also considered the efficiency of

converters in our measurement presentation. Figure 5.8 shows the result of this experiment. The results are very much aligned with our simulation results.

5.6 Conclusion and Discussion

In this chapter, we provided a comprehensive feasibility study to show that future indoor mmWave access points can power up IoT devices. In fact, our results showed that mmWave systems are a better candidate for wireless power transfer compared to the systems which use lower frequency RF signals. However, to enable this vision we needed to address multiple challenges. The most important challenge was to enable very low power beam alignment architecture and link establishment for mmWave power transfer. We presented mmCharge which introduces a new system based on frequency scanning technique and combined it with a backscatter technique to enable IoT devices to harvest energy from mmWave access point while consuming a minimum amount of energy. We believe this system provides the first step toward enabling future mmWave access points to transfer power to IoT devices besides enabling connectivity. Looking into the future, the design of mmCharge could be further extended to address certain challenges.

The first challenge is mode switching. The power harvester needs to switch between the backscatter (beam alignment) mode and harvesting mode. This requires the harvester to know when beam searching is done by the AP. One potential solution is to use a power divider, by which the harvester is always reflecting while it is also harvesting some power. However, this solution reduces the efficiency of the system since some of the received power is always reflected. Another solution is to design a switch which is triggered by the fluctuation in received power. In particular, when the beam searching is done and the received power remains stable, the switch will be triggered and switch the node to the harvesting mode. Exploring the effectiveness of these solutions is an interesting research direction.

The second challenge is the receiver sensitivity of the AP. mmCharge solves the self-

interference problem by modulating the reflected signal. However, this requires the AP's receiver to have high sensitivity to detect the reflected signal. In particular, the backscattered signal should be at least 5dB higher than the AP's noise floor to be detectable. Considering an AP with a typical noise floor of -86 dBm, the backscattered signal should be stronger than -81 dBm. Our preliminary results shows that this is achievable for the ranges which our system targets. However, a comprehensive study and experimental evaluation is required to confirm this.

CHAPTER 6

Summary and Future Work

This thesis illustrates how integrating passive beamforming into wireless communication, sensing, and power transfer can catalyze a host of new applications. We have meticulously designed and constructed comprehensive systems for communication, sensing, and power transfer utilizing Frequency Scanning Antenna (FSA) technology. These systems are seamlessly integrate with existing wireless protocols, significantly boosting their range, performance and enabling new capabilities. Here, we provide a summary of our work and propose some potential directions for future research.

6.1 Summary

In this section we summarize the main contributions of this thesis. In this thesis, we introduce three pieces of work to solve the challenges of modern wireless networks using passive beamforming:

mmXtend: An On-Demand mmWave Repeater to Solve mmWave Signal Blockage We present mmXtend, the first repeater which uses passive beamforming to solve the blockage problem of mmWave networks in outdoor and indoor scenarios. mmXtend is low-cost, low-power, and can be seamlessly deployed whenever and wherever is needed without needing to modify the communication end-points. We introduce a novel design which enables the repeater to perform 2D passive beamforming, providing reliable high-data-rate connectivity to thousands of users even when they are hundreds of meters away from the

base station and their line-of-sight path to it is blocked

Wi-Pro: A Plug-and-Play Module to Enhance WiFi Performance We present Wi-Pro, a new plug-and-play FSA antenna which can be integrated with any commodity WiFi devices, even low-power IoT devices with a single transceiver chain. By combining FSA with the inherent features of existing WiFi protocol, Wi-Pro is able to improve the performance of WiFi for both communication and direction measurement. In terms of communication, Wi-Pro is able to focus the signal of a particular RU toward the designated user, which greatly increases data rate and communication distance of individual users in the network. In terms of direction measurement, Wi-Pro is able to measure the direction of any WiFi devices in the vicinity, including low-cost, low-power devices with a single transceiver chain, without requiring firmware or chipset updates. Finally, we implemented Wi-Pro and evaluated its performance in various indoor settings.

mmCharge: A mmWave Power Transfer System to Increase the Range of mmWave Power Transfer We first provide a comprehensive feasibility study to show that mmWave access points are more suitable for powering IoT devices compared to lower frequency RF systems and it has the potential to power up low-power IoT devices. We present mmCharge which introduces a new system based on passive beamforming and combined it with a backscatter technique to enable IoT devices to harvest energy from mmWave access point while consuming a minimum amount of energy. We develope a low-power beam alignment and link establishment protocol based on FSA for mmWave energy transfer. We believe this paper provides the first step toward enabling future mmWave access points to transfer power to IoT devices besides enabling connectivity.

6.2 Future Work

In this section we discuss some potential future directions of using passive beamforming in wireless systems.

6.2.1 Enabling Dual-Sided Passive Beamforming for mmWave Repeater

In this thesis we introduced mmXtend, which uses Rotman Lens and FSA to perform 2D passive beamforming to a crowd of users. One limitation of our mmXtend prototype is the use of fixed beam horn antennas for the backhaul connectivity. This potentially limits the ability of mmXtend to receive signals from other base stations and requires reconfiguration of the backhaul beam every time the repeater is moved. To address this challenge future research could focus on enabling 2D passive beamforming not only for the repeater-to-user link but also for the repeater-to-base station link. This adaptation would allow the repeater to receive signals from base stations at different angles, eliminating the need for manual adjustment of the backhaul antenna upon initial deployment or relocation of the repeater. However, integrating a dual-sided 2D beamforming system onto a single PCB presents a new set of hardware design challenges.

6.2.2 Enhancing RFID Performance Using FSA

A promising avenue for future research is the integration of FSA with RFID (Radio Frequency Identification) systems. RFID technology comprises two principal components: an RFID tag and an RFID reader. A notable limitation of current RFID systems is their restricted operational range [WCA22]. Enhancing the reader's antenna gain extends this range but at the expense of a narrower beam, consequently diminishing the coverage angle. FSA offers a viable approach to facilitate passive beamforming in multiple directions. However, steering the FSA's beam requires the transmission of signals at varying frequencies. RFID readers typically perform frequency hopping, periodically transmitting signals at different frequencies to mitigate interference from other RFID readers or nearby wireless transmitters. This characteristic of frequency hopping, when combined with the beamforming capabilities of FSA, allows the reader to direct a high-gain, narrow beam in various directions. Such an approach not only amplifies the working distance of RFID systems but also maintains

a broad angle of coverage. Another challenge of RFID is interference between RFID tags. Today's RFID tags adopt ALOHA for medium access control. However, the time delay of ALOHA algorithm may hinder the performance of RFID in scenarios with a large number of tags. The beam steering feature of FSA could also allows tags in different directions to reflect using different signal frequencies, which may potentially improve the efficiency of tag communication. However, the limited working bandwidth of RFID presents a significant challenge in designing an FSA with an extensive angle of coverage.

6.2.3 Combining Power Harvesting and Backscatter Communication

Backscatter technology is a communication method that enables devices to transmit data by reflecting modulated wireless signals off their antennas [MCA21, AA21, ADM20, DAB21, AMA18]. This technique is known for its low power consumption and simplicity, making it highly valuable in various fields such as IoT. Previous work has shown the potential of using backscatter and FSA to enable two-way mmWave communication [LMR23]. In this thesis, we present mmCharge, illustrating how FSA and backscatter can be used together to increase the range of mmWave power harvesting. Looking ahead, a potential area of research lies in integrating backscatter with FSA for simultaneous power transfer and communication. This integration could significantly prolong the operational lifespan of IoT devices. Nonetheless, this advancement hinges on the development of circuitry capable of flexibly alternating or balancing between power harvesting and communication modes.

6.3 Closing Remarks

In summary, this thesis serves as a pivotal exploration into the cross-layer approach for enhancing wireless system performance. It bridges the gap between antenna hardware design, signal processing, and wireless network protocols, offering a comprehensive perspective on improving the overall efficacy of wireless systems. We demonstrate that FSA provide a

low-power low-complexity method for beamforming and beam steering based on signal frequency, introducing a novel approach to overcoming the challenges in contemporary wireless networks. Our research serves as a fundamental exploration in the development of comprehensive systems encompassing communication, sensing, and wireless power transfer using FSA. It sets a solid foundation for subsequent advancements and future research in this field.

REFERENCES

[3GP17a] 3GPP. "3GPP TR 38.802 Release 14 - 6.1.6.1 Beam Management." https://www.3gpp.org/ftp/Specs/archive/38_series/38.802/, 2017.

[3GP17b] 3GPP. "3GPP TR 38.802 Release 14 - 6.2.3.1 Synchronization signal and DL broadcast signal/channel structure." https://www.3gpp.org/ftp/Specs/archive/38_series/38.802/, 2017.

[3GP21a] 3GPP. "3GPP TS 38.104 Release 17 - 5.3A BS channel bandwidth for CA." https://www.3gpp.org/ftp/Specs/archive/38_series/38.104/, 2021.

[3GP21b] 3GPP. "3GPP TS 38.104 Release 17 - 5.4.3 Synchronization Raster." https://www.3gpp.org/ftp/Specs/archive/38_series/38.104/, 2021.

[3GP22] 3GPP. "3GPP TS 38.306 V17.3.0 - 5 UE radio access capability parameters." https://www.3gpp.org/ftp/Specs/archive/38_series/38.306/, 2022.

[3GP23] 3GPP. "3GPP TS 38.101-2 Release 18 - 5.2 Operating Bands." https://www.3gpp.org/ftp/Specs/archive/38_series/38.101-2/, 2023.

[5GW20] 5GWorldPro.com. "What are 5G Beam management procedures." https://www.5gworldpro.com/5g-knowledge/what-are-5g-beam-management-procedures.html, 2020.

[AA21] Ali Abedi and Omid Abari. "Can WiFi Backscatter Achieve the Range of RFID? Nulling to the Rescue." In *Proceedings of the Twentieth ACM Workshop on Hot Topics in Networks*, pp. 171–177, 2021.

[ABD17] Omid Abari, Dinesh Bharadia, Austin Duffield, and Dina Katabi. "Enabling high-quality untethered virtual reality." In *14th {USENIX} Symposium on Networked Systems Design and Implementation ({NSDI} 17)*, pp. 531–544, 2017.

[ADM20] Ali Abedi, Farzan Dehbashi, Mohammad Hossein Mazaheri, Omid Abari, and Tim Brecht. "Witag: Seamless wifi backscatter communication." In *Proceedings of the Annual conference of the ACM Special Interest Group on Data Communication on the applications, technologies, architectures, and protocols for computer communication*, pp. 240–252, 2020.

[AHR16] Omid Abari, Haitham Hassanieh, Michael Rodreguiz, and Dina Katabi. "Poster: A millimeter wave software defined radio platform with phased arrays." In *Proceedings of the 22nd Annual International Conference on Mobile Computing and Networking*, pp. 419–420, 2016.

[AMA18] Ali Abedi, Mohammad Hossein Mazaheri, Omid Abari, and Tim Brecht. "Witag: Rethinking backscatter communication for wifi networks." In *Proceedings of the 17th ACM Workshop on Hot Topics in Networks*, pp. 148–154, 2018.

[App23] Apple. "iPhone 14 Pro Technical Spec." `https://www.apple.com/iphone-14-pro/specs/`, 2023.

[BJR17] Nikola Boskovic, Branka Jokanovic, and Milos Radovanovic. "Printed frequency scanning antenna arrays with enhanced frequency sensitivity and sidelobe suppression." *IEEE Transactions on Antennas and Propagation*, **65**(4):1757–1764, 2017.

[Bri53] Leon Brillouin. *Wave propagation in periodic structures: electric filters and crystal lattices*, volume 2. Dover publications, 1953.

[CHW10] Yu Jian Cheng, Wei Hong, Ke Wu, and Yong Fan. "Millimeter-wave substrate integrated waveguide long slot leaky-wave antennas and two-dimensional multibeam applications." *IEEE Transactions on Antennas and Propagation*, **59**(1):40–47, 2010.

[CLC20] Qiang Chen, Zhihao Liu, Yuguo Cui, Haotian Cai, and Xing Chen. "A Metallic Waveguide-Integrated 35-GHz Rectenna With High Conversion Efficiency." *IEEE Microwave and Wireless Components Letters*, **30**(8):821–824, 2020.

[CMG23] Kun Woo Cho, Mohammad H Mazaheri, Jeremy Gummeson, Omid Abari, and Kyle Jamieson. "{mmWall}: A Steerable, Transflective Metamaterial Surface for {NextG}{mmWave} Networks." In *20th USENIX Symposium on Networked Systems Design and Implementation (NSDI 23)*, pp. 1647–1665, 2023.

[CVF17] René Camblor, Samuel Ver Hoeye, Miguel Fernandez, Carlos Vázquez Antuña, and Fernando Las-Heras. "Full 2-D submillimeter-wave frequency scanning array." *IEEE Transactions on Antennas and Propagation*, **65**(9):4486–4494, 2017.

[DAB21] Farzan Dehbashi, Ali Abedi, Tim Brecht, and Omid Abari. "Verification: can wifi backscatter replace RFID?" In *Proceedings of the 27th Annual International Conference on Mobile Computing and Networking*, pp. 97–107, 2021.

[Das23] Dassault Systèmes. "CST STUDIO SUITE." Computer software, 2023. Available: https://www.3ds.com/products-services/simulia/products/cst-studio-suite/.

[Dev22] Analog Devices. "ADL8142: GaAs, pHEMT, MMIC, Low Noise Amplifier, 23 GHz to 31 GHz Data Sheet (Rev. A)." `https://www.analog.com/media/en/technical-documentation/data-sheets/adl8142.pdf`, 2022.

[DJI23] DJI. "DJI Consumer Drones Comparison." https://www.dji.com/products/comparison-consumer-drones, 2023.

[EAH15] Mohammed E Eltayeb, Ahmed Alkhateeb, Robert W Heath, and Tareq Y Al-Naffouri. "Opportunistic beam training with hybrid analog/digital codebooks for mmWave systems." In *GlobalSIP*, pp. 315–319. IEEE, 2015.

[EHT20] Aline Eid, Jimmy GD Hester, and Manos M Tentzeris. "Rotman lens-based wide angular coverage and high-gain semipassive architecture for ultralong range mm-wave RFIDs." *IEEE Antennas and Wireless Propagation Letters*, **19**(11):1943–1947, 2020.

[EHT21a] Aline Eid, Jimmy Hester, and Manos Tentzeris. "5G as a Wireless Power Grid." *Scientific Reports*, 01 2021.

[EHT21b] Aline Eid, Jimmy GD Hester, and Manos M Tentzeris. "5G as a wireless power grid." *Scientific Reports*, **11**(1):636, 2021.

[ENA16] Mohamed El Rayes, Gihan Nagib, and Wahied Abdelaal. "A Review on Wireless Power Transfer." *International Journal of Engineering Trends and Technology (IJETT)*, **40**:272, 10 2016.

[Exp21] Mobile Experts. "White Paper: 5G mmWave Repeaters Cut Costs in Half." https://mobile-experts.net/reports/p/white-paper-semiconductors-for-oran-ss6db, 2021.

[FCC23a] FCC. "FCC EIRP Limit for Outdoor Base Station in the 24 GHz, 28 GHz and 39 GHz bands." https://www.ecfr.gov/current/title-47/chapter-I/subchapter-B/part-30, 2023.

[FCC23b] FCC. "FCC EIRP Limit for Wireless Access Points." https://www.ecfr.gov/current/title-47/chapter-I/subchapter-A/part-15, 2023.

[FCC23c] FCC. "FCC mmWave Transmit Power Regulation." https://www.ecfr.gov/current/title-47/chapter-I/subchapter-B/part-30, 2023.

[FMT17] Valerio Frascolla, Federico Miatton, Gia Khanh Tran, Koji Takinami, Antonio De Domenico, Emilio Calvanese Strinati, Konstantin Koslowski, Thomas Haustein, Kei Sakaguchi, Sergio Barbarossa, et al. "5G-MiEdge: Design, standardization and deployment of 5G phase II technologies: MEC and mmWaves joint development for Tokyo 2020 Olympic games." In *2017 IEEE Conference on Standards for Communications and Networking (CSCN)*, pp. 54–59. IEEE, 2017.

[For] Forbes. ""2018 Roundup Of Internet Of Things Forecasts And Market Estimates".".

[FRT22] FRTek. "FRTek 28GHz 5G Wireless Optical Distributed Repeater." `http://www.frtek.com/en/board/board.php?bo_table=wireless&cate=DAS&idx=101`, 2022.

[GHY21] Zhihao Gu, Taiwei He, Junwei Yin, Yuedong Xu, and Jun Wu. "TyrLoc: A Low-Cost Multi-Technology MIMO Localization System with a Single RF Chain." In *Proceedings of the 19th Annual International Conference on Mobile Systems, Applications, and Services*, MobiSys '21, p. 228–240, New York, NY, USA, 2021. Association for Computing Machinery.

[GLP23] Alejandro Gil-Martinez, José Antonio López-Pastor, Miguel Poveda-García, Astrid Algaba-Brazález, David Cañete-Rebenaque, and José Luis Gómez-Tornero. "Monopulse Leaky-Wave Antennas for RSSI-based Direction Finding in Wireless Local Area Networks." *IEEE Transactions on Antennas and Propagation*, 2023.

[GPL21] Alejandro Gil-Martínez, Miguel Poveda-García, Jose Antonio López-Pastor, Juan Carlos Sánchez-Aarnoutse, and José Luis Gómez-Tornero. "Wi-Fi direction finding with frequency-scanned antenna and channel-hopping scheme." *IEEE Sensors Journal*, **22**(6):5210–5222, 2021.

[GPO21] Jean-Baptiste Gros, Vladislav Popov, Mikhail A Odit, Vladimir Lenets, and Geoffroy Lerosey. "A reconfigurable intelligent surface at mmWave based on a binary phase tunable metasurface." *IEEE Open Journal of the Communications Society*, **2**:1055–1064, 2021.

[Gua18] Dong-Fang Guan et al. "Scanning rate enhancement of leaky-wave antennas using slow-wave substrate integrated waveguide structure." *IEEE Transactions on Antennas and Propagation*, **66**(7):3747–3751, 2018.

[GYS20] Yasaman Ghasempour, Chia-Yi Yeh, Rabi Shrestha, Daniel Mittleman, and Edward Knightly. "Single shot single antenna path discovery in THz networks." In *Proceedings of the 26th Annual International Conference on Mobile Computing and Networking*, pp. 1–13, 2020.

[HAB20] Ali Hajimiri, Behrooz Abiri, Florian Bohn, Matan Gal-Katziri, and Mohith H Manohara. "Dynamic focusing of large arrays for wireless power transfer and beyond." *IEEE Journal of Solid-State Circuits*, **56**(7):2077–2101, 2020.

[HAB23] Seyed Ali Hajimiri, Behrooz Abiri, Florian Bohn, and Farhud Tebbi. "Dynamic focusing and tracking for wireless power transfer arrays.", May 23 2023. US Patent 11,659,355.

[HAR18a] Haitham Hassanieh, Omid Abari, Michael Rodriguez, Mohammed Abdelghany, Dina Katabi, and Piotr Indyk. "Fast millimeter wave beam alignment." In

Proceedings of the 2018 Conference of the ACM Special Interest Group on Data Communication, pp. 432–445, 2018.

[HAR18b] Haitham Hassanieh, Omid Abari, Michael Rodriguez, Mohammed Abdelghany, Dina Katabi, and Piotr Indyk. "Fast millimeter wave beam alignment." In *Proceedings of the 2018 Conference of the ACM Special Interest Group on Data Communication*, pp. 432–445, 2018.

[IEE21a] IEEE. "IEEE 802.11ax-2021." `https://standards.ieee.org/ieee/802.11ax/7180/`, 2021.

[IEE21b] IEEE. "IEEE Standard for 802.11ay." `https://standards.ieee.org/ieee/802.11ay/6142/`, 2021.

[Ito04] Tatsuo Itoh. "Periodic structures for microwave engineering." In *MWE Microw. Workshop*, 2004.

[JCI12] David R. Jackson, Christophe Caloz, and Tatsuo Itoh. "Leaky-Wave Antennas." *Proceedings of the IEEE*, **100**(7):2194–2206, 2012.

[JLR21] Zhiping Jiang, Tom H Luan, Xincheng Ren, Dongtao Lv, Han Hao, Jing Wang, Kun Zhao, Wei Xi, Yueshen Xu, and Rui Li. "Eliminating the barriers: Demystifying wi-fi baseband design and introducing the picoscenes wi-fi sensing platform." *IEEE Internet of Things Journal*, **9**(6):4476–4496, 2021.

[JWG19] Suraj Jog, Jiaming Wang, Junfeng Guan, Thomas Moon, Haitham Hassanieh, and Romit Roy Choudhury. "{Many-to-Many} Beam Alignment in Millimeter Wave Networks." In *16th USENIX Symposium on Networked Systems Design and Implementation (NSDI 19)*, pp. 783–800, 2019.

[KCQ16] Amin Kianinejad, Zhi Ning Chen, and Cheng-Wei Qiu. "Low-loss spoof surface plasmon slow-wave transmission lines with compact transition and high isolation." *IEEE Transactions on Microwave Theory and Techniques*, **64**(10):3078–3086, 2016.

[Key23] Keysight. "Keysight 5G NR R&D Testbed." `https://www.keysight.com/us/en/products/modular/reference-solutions/5g-waveform-generation-analysis-testbed-reference-solution.html`, 2023.

[KGK14] Swarun Kumar, Stephanie Gil, Dina Katabi, and Daniela Rus. "Accurate indoor localization with zero start-up cost." In *Proceedings of the 20th annual international conference on Mobile computing and networking*, pp. 483–494, 2014.

[KHL22] Weiyang Kong, Yun Hu, Jiawang Li, Lei Zhang, and Wei Hong. "2-D Orthogonal Multibeam Antenna Arrays for 5G Millimeter-Wave Applications." *IEEE Transactions on Microwave Theory and Techniques*, **70**(5):2815–2824, 2022.

[KJB15] Manikanta Kotaru, Kiran Joshi, Dinesh Bharadia, and Sachin Katti. "Spotfi: Decimeter level localization using wifi." In *Proceedings of the 2015 ACM Conference on Special Interest Group on Data Communication*, pp. 269–282, 2015.

[KM14] Joongheon Kim and Andreas F Molisch. "Fast millimeter-wave beam training with receive beamforming." *Journal of Communications and Networks*, **16**(5):512–522, 2014.

[KZ13] Shaya Karimkashi and Guifu Zhang. "A dual-polarized series-fed microstrip antenna array with very high polarization purity for weather measurements." *IEEE transactions on antennas and propagation*, **61**(10):5315–5319, 2013.

[KZK13] Shaya Karimkashi, Guifu Zhang, Ahmed A Kishk, Wascar Bocangel, Redmond Kelley, John Meier, and Robert D Palmer. "Dual-polarization frequency scanning microstrip array antenna with low cross-polarization for weather measurements." *IEEE transactions on antennas and propagation*, **61**(11):5444–5452, 2013.

[li2] "Anonymized workshop paper.".

[LLI18] Belen Larumbe, Jaime Laviada, Asier Ibáñez-Loinaz, and Jorge Teniente. "Real-time imaging with frequency scanning array antenna for industrial inspection applications at W band." *Journal of Infrared, Millimeter, and Terahertz Waves*, **39**:45–63, 2018.

[LLL16] Shichao Li, Chao Li, Wei Liu, Zhaoyang Sun, Shinan Lang, Zheng Lu, Xiaojuan Zhang, and Guangyou Fang. "Study of terahertz superresolution imaging scheme with real-time capability based on frequency scanning antenna." *IEEE Transactions on Terahertz Science and Technology*, **6**(3):451–463, 2016.

[LLR22] Tianxiang Li, Haofan Lu, Reza Rezvani, Ali Abedi, and Omid Abari. "Bringing wifi localization to any wifi devices." In *Proceedings of the 21st ACM Workshop on Hot Topics in Networks*, pp. 46–52, 2022.

[LMR23] Haofan Lu, Mohammad Mazaheri, Reza Rezvani, and Omid Abari. "A Millimeter Wave Backscatter Network for Two-Way Communication and Localization." In *Proceedings of the ACM SIGCOMM 2023 Conference*, pp. 49–61, 2023.

[LWL17] Yujian Li, Junhong Wang, and Kwai-Man Luk. "Millimeter-wave multibeam aperture-coupled magnetoelectric dipole array with planar substrate integrated beamforming network for 5G applications." *IEEE transactions on antennas and propagation*, **65**(12):6422–6431, 2017.

[LWN15] Xiao Lu, Ping Wang, Dusit Niyato, Dong In Kim, and Zhu Han. "Wireless Networks With RF Energy Harvesting: A Contemporary Survey." *IEEE Communications Surveys & Tutorials*, **17**(2):757–789, 2015.

[MAA19a] Mohammad H Mazaheri, Soroush Ameli, Ali Abedi, and Omid Abari. "A millimeter wave network for billions of things." In *Proceedings of the ACM Special Interest Group on Data Communication*, pp. 174–186. 2019.

[MAA19b] Mohammad H Mazaheri, Soroush Ameli, Ali Abedi, and Omid Abari. "A millimeter wave network for billions of things." In *Proceedings of the ACM Special Interest Group on Data Communication*, pp. 174–186. 2019.

[Mai17] Robert J Mailloux. *Phased array antenna handbook*. Artech house, 2017.

[MCA21] Mohammad Hossein Mazaheri, Alex Chen, and Omid Abari. "Mmtag: A millimeter wave backscatter network." In *Proceedings of the 2021 ACM SIGCOMM 2021 Conference*, pp. 463–474, 2021.

[Met18] Metawave. "Successful Demonstration of 28GHz-Band 5G Using World's First Meta-Structure Technology." `https://www.metawave.com/post/successful-demonstration-of-28ghz-band-5g-using-world-s-first-meta-structure-t` 2018.

[Met21] Metawave. "Metawave Turbo." `https://www.metawave.com/post/metawave-selects-analog-devices-beamforming-technology-for-turbo-5g-repeater`, 2021.

[Mez18] Marco Mezzavilla et al. "End-to-end simulation of 5G mmWave networks." *IEEE Communications Surveys & Tutorials*, **20**(3):2237–2263, 2018.

[mov] movandi. "Movandi 5G Repeaters." https://movandi.com/smart-repeaters/.

[MRG23] Mohammad Mazaheri, Rafael Ruiz, Domenico Giustiniano, Joerg Widmer, and Omid Abari. "Bringing Millimeter Wave Technology to Any IoT Device." In *Proceedings of the 29th Annual International Conference on Mobile Computing and Networking*, pp. 1–15, 2023.

[ND95] A Nesic and S Dragas. "Frequency scanning printed array antenna." In *IEEE Antennas and Propagation Society International Symposium. 1995 Digest*, volume 2, pp. 950–953. IEEE, 1995.

[Nok23] Nokia. "DJI Consumer Drones Comparison." `https://www.nokia.com/networks/mobile-networks/airscale-radio-access/mmwave-radio/`, 2023.

[NST16] Med Nariman, Farid Shirinfar, Anna Papió Toda, Sudhakar Pamarti, Ahmadreza Rofougaran, and Franco De Flaviis. "A compact 60-GHz wireless power transfer system." *IEEE Transactions on Microwave Theory and Techniques*, **64**(8):2664–2677, 2016.

[PGC20] Miguel Poveda-García, Antonio Gómez-Alcaraz, David Cañete-Rebenaque, Alejandro Santos Martinez-Sala, and José Luis Gómez-Tornero. "RSSI-based direction-of-departure estimation in Bluetooth low energy using an array of frequency-steered leaky-wave antennas." *IEEE Access*, **8**:9380–9394, 2020.

[PGP17] Henna Paaso, Nikhil Gulati, Damiano Patron, Aki Hakkarainen, Janis Werner, Kapil R Dandekar, Mikko Valkama, and Aarne Mämmelä. "DoA estimation using compact CRLH leaky-wave antennas: Novel algorithms and measured performance." *IEEE Transactions on Antennas and Propagation*, **65**(9):4836–4849, 2017.

[PLS20] Chandan Pradhan, Ang Li, Lingyang Song, Branka Vucetic, and Yonghui Li. "Hybrid precoding design for reconfigurable intelligent surface aided mmWave communication systems." *IEEE Wireless Communications Letters*, **9**(7):1041–1045, 2020.

[qua] "The Benefits of OFDMA for Wi-Fi 6." `https://www.qualcomm.com/content/dam/qcomm-martech/dm-assets/documents/ofdma_white_paper.pdf`. Accessed: 2023-09-16.

[Qua18] Qualcomm. "VR and AR pushing connectivity limits." `https://www.qualcomm.com/media/documents/files/vr-and-ar-pushing-connectivity-limits.pdf`, 2018.

[Qua19] Qualcomm. "5G NR mmWave outdoor and indoor deployment strategy." `https://www.qualcomm.com/media/documents/files/deploying-5g-nr-mmwave-for-indoor-outdoor.pdf`, 2019.

[QYZ22] Kun Qian, Lulu Yao, Xinyu Zhang, and Tse Nga Ng. "MilliMirror: 3D printed reflecting surface for millimeter-wave coverage expansion." In *Proceedings of the 28th Annual International Conference on Mobile Computing And Networking*, pp. 15–28, 2022.

[Rem23] Remcom Inc. "Wireless InSite." Computer software, 2023. Available: https://www.remcom.com/wireless-insite-em-propagation-software.

[RKK12] Hariharan Shankar Rahul, Swarun Kumar, and Dina Katabi. "JMB: scaling wireless capacity with user demands." *ACM SIGCOMM Computer Communication Review*, **42**(4):235–246, 2012.

[RQH20] Pei Ren, Xiuquan Qiao, Yakun Huang, Ling Liu, Schahram Dustdar, and Junliang Chen. "Edge-assisted distributed DNN collaborative computing approach for mobile web augmented reality in 5G networks." *IEEE Network*, **34**(2):254–261, 2020.

[RVM12] Dinesh Ramasamy, Sriram Venkateswaran, and Upamanyu Madhow. "Compressive tracking with 1000-element arrays: A framework for multi-Gbps mm wave cellular downlinks." In *2012 50th Annual Allerton Conference on Communication, Control, and Computing (Allerton)*, pp. 690–697. IEEE, 2012.

[Sch86] Ralph Schmidt. "Multiple emitter location and signal parameter estimation." *IEEE transactions on antennas and propagation*, **34**(3):276–280, 1986.

[Sha22] ShareTechnote.com. "5G/NR - Beam Management." `https://www.sharetechnote.com/html/5G/5G_Phy_BeamManagement.html`, 2022.

[SNR20] Stefano Savazzi, Monica Nicoli, and Vittorio Rampa. "Federated learning with cooperating devices: A consensus approach for massive IoT networks." *IEEE Internet of Things Journal*, **7**(5):4641–4654, 2020.

[SPZ18] Sanjib Sur, Ioannis Pefkianakis, Xinyu Zhang, and Kyu-Han Kim. "Towards scalable and ubiquitous millimeter-wave wireless networks." In *Proceedings of the 24th Annual International Conference on Mobile Computing and Networking*, pp. 257–271, 2018.

[SRT19] David A Schneider, Markus Rösch, Axel Tessmann, and Thomas Zwick. "A low-loss W-band frequency-scanning antenna for wideband multichannel radar applications." *IEEE Antennas and Wireless Propagation Letters*, **18**(4):806–810, 2019.

[Sta] Statista. ""Number of Internet of Things (IoT) connected devices worldwide from 2019 to 2030".".

[SVL21] Hooman Saeidi, Suresh Venkatesh, Xuyang Lu, and Kaushik Sengupta. "Thz prism: One-shot simultaneous localization of multiple wireless nodes with leaky-wave thz antennas and transceivers in cmos." *IEEE Journal of Solid-State Circuits*, **56**(12):3840–3854, 2021.

[SWC23] Chaoyun Song, Lei Wang, Zhensheng Chen, George Goussetis, Guy AE Vandenbosch, and Yi Huang. "Wideband mmWave Wireless Power Transfer: Theory, Design and Experiments." In *2023 17th European Conference on Antennas and Propagation (EuCAP)*, pp. 1–5. IEEE, 2023.

[Sys23] Voltaic Systems. "1 Watt 6 Volt Solar Panel." `https://voltaicsystems.com/1-watt-panel/`, 2023.

[SZR16] Sanjib Sur, Xinyu Zhang, Parmesh Ramanathan, and Ranveer Chandra. "BeamSpy: Enabling robust 60 GHz links under blockage." In *13th {USENIX} Symposium on Networked Systems Design and Implementation ({NSDI} 16)*, pp. 193–206, 2016.

[TBS21] Sergei Tutelian, Dmitry Bankov, Dmitri Shmelkin, and Evgeny Khorov. "IEEE 802.11 ax OFDMA resource allocation with frequency-selective fading." *Sensors*, **21**(18):6099, 2021.

[Tim] Economic Times. ""Households have 10 connected devices now, will rise to 50 by 2020".".

[TSK18] Xin Tan, Zhi Sun, Dimitrios Koutsonikolas, and Josep M Jornet. "Enabling indoor mobile millimeter-wave networks based on smart reflect-arrays." In *IEEE INFOCOM 2018-IEEE Conference on Computer Communications*, pp. 270–278. IEEE, 2018.

[Twe22] Tweet4Technology.com. "5G NR: 5G-NR Cell Search Procedure." `https://tweet4technology.blogspot.com/2019/10/5g-cell-search-procedure.html`, 2022.

[VD14] Christopher Valenta and Gregory Durgin. "Harvesting Wireless Power: Survey of Energy-Harvester Conversion Efficiency in Far-Field, Wireless Power Transfer Systems." *Microwave Magazine, IEEE*, **15**:108–120, 06 2014.

[VGA13] Carlos Vázquez, Cebrian Garcia, Yuri Alvarez, Samuel Ver-Hoeye, and Fernando Las-Heras. "Near field characterization of an imaging system based on a frequency scanning antenna array." *IEEE transactions on antennas and propagation*, **61**(5):2874–2879, 2013.

[VKM21] Sarath Sankar Vinnakota, Runa Kumari, Himanshu Meena, and Basudev Majumder. "Rectifier integrated multibeam Luneburg lens employing artificial dielectric as a wireless power transfer medium at mm wave band." *IEEE Photonics Journal*, **13**(3):1–14, 2021.

[VSS14] Shruti Vashist, MK Soni, and PK Singhal. "A review on the development of Rotman lens antenna." *Chinese Journal of Engineering*, **2014**(11):1–9, 2014.

[WCA22] Ju Wang, Liqiong Chang, Omid Abari, and Srinivasan Keshav. "How Manufacturers Can Easily Improve Working Range of Passive RFIDs." In *2022 19th Annual IEEE International Conference on Sensing, Communication, and Networking (SECON)*, pp. 452–460. IEEE, 2022.

[WCC17] Xiaoli Wang, Aakanksha Chowdhery, and Mung Chiang. "Networked drone cameras for sports streaming." In *2017 IEEE 37th International Conference on Distributed Computing Systems (ICDCS)*, pp. 308–318. IEEE, 2017.

[WCH18] Ya Fei Wu, Yu Jian Cheng, and Zi Xuan Huang. "Ka-band near-field-focused 2-D steering antenna array with a focused Rotman lens." *IEEE Transactions on Antennas and Propagation*, **66**(10):5204–5213, 2018.

[WHW22] Mahmoud Wagih, Geoffrey S. Hilton, Alex S. Weddell, and Steve Beeby. "Millimeter-Wave Power Transmission for Compact and Large-Area Wearable IoT Devices Based on a Higher Order Mode Wearable Antenna." *IEEE Internet of Things Journal*, **9**(7):5229–5239, 2022.

[Wik23] Wikipedia. "5G NR Frequency Bands." `https://en.wikipedia.org/wiki/5G_NR_frequency_bands`, 2023.

[WWB20] Mahmoud Wagih, Alex S. Weddell, and Steve Beeby. "Millimeter-Wave Power Harvesting: A Review." *IEEE Open Journal of Antennas and Propagation*, **1**:560–578, 2020.

[WZC20] Geng-Bo Wu, Qing-Le Zhang, Ka Fai Chan, Bao-Jie Chen, and Chi Hou Chan. "Amplitude-modulated leaky-wave antennas." *IEEE Transactions on Antennas and Propagation*, **69**(7):3664–3676, 2020.

[XGZ19] Shen-Da Xu, Dong-Fang Guan, Qingfeng Zhang, Peng You, Shangkun Ge, Xiao-Xiang Hou, Zhang-Biao Yang, and Shao-Wei Yong. "A wide-angle narrowband leaky-wave antenna based on substrate integrated waveguide-spoof surface plasmon polariton structure." *IEEE Antennas and Wireless Propagation Letters*, **18**(7):1386–1389, 2019.

[XJ13] Jie Xiong and Kyle Jamieson. "ArrayTrack: A Fine-Grained Indoor Location System." In *10th USENIX Symposium on Networked Systems Design and Implementation (NSDI 13)*, pp. 71–84, Lombard, IL, April 2013. USENIX Association.

[XWZ09] Feng Xu, Ke Wu, and Xiupu Zhang. "Periodic leaky-wave antenna for millimeter wave applications based on substrate integrated waveguide." *IEEE Transactions on Antennas and Propagation*, **58**(2):340–347, 2009.

[Zha13] Hang Zhao et al. "28 GHz millimeter wave cellular communication measurements for reflection and penetration loss in and around buildings in New York city." In *2013 IEEE international conference on communications (ICC)*, pp. 5163–5167. IEEE, 2013.

[zim] "Zimaboard." `https://www.zimaboard.com/`.

[ZKQ17] Sun Zhan-shan, Ren Ke, Chen Qiang, Bai Jia-jun, and Fu Yun-qi. "3D radar imaging based on frequency-scanned antenna." *IEICE Electronics Express*, **14**(12):20170503–20170503, 2017.

[ZMZ13] Dmitry Zelenchuk, Alejandro Javier Martinez-Ros, Tomas Zvolensky, Jose Luis Gomez-Tornero, George Goussetis, Neil Buchanan, David Linton, and Vincent Fusco. "W-band planar wide-angle scanning antenna architecture." *Journal of Infrared, Millimeter, and Terahertz Waves*, **34**:127–139, 2013.

[ZWH19] Guangxu Zhu, Yong Wang, and Kaibin Huang. "Broadband analog aggregation for low-latency federated edge learning." *IEEE Transactions on Wireless Communications*, **19**(1):491–506, 2019.

[ZWL16] Xiongwen Zhao, Qi Wang, Shu Li, Suiyan Geng, Mengjun Wang, Shaohui Sun, and Zhu Wen. "Attenuation by human bodies at 26-and 39.5-GHz millimeter wavebands." *IEEE Antennas and Wireless Propagation Letters*, **16**:1229–1232, 2016.